Thermal Performances of Two-metal Micro Heat Pipes (TMMHP)

by

KMN Sarwar Iqbal

A Thesis Submitted to the Board of Examiners in Partial Fulfillment of the Requirements for the Degree of

DOCTOR OF PHILOSOPHY IN MECHANICAL ENGINEERING

Department of Mechanical and Chemical Engineering
Islamic University of Technology (IUT), OIC
Gazipur, Bangladesh

August 2014

Declaration of Candidate

It is hereby declared that this thesis or any part of it has not been submitted elsewhere for the award of any Degree or Diploma.

_____

Prof. Dr. Md. Abdur Razzaq Akhanda
Head, Mechanical and Chemical Engineering
Islamic University of Technology (IUT), OIC
Gazipur
Date: August 12, 2014

_____

KMN Sarwar Iqbal
Student No. 101701
Academic Year: 2011-14
Date: August 12, 2014

May it be a pathway for Ishraq and Tashfia
to go for even higher study
(ameen)

Table of Contents

N.B. A CD containing the whole thesis is provided in the pocket of the back cover.

List of Tables

List of Figures

Nomenclature

A_e surface area of the evaporator, m^2

A_c surface area of the condenser, m^2

C_p specific heat at constant pressure, $kJ/kg.^oC$

$C_{p,w}$ specific heat of water at constant pressure, $kJ/kg.^oC$

d_H hydraulic diameter of the heat pipe, *(m)*

d_T profile height of the heat pipe, *(m)*

h heat transfer coefficient for terminal temperature difference of the fluid, $kW/m^2.^oC$

h_{eff} effective heat transfer coefficient of the fluid for average terminal temperature difference, $kW/m^2.^oC$

k thermal conductivity of metal, *W/m.K*

l length of the heat pipe, *m*

Δl thickness of the shell of the heat pipe, *m*

l_a length of the adiabatic section, *m*

l_e length of the evaporator, *m*

l_c length of the condenser, *m*

l_{eff} effective length of the heat pipe, *m*

$\dot{m}$ coolant water flow rate, *kg/s*

P_{eva} pressure in the evaporator, *Pa* (N/m^2)

P_{con} pressure in the condenser, *Pa* (N/m^2)

ΔP_{cap} total capillary pressure drop, *Pa* (N/m^2)

ΔP_{eva} pressure drop at the evaporator, *Pa* (N/m^2)

ΔP_{liq} liquid (condensate) pressure drop, *Pa* (N/m^2)

p pressure of the fluid, *kPa*

q heat input, *Watt (Joules/s)*

Δp terminal pressure drop, *kPa*

Δp_{eff} effective pressure drop at terminal average pressure, *kPa*

q" heat flux, kW/m^2

$q"_{e,\,eff}$ effective heat flux through the evaporator shell by conduction, kW/m^2

$q"_{e,\,s}$ heat flux at the evaporator surface supplied by heater, kW/m^2

$q"_{c,\,s,}$ dissipated heat flux from the condenser surface by convection cooling, kW/m^2

$q"_{c,\,eff}$ effective heat flux dissipated through the condenser shell by conduction, kW/m^2

Q_{in} heat enters the evaporator boundary, *Joule (J)*

Q_{out} heat exits the condenser boundary, *Joule (J)*

$R_{eff,}$ effective thermal resistance, $^oC/W$

T_1-T_5 temperatures of the fluids in the micro heat pipe, ^oC

T_{1s}-T_{5s} temperatures of the heat pipe surface at the locations of T_1-$T_{5,}$ ^oC

ΔT temperature difference between two sides of the shell of heat pipe

T_e average temperature at the evaporator, ^oC

T_{es} average surface temperature at the evaporator, ^oC

T_{cs} average surface temperature at the condenser, ^oC

T_{eva} temperature at the evaporator, ^oC

T_{con} temperature at the condenser, ^oC

T_{adi} temperature at the adiabatic section, ^oC

T_{sat} temperature of the saturated vapor (T_3), ^oC

T_c average temperature at the condenser, ^oC

$T_{w,c}$ wall temperature at the condenser, ^oC

$T_{w,\infty}$ ambient temperature of water, ^oC

U overall heat transfer coefficient, $kW/m^2.^oC$

ρ density of the fluid, kg/m^3

ρ_c density of the fluid at the condenser, kg/m^3

ρ_e density of the fluid at the evaporator, kg/m^3

φ dimensionless correlation constant

θ angle of inclination, degree (^{o})

Subscripts:

c, condenser
e, evaporator
eff, effective
p, constant pressure
s, surface of the heat pipe
w wall
1-5, positions of thermocouples

Acknowledgements

In the name of Allah, the most merciful and the most gracious to Whom I submit myself with utmost gratitude for granting me such a great opportunity to arrive at the highest podium of academia with success and honor.

The author sincerely acknowledges the continuous guidance and untiring effort paid by the thesis supervisor Prof. Dr. Md. Abdur Razzaq Akhanda, to accomplish the research work in due time. Next, my sincere thank goes to Prof. Dr. A. K. M. Sadrul Islam whose careful monitoring on my research method specially in the area of validation of my experiments remains as a milestone towards achieving this Ph.D. Sincere appreciation also goes to Dr. Faisal Kader, whose advices have always been encouraging. Prof. Dr. Mohammad Ali of BUET has been caringly inquisitive to me that lead the work further ahead. Especially I am grateful to the reverend octogenarian Professor Dr. M. H. Khan, formerly Vice-chancellor of BUET, who is kind enough to review my work thoroughly and repeatedly. Otherwise his revision, the thesis could not get its present status at all. I convey my heartiest thanks to him and wish him a long healthy and peaceful life. Sincere thanks go to Mr. Abu Hossain of Air-conditioning and Refrigeration lab who spent many extra hours with me during the experimenting session beyond his scheduled office hours.

I would like to thank my employer Prof. Dr. M. Alimullah Miyan, Founder and Vice-chancellor of IUBAT—International University of Business Agriculture and Technology, for his kind approval and encouragement throughout my career. I woe to my colleague Mr. Dilip Kumar Das, Asst. Prof. in quantitative sciences, who helped me in mathematical needs and my beloved student of ME, Md. Aminul Islam who helped me a lot in preparing the figures of experimental setup by AutoCAD. I would like to especially thank my young colleague Dr. Abhijit Saha, Associate Professor in Computer Science and Engineering department who never loses patience in spending hours to decorate my thesis from his time constraints. I cannot leave before offering thanks to Zainul Abedin, my technician at Mechatracks Ltd. who has worked day and night to construct the best possible micro heat pipes for this experiment. And many others associated with my success in this program still remain uncalled in black and white, but are engraved in my heart.

My thanks with tear and cheer will never reach my parents as both of them passed away in the middle of my career. Lastly but never ending, I would offer thanks to my wife Mohua, who used to remain awake with me till late of many nights while encouraging me with good words. Best of all, I regain the lost strength which is vital to carry on this hard work when my lovely son and daughter, Ishraq and Tashfia, stand by me with their innumerable questions and queries about my research.

August 2014 KMN Sarwar Iqbal

Abstract

Electronic machines are rapidly being developed with the increasing benefits but, getting smaller in sizes resulting in more thermal stress. In an attempt to manage this stress, a comparative study is conducted between a two-metal (Cu-Ag) micro heat pipe (TMMHP) and the presently utilized single-metal (Cu) micro heat pipe (SMMHP). Thermal effects of three TMMHPs of circular, triangular, square cross sections plus one convergent-divergent of circular cross section at steady state are experimentally investigated. The tubes have three common basic dimensions – 150 mm long hollow axial space, 3.0 ± 0.3 mm hydraulic diameter and 0.3 mm thickness. The evaporator and condenser sections are made of pure copper (k = 398 W/m-K) and pure silver (k = 429 W/m-K) having lengths of 45 mm and 60 mm respectively. The adiabatic section is made of two parts – first half is made with copper and the second half is made with silver, each part having length of 22.5 mm. All the joints were brazed with silver. Water and three low boiling point liquids – ethanol, methanol and iso-propanol – are used as working liquids. In consideration of the usage of the actual equipment, tests are conducted by placing the heat pipe at three different orientations – horizontal, vertical and at 45^{o} inclination. To provide heat flux, SGW36 (Ni-Cr) electric heater-coil is coiled around the evaporator simulating the heat-generation of an actual device, and simultaneously the condenser section is directly cooled by water in an annular space. Internal fluid-flow is considered one dimensional. Ten calibrated K-type thermocouples are installed at different locations – five of them are to measure the temperatures of internal fluid and five are used to measure the surface temperatures of the tube at different axial locations. Temperatures are recorded by digital electronic thermometers. Unlike in the SMMHP, it is found that the boiling and super heat effects in the evaporator of TMMHP transforms the two-phase flow into a single phase superheated vapor flow, which increases TMMHP's heat transfer capability to three and half times the capacity of SMMHP. Such an enhanced heat transfer coefficient may be initiated from the improved convection which is developed from the different heat conductivity of metals that enables the TMMHP to reject heat at higher rate through its condenser than the rate it can take heat in through its evaporator.

Chapter 1

Introduction

The thermal engineering legend American inventor Jacob Perkins patented hermetic tube boiler in 1839, which was used to be deployed in locomotives and bakers' ovens in England. These tubes were later modified by his descendent Angier March Perkins, and in 1936 he patented it as Perkins Tube. Depending on their applications Perkins Tube could be as short as a hypodermic needle, or as long as 24 feet [1]. Eventually, this Perkins Tube became the inspiration for George Grover of Los Alamos National Research Laboratory to introduce the modern heat pipes. George Grover is the first person who successfully introduced the theory of capillary force as a natural pump to drive working fluid within the heat pipe from its condenser to evaporator [1]. Since then the concept of heat pipe became widespread and has been developing categorically for implementation in different industries.

1.1 Physical description of heat pipe and its varieties

Heat pipe is simply a metal pipe which is evacuated and filled with a liquid before being sealed off at both ends. These ends are evaporating and condensing zones where the middle part is insulated, called adiabatic zone, to avoid the heat loss or gain (Fig. 1.1). The working fluid may be a single compound (i.e. water, acetone etc.) or a homogeneous mixture of multiple compounds, called azeotrope, which maintains common thermodynamic properties (i.e. boiling, freezing etc.). A wick is shaped accordingly, and inserted within the heat pipe spanning end to end to let the condensate crawl back to the evaporating zone. The wick can be made of stainless steel mesh, sintered metal powder, fiber, wire braid etc.. In micro heat pipe (MHP), the presence of sharp or non circular edges [2], and in other case, radially etched micro grooved inner wall of the MHP are also replacing wick that provides the capillary action.

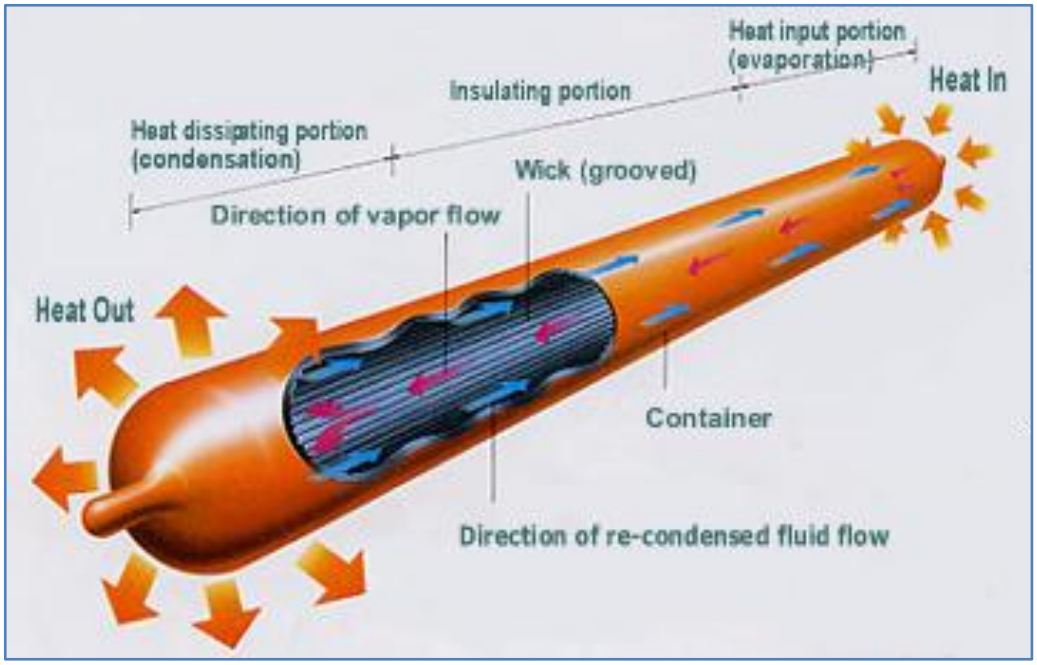

Figure 1.1 Components of heat pipe [3]

Modern heat pipes are manufactured in many forms: miniature heat pipe, flat miniature heat pipe (FMHP), micro heat pipe (MHP), parallel micro heat pipe (PMHP), capillary pumped loop heat pipe (CPLHP), variable conductance heat pipe (VCHP) etc. along with many other sub classifications. However, characteristically, all the heat pipes follow the same thermodynamic cycle.

1.2 Thermodynamic cycle of heat pipe

While surveying the literature, it is found that some researchers mistakenly explain the thermofluid cycle (liquid-vapor-liquid) as thermodynamic cycle [4]. When a working fluid or a system returns to its original state after completing all the processes of heat addition and rejection, then the whole process is called to be a thermodynamic cycle completed by the fluid or the system. The definition is available in any undergraduate thermodynamics text book. However, heat pipe operates following an ideal thermodynamic cycle which is described below.

1-2: Surroundings heat energy, Q_{in}, enters the evaporator boundary to be absorbed by the working liquid to develop vapor at constant pressure P_{eva} and temperature T_{eva}.

2-3: Vapor, energized by Q_{in} at T_{eva}, is driven by the vapor pressure P_{eva} that exits the evaporator boundary, and then travels isothermally at T_{adi} which enters the condenser boundary of lower temperature and lower pressure zone of T_{con} P_{con} respectively.

[$T_{eva} > T_{con}$,` $P_{eva} > P_{con}$ *and* $T_{eva} = T_{adi}$]

3-4: Heat energy, Q_{in}, is released by the energized vapor to become condensed at the condenser boundary at constant pressure P_{con} and temperature T_{con}.

4-1: Heat energy, Q_{out}, exits the condenser boundary to dissipate into the surroundings at constant temperature T_{con} and pressure P_{con}.

After completing the above four steps of thermodynamic cycle, the condensate returns to the evaporator by the capillary action of the wick to complete the thermofluid cycle.

All the above phases are summarized in Fig. 1.2 with small deviation. A little upside-cup curve 2'-2 confirms the nonlinear heat addition to the vapor within the adiabatic section which originates from the residual heat accumulated within the adiabatic section. It is easily noticed in Fig. 1.1 and Fig. 1.2 that there is no work output in the cycle that indicates the heat balance, $Q_{in} = Q_{out}$, occurs within the heat pipe system which verifies the first law of thermodynamics.

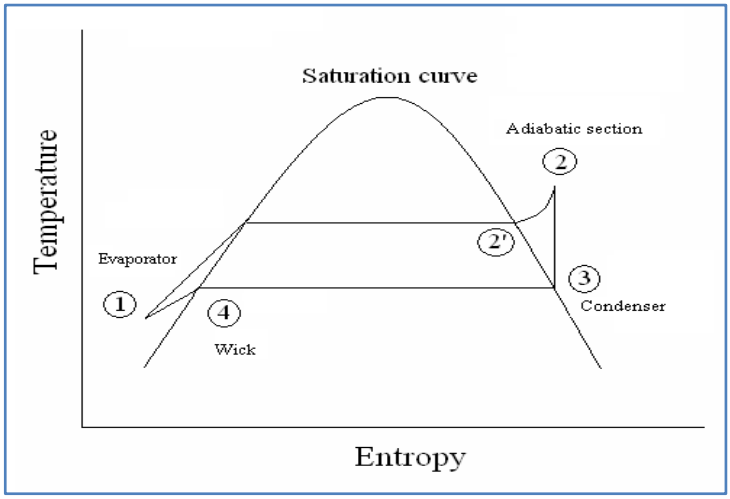

Figure 1.2 Thermodynamic cycle of a heat pipe with wick [5]

1.3 Principle of heat pipe

Heat pipe is a self explanatory device (Fig. 1.1). Heat enters through its evaporator (hot end – wherein the liquid content at relatively lower temperature is stored), and is being absorbed by the liquid until it is saturated liquid. Heat is transferred peripherally through the case and reaches the wick. This causes the liquid to evaporate and transfer energized mass from the wick to the vapor core. This addition of energized mass in the vapor core increases the pressure of the vapor at the evaporator end of the pipe, thus creating a pressure differential that drives vapor flow to the condenser end of the heat pipe. Since it is not desired that the carried-away-heat by the vapor be dissipated nearby the evaporator, so is not the "dry out" situation (when the evaporator is lacking any liquid to evaporate). Thus heat is being carried away by the mass through the insulated portion of the heat pipe leading to the condenser (cold end – for dumping out). How far the condenser of the heat pipe is required to work that depends on the amount of heat which is being absorbed by the working liquid through the evaporator while assuming that the vapor travels adiabatically. Eventually, the vapor travels up to the condenser of the heat pipe where the kinetic vapor comes to a halt by giving up all of its absorbed heat (latent heat of condensation) to the cold interface and becomes liquid again. Then the liquid is rerouted to the evaporator end through capillary action – this is accomplished by the wick inserted within the container or

through the gravitation assisted grooves spanning from condenser to evaporator. The process starts over again to continue the removal of heat from heat source. Since the vapor condenses with at a small temperature drop at the condenser end while it delivers a large heat flux into the heat sink, heat pipe is also called “superconductor”. Heat pipes with liquid metal working fluids can have a thermal conductance of a thousand times greater than the best solid metal conductors, silver or copper. Heat pipes, that utilize water as the working fluid, can have a thermal conductance greater than the best metallic conductors [6]. This is because the heat transfer in a heat pipe utilizes the phase change of the working fluid (by absorbing latent heat of evaporation), where a high amount of heat can be transferred with very little temperature difference between the source and the sink.

Fig.1.3a shows the basic principle of heat pipe with wick. Fig.1.3b is schematically showing liquid-vapor interface within the heat pipe (HP) when it is in operation. It is noticed that as the condensate approaches closer to the evaporator, the number of meniscus along the liquid axis also grows higher – continuous liquid pressure drop is the reason behind such change. At the same time, the radius of curvature of the meniscus also becomes smaller. Another observation is the constantly changing annulus diameter of the liquid-vapor interface which is the minimum at the beginning of condenser but grows larger as the liquid advances towards the evaporator. This happens because the advancing liquid faces the increasing resistance from the increasing velocity of the vapor. However, irrespective of the orientation of HP, to deliver the liquid from condenser to evaporator the capillary force must overcome all the resistance forces generated within the HP [7, 8]. In Fig. 1.3b, it is seen that the capillary pressure difference equals the sum of the vapor pressure drop plus the liquid pressure drop. Comparing with the thermodynamic cycle (sec 1.2) it can be checked that the capillary pressure difference equals the difference between evaporation pressure and the condensation pressure, plus the liquid pressure drop of the working fluid. Thus the total pressure drop can be summarized as below in Eq 1.1.

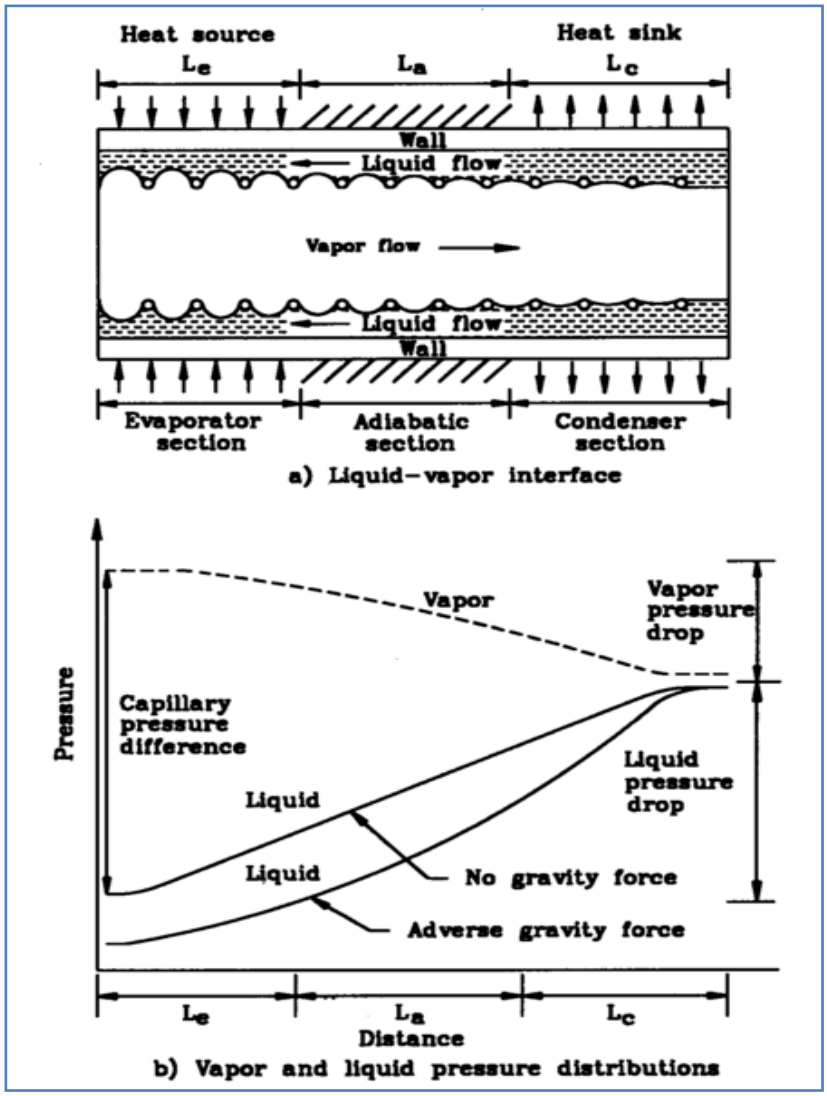

Figure 1.3 Principle of heat pipe with wick [7]

$$Or\ \Delta P_{cap} = (P_{eva} - P_{con}) + \sum \Delta P_{liq} \dots\dots\dots\dots\dots\dots\dots\dots\dots\dots\dots\dots\dots\dots (1.1)$$

But, to transport the working liquid from the condenser to the evaporator, the capillary pressure must overcome all the pressure drops occurring along the path. Thus *eqn. 1.1* can be rewritten as *eqn 1.2* which is as follows.

$$\Delta P_{cap} \geq \sum \Delta P_{eva} + \sum \Delta P_{liq} \dots\dots\dots\dots\dots\dots\dots\dots\dots\dots\dots\dots\dots\dots (1.2)$$

The vapor pressure drop is caused by the friction at the inner wall of the container or the wick material at one end, and at the liquid-vapor interface on the other end. Further the liquid pressure drop in the HP includes three different types of drops – liquid pressure drop within the condenser at the onset of journey towards evaporator, pressure drop due to the friction force which arises from the use of wick and the pressure drop due to the flow against gravitation force. Moreover, it is observeable during an operation cycle, the highest pressure is recorded at the evaporator where evaporation initiates while the lowest pressure is also recorded here upon returning vapor as liquid. Such a contrast is obvious because of gaining and loosing the kinetic energy by the working fluid during the phase change. We notice the effect of gravitation on the liquid's homebound path from the condenser to the evaporator. When the returning path is under the gravitational pull the liquid's pressure gradient is constant and uniformly distributed almost everywhere along the HP; but when it comes against the effect of gravitation, the relation becomes nonlinear. This nonlinearity is developed from the viscous effect (of the liquid) and friction force (at the liquid-vapor interface) combined, which are being tamed by the capillary force of the crawling liquid in the presence of gravitation force.

1.4 Miniature heat pipe

Miniature heat pipe is very small compared with the heat pipe and medium size heat pipe, but it functions on the same principle as the heat pipe does. Miniature heat pipe is used in high heat flux generating devices.

1.5 Micro heat pipe (MHP)

Cotter defined a micro heat pipe as "so small that the mean curvature of the liquid-vapor interface is comparable in magnitude to the reciprocal of the hydraulic radius of the total flow channel" [9]. The theory can be characterized by the equation: $r_c / r_h \geq 1$ where r_c is the capillary radius, and r_h is the hydraulic radius of the flow channel [10]. However, the specification of the MHP has been set as "A micro heat pipe is a wickless, non-circular channel with a diameter of 10 μm to 500 μm and a length of

about 10 mm to 20 mm" [11]. Nevertheless, till writing of the report, specification for the MHP has been adapted to the maximum of 3 mm hydraulic diameter and longer than 20 mm of lengths [6, 11, 25].

The theory of micro heat pipe was introduced by Cotter in 1984, and has received considerable attention in the past two decades of electronics development. Researchers have found that the reduction in the temperature of a typical semi-conductor device exponentially increases the reliability and durability of it [12 - 15]. The interest extends further from the possibility of achieving the extremely high heat fluxes near 1000 W/cm^2, needed for future generation electronics cooling application [16]. One of the prime advantages of micro heat pipe is its size. It has dimensions in microns and can be fabricated on the substrate itself. This helps in removing heat directly from a hotspot (locally accumulated heat). It is a passive heat transfer device [17]. The micro heat pipe is being looked at as one of the emerging technologies in thermal cooling: it helps in overall cooling of the electronic device and also results in uniform thermal distribution [18]. For instance, first heat pipe in laptop was used in 1994 [19].

1.6 Advantages of using MHP

- **High heat flux transportability:** The advantage of heat pipes over many other heat-dissipation mechanisms is their great efficiency in transferring heat. They are a fundamentally better heat conductor than an equivalent cross-section of solid copper. Some heat pipes have demonstrated a heat flux 230 MW/m^2 [20].
- **Less temperature difference** needed to transport heat than traditional materials (heat conductivity up to 90 times greater than that of copper of the same size) [5] resulting, in low thermal resistance [10].

1.7 Limitations of MHP applications

- **Capillary limit:** It is the disability of wick or the groove lines to drive the working fluid from the condenser to evaporator. In this situation, capillary

pressure is unable to overcome the sum of the pressure drops leading in failure to move fluid along the wick or grooves. Thus the evaporator experiences dry out and ultimately malfunctions the MHP.

- **Boiling limit:** When boiling occurs by the excessive radial heat flux in the oncoming fluid of the wick or groove lines away from the evaporator leading to dry out in the evaporator [5].
- **Entrainment Limit:** At high vapor velocities, droplets of liquid in the wick get detached from the wick and sent into the vapor flow that results in dry out.
- **Sonic limit:** This occurs usually during startup of heat pipe when the vapor velocity reaches sonic speed at the evaporator and the flow becomes choked. Even at the increased pressure difference no change in vapor velocity is observed. Thus heat is accumulated in the evaporator and exposed to nearby area.
- **Viscous limit:** At low temperatures, the pressure difference between evaporator and condenser is not strong enough to overcome the viscous force of the fluid, thus hinders the flow of vapor into the condenser [5] and heat transportation stops.
- **Vapor Continuum flow limitation:** For small heat pipes, such as micro heat pipes and for heat pipes with very low operating temperatures, the vapor flow in the heat pipe may be in the free molecular or rarefied condition. The heat transport capability under this condition is limited because the continuum vapor state has not been reached.

1.8 Objective of the study

The objective of the study is to investigate the thermal performances of micro heat pipes of different thermal conductivity (two-metal, i.e. Cu-Ag) using different working liquids of low boiling point at different orientations with different tube cross sections. The two metals are selected where copper is for the evaporator and silver is for the condenser to allow heat transfer at a higher rate towards condensation because of the higher conductivity of silver than copper. The high conductivity silver made condenser

has the capability to dissipate more heat than the low conductivity copper made evaporator can take in. Various cross sectional geometries (circular, triangular, square and convergent-divergent tube of circular cross sectional area) will be producing the varying pressure gradient within the heat pipe that will also affect the heat transfer coefficient (HTC). Different positions – horizontal, inclined at 45^{o} and vertical – will affect the fluid flow regime because of gravitational effect and ultimately affect the HTC. Different fluids – inorganic and organic – are chosen for observing the effect of thermophysical and chemical properties on the HTC. It is expected that the investigation will be helpful to find an improved geometry of heat pipe, its material as well as the working liquid used in it to get a high-valued heat transfer coefficient.

Chapter 2

Literature Review

Study on heat pipe began since 1942 by R. S. Gaugler of General Motors, USA proposed first [1]. However, heat pipe did not receive a target oriented attention until 1963 when Grover et al. [21] changed the heat pipe's condensate-returning mechanism from its confined gravitation-fed state to the simple capillary-force action of wick structure inserted in it. Subsequently the results were published in the Journal of Applied Physics in 1964. Since then the researches were going on in academia as well as in R & D labs of many industries, i.e. NASA, Los Alamos National Research Laboratory, RCA etc.. By the U.S. government funding, between 1964 and 1966, RCA was the first corporation to undertake research and development of heat pipes for commercial applications [22]. Starting in the 1980s Sony began incorporating heat pipes into the cooling schemes for some of its commercial electronic products instead of the more traditional finned heat sink with and without forced convection. But, twenty years later in 1984 T. P. Cotter first introduced the idea of "micro" heat pipes [1].

2.1 Developments of heat pipe

Numerous works are done on the heat pipes till the date; some of the related works are being discussed here based on different test parameters.

2.1.1 One dimensional steady-state analysis

The first steady-state model specifically designed for use in modeling of micro heat pipes was proposed by Cotter [9] in 1984. Chen et al. [23] worked on a typical steady-state, one-dimensional model for annular condensation in horizontal micro channels which was developed based on the Young-Laplace equation. Nadgauda [17] worked on two different matters as working fluid – DI water and Mercury in his Master's thesis. Although he has found the mercury as a good heat conductor but it was

difficult to fill up the micro heat pipe and sealing. Additionally a common fear exists about its radioactive property; people may not be interested using this liquid metal as a working fluid.

No conductive and convective heat transfer occurs in a vacuum; based on the principle Moon et al. [24] tested the MHPs which have a triangular cross-section with curved sides and a rectangular cross-section with curved sides. The material of the MHP is copper and the working fluid of it is pure water. The test was performed in a vacuum chamber to minimize heat loss. The operating temperatures of the MHP were considered from 60°C to 90 °C. They have found the MHP with triangular cross-section can dissipate up to a thermal load of 7 W.

Mahmood [6] at Islamic University of Technology (IUT), OIC has performed tests on different cross sections of MHP of the same hydraulic diameter charged with water at different inclinations. It was found that the best heat transfer coefficient at the circular cross section was at an angle of 90^{o}.

Hossain et al. [25] explored the boiling-condensation phenomenon in MHP in diversified ways. The experiment of investigating thermal performance of MHP was done by varying the angle of inclination, coolant flow rates, working fluids and heat inputs. From the results they concluded that the coolant flow rate has an insignificant effect on the performance of MHP, rather Performance of MHP depends upon angle of inclination. Better performance was found for an inclination angle of 70^{o}. It was found that overall heat transfer coefficient is higher for higher heat input.

2.1 .2 Studies on wickless micro heat pipes

In order to reduce the viscous shear force between liquid and vapor flow and separate them, Kang et al. [26] designed the radially grooved micro heat pipes (MHPs) with a three-layer structure. Experiments were conducted to evaluate the performance of wafers with three different wafer fill rates at different input powers. After the evaluation, the MHP with 70% fill rate showed the best performance as compared to samples with smaller fill rates.

2.1.3 Investigation on micro and miniature heat pipes

Vasiliev [16] investigated the differences and complications between Micro and miniature heat pipes due to their small size. A short review on the micro and miniature heat pipes is presented in his paper.

Moon et al. [27] investigated the thermal performance of MHPs with cross sections of polygon. They found cross section diameter with smaller than 2 mm has significant effect on the length of MHP regarding thermal performance because of pressure losses by friction at the vapor–liquid interface and the capillary limitation of condensed fluid also dominant as in the increase of length. Kimura et al. [28] confirmed the heat transfer characteristic in their experiment and proposed a prediction method for maximum heat transfer rate. They observed that the longer the evaporation and condensation takes, the higher the heat transfer rate occurs in MHP disagreeing with Iqbal and Akhanda who studied the TMMHP [29, 30].

Faghri [31, 32] wished to consider the thermal resistances in condensation and evaporation parts of micro-heat pipe with triangular grooves. They analyzed a triangular micro heat pipe in which the corners act as a wick.

2.1.4 Experiments on various fill ratios and cross sections

Le Berre et al. [33] studied experimentally the performance of a micro heat pipe array for various filling charges under various experimental conditions. The micro heat pipe array was 20mm × 20mm and consisted of 27 parallel triangular shaped channels, 500μm wide and 350μm deep, giving a void fraction of 11%. They defined an effective thermal conductivity as the thermal conductivity of a homogeneous material which would lead to the same temperature field under the same conditions. The measurements indicated that the use of micro heat pipes increases the effective thermal conductivity to about 200 W/m.K.

2.1.5 Heat pipe experiments on miscellaneous test parameters

Polymer-based flat heat pipes (PFHPs) with a thickness on the order of 1 mm have been successfully developed and tested by Oshman et al. [34]. An experimental study was conducted to examine the PFHP performance. The test data demonstrated that the PFHP can operate with a heat flux of 11.94 W/cm^2 and results in effective thermal conductivity ranging from 650 to 830 $W/m \cdot K$, with the value varying with the input heat flux and the tilt angle.

Yamamoto et al. [35] experimentally found the heat pipe's geometrical influence on the heat transport capability. The worked on a high performance MHP and confirmed the larger the diameter, the higher the rate of heat transfer.

Sreenivasa et al. [36] determined the optimum fill ratio in miniature heat pipe which indicates the same performance the evaporator section was half filled rather than filling in full. Akhanda et al. [37] tested an air cooled condenser to investigate the thermal performance of MHPs charged with different fluids and oriented a different inclinations. Cao and Gao [38] developed a wickless network of heat pipe for high heat flux study and applications. Thereupon, studies on the application of MHP having the diameter of 3mm for cooling of the notebook PCCPU have been actively conducted by the American and Japanese companies specializing in the heat pipes [39 - 41].

2.1.6 Heat pipes using nano-fluids

Kole and Dey [42] investigated thermal performance using Cu-distilled water nano-fluid, which enhanced thermal conductivity by 15% at 30^o C. Chiang et al. [43] developed a magnetic-nanofluid (MNF) heat pipe (MNFHP) with magnetically enhanced thermal properties. The results showed that an optimal thermal conductivity exists in the applied field of 200 Oe.

Throughout the survey, all the researchers have struggled to build a common but fundamental thermal relationship among three principal elements of heat pipe – working fluid, wick and shell. This relationship is based on that the working fluid obeys

thermodynamics and shell follows the modes of heat transfer while the wick collaborates the tow by keeping the processes unaltered. An efficient thermodynamic approach to produce a *single-phase-flow* of fluid (i.e. super heated vapor) will assure the maximum heat generation within the heat pipe's evaporator which will adiabatically be carried to the condenser port. Next, a large negative pressure gradient needs to be produced by the condenser to dissipate heat through the shell of condenser by conduction and convection modes.

2.2 Scope of the present study

Till now, it is found that only a single metal or bimetal alloy has been used to manufacture heat pipes including varieties of isometric geometry. In these cases, heat transfer occurs only at constant heat conductivity at both ends of MHP. No individual or company has attempted to investigate MHP with two different metals of thermal conductivity. Thus, a two-metal micro heat pipe (TMMHP) made with two different metals (i.e. Cu and Ag) of close heat conductivity (i.e. 398 W/m-K for copper and 429 W/m-K for silver) to have *different heat conductivity* is selected by the author for his doctoral thesis. For detailed study, four TMMHPs of circular, triangular [29], square [30] and convergent-divergent of circular cross sections as well as four different working liquids of low boiling point (i.e.water, ethanol, methanol and iso-propanol) are selected. All the four cross sections of TMMHP hold 3.0±0.3 mm hydraulic diameter. Moreover, the convergent-divergent TMMHP will produce the *different pressure gradient* because of its geometry. Each TMMHP is tested with all four fluids while the circular one with water is taken as a reference. A series of heat inputs ranging from 2W to 16 W are supplied to the evaporator keeping the MHP horizontally to study the heat transfer behavior of fluids. Then it is reexamined at 45^{o} inclination and vertical (evaporator uphill) position while the condenser is being cooled by water at a constant flow-rate of 400 ml/min.

At the end, the fluid temperatures within the TMMHP as well as the surface temperatures at designated locations at steady state are recorded. Then the experimental data are recorded to compare with the results of other researchers.

Chapter 3

Experimental Measurements and Test Procedures

3.1 Experimental measurements

The experimental set up essentially consists of a TMMHP, a water storage tank, a measuring cup, a power source and a digital thermometer. There are four different shapes of TMMHPs (i.e. circular, triangular, square cross section and a convergent-divergent of circular cross section) used in this experiment that are made on a 3.0±0.3 mm hydraulic diameter and are of same length.

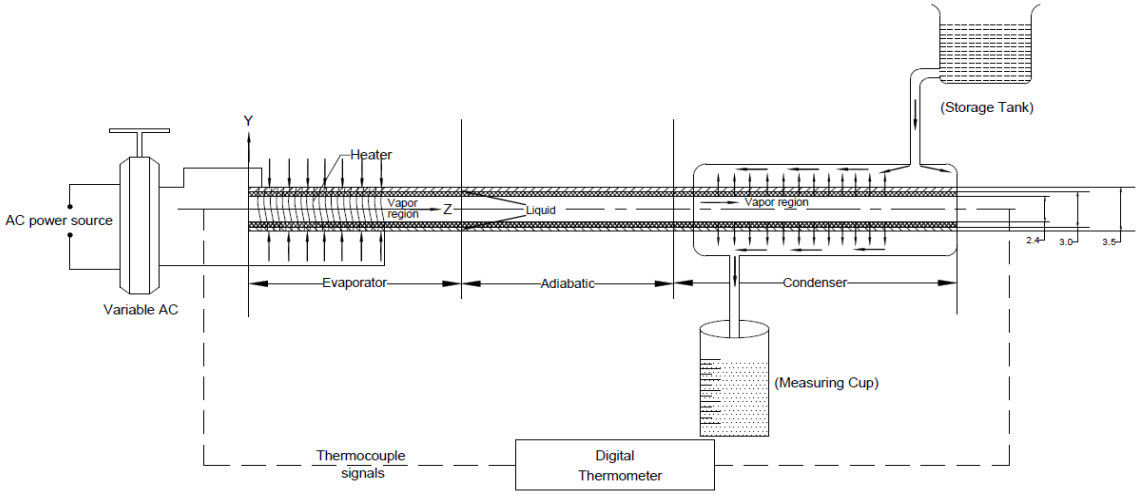

Figure 3.1 Schematic diagram of the experimental setup at horizontal position

Storage Tank holds the coolant (water) that is positioned above the heat pipe section while the measuring cup is placed below the heat pipe to ensure the gravitation fed coolant flow is gravitation fed. The power source includes a voltage regulator to provide the required voltage to create exact power output for the heat generation on to the evaporator of TMMHP. A digital thermometer is used which is an electronic thermometer that can show temperature of designated points by the help of a selector switch. Fig. 3.1 shows the schematic diagram of the experimental set up which is common to all four TMMHPs.

3.1.1 Specifications of different TMMHP

Physical dimensions of all four TMMHPs are shown in the Tables (3.1-3.4) below.

Table 3.1 Physical Dimensions of TMMHP (Circular)

Specifications	Dimensions	Materials
Heat pipe total length	150 mm	Copper & Silver
Evaporator section length	45 mm	Copper
Adiabatic section length	45 mm (22.5+22.5)	Copper & Silver
Condenser section length	60 mm	Silver
Heat pipe inner diameter	3.0 mm	
Heat pipe outer diameter	3.6 mm	
Hydraulic diameter	3.0 mm	
Heat pipe wall thickness	0.3 mm	
Mesh number of wick	7 holes per cm	
Wick thickness	0.3 mm	
Working fluid	Methanol, Ethanol, Iso-propanol and Water	
No. of circumferential heater in the evaporator section	1 [SGW36]	
Insulating material	Asbestos rope	

Table 3.2 Physical Dimensions of TMMHP (Triangular)

Specifications	Dimensions	Materials
Heat pipe total length	150 mm	Copper & Silver
Evaporator section length	45 mm	Copper
Adiabatic section length	45 mm(22.5+22.5)	Copper & Silver
Condenser section length	60 mm	Silver
Heat pipe each side length	4.0 mm	
Heat pipe profile height	3.5 mm	
Hydraulic diameter	3.0 mm	
Heat pipe wall thickness	0.3mm	
Mesh number of wick	7 holes per cm	
Wick thickness	0.3 mm	
Working fluid	Methanol, Ethanol, Iso-propanol and /Water	
No. of surrounding heater in the evaporator section	1 [SGW36]	
Insulating material	Asbestos rope	

Table 3.3 Physical Dimensions of TMMHP (Square)

Specifications	Dimensions	Materials
Heat pipe total length	150 mm	Copper & Silver
Evaporator section length	45 mm	Copper
Adiabatic section length	45 mm(22.5+22.5)	Copper & Silver
Condenser section length	60 mm	Silver
Heat pipe each side length	3.6 mm	
Heat pipe profile height	3.0 mm	
Hydraulic diameter	3.0 mm	
Heat pipe wall thickness	0.3 mm	
Mesh number of wick	7 holes per cm	
Wick thickness	0.3 mm	
Working fluid	Methanol, Ethanol, Iso-propanol and Water	
No. of surrounding heater in the evaporator section	1 [SGW36]	
Insulating material	Asbestos rope	

Table 3.4 Physical Dimensions of TMMHP (Convergent-Divergent, circular)

Specifications	Dimensions	Materials
Heat pipe total length	150 mm	Copper & Silver
Evaporator section length	45 mm	Copper
Adiabatic section length	45 mm(22.5+22.5)	Copper & Silver
Condenser section length	60 mm	Silver
Divergent side diameter	4.5 mm	
Convergent side diameter	3.0 mm	
Heat pipe profile height	3.8 mm	
Heat pipe wall thickness	0.3mm	
Hydraulic diameter	3.0 mm	
Mesh number of wick	7 holes per cm	
ick thickness	0.3 mm	
Working liquids	Ethanol, Methanol, Iso-propanol and Water	
No. of surrounding heater in the evaporator section	1 [SGW36]	
Insulating material	Asbestos rope	

3.1.2 Positions of thermocouples on different heat pipes

There are ten K-type thermocouples attached to the heat pipe – five of them are to sense the temperatures of the working fluid flowing within the heat pipe and five are to sense the surface temperatures at the same locations. Those positions on all four TMMHPs are shown in Tables (3.2-3.5) below.

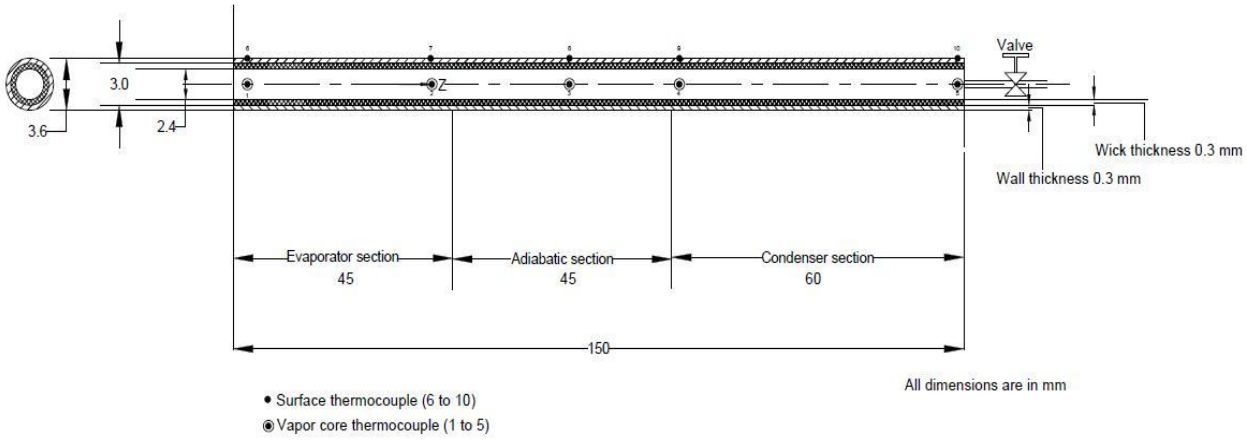

Figure 3.2 Positions of thermocouples along the TMMHP (Circular)

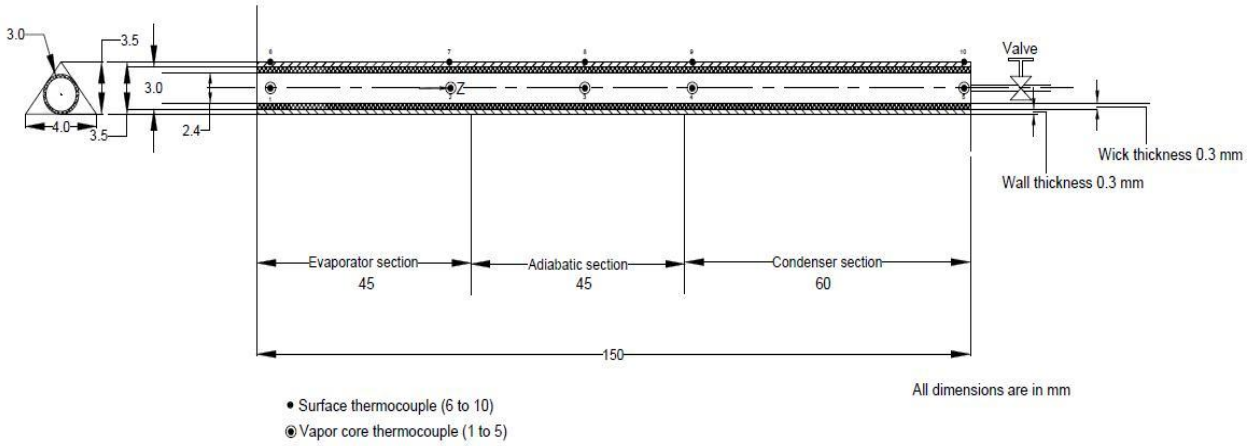

Figure 3.3 Positions of thermocouples along the TMMHP (Triangular)

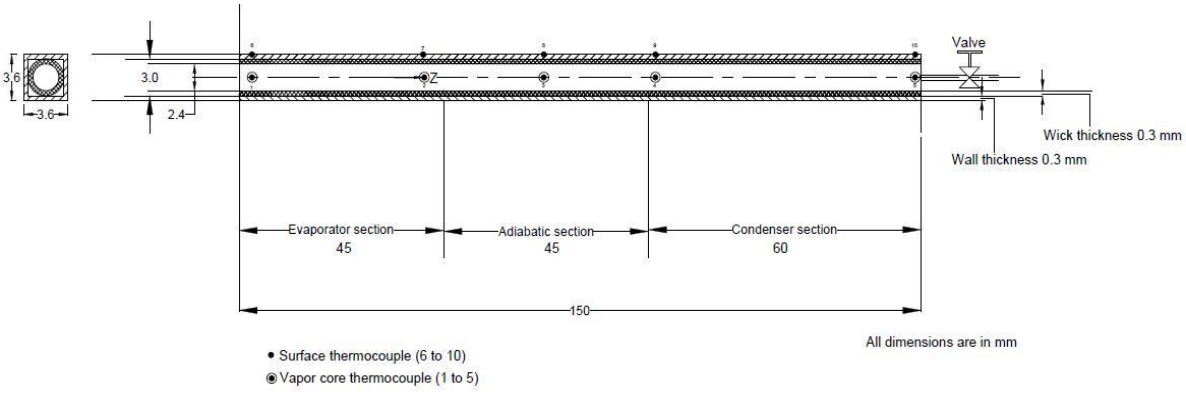

Figure 3.4 Positions of thermocouples along the TMMHP (Square)

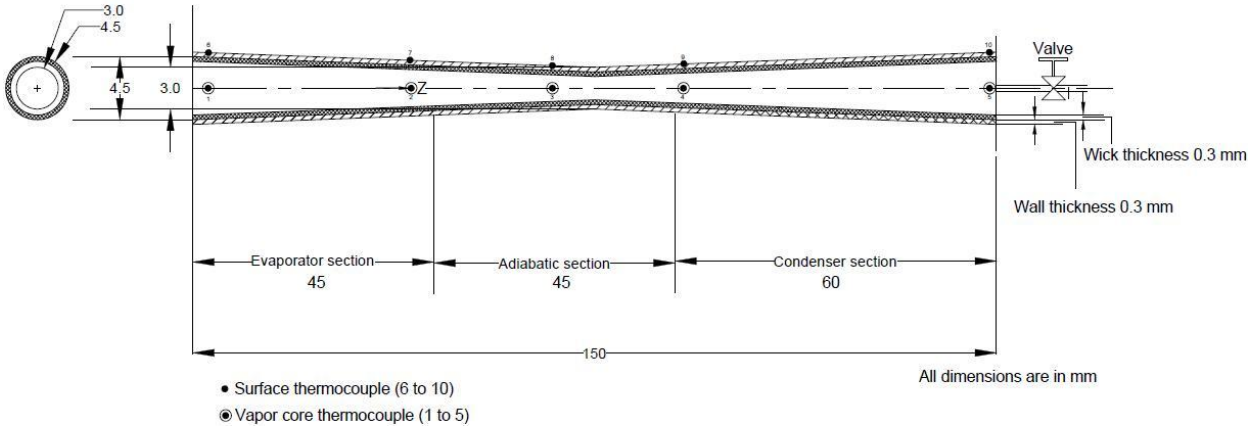

Figure 3.5 Positions of thermocouples along the TMMHP (Convergent-Divergent)

It is noteworthy to inform that the adiabatic section assigned in between evaporator and condenser of the heat pipe is

- to isolate the evaporator and condenser section
- to simulate the actual situation of how far the heat will be taken away from the heat source.

All the TMMHPs are manufactured and commissioned at Mechatracks Ltd., Dhaka, an R&D institute of which the Managing Director is author himself. The ingots of pure copper and silver are rolled to the sheet of appropriate thickness, and curved by sheet rolling process, and then the seam line is brazed with silver. Later, the tubes are tempered to release the residual stress due to cold work for rolling.

3.1.3 Photographic views of different TMMHP in operation

Venue: Aircondition and Refrigeration Laboratory, IUT, OIC, Dhaka, Bangladesh

Circular (axial)

Circular (lateral)

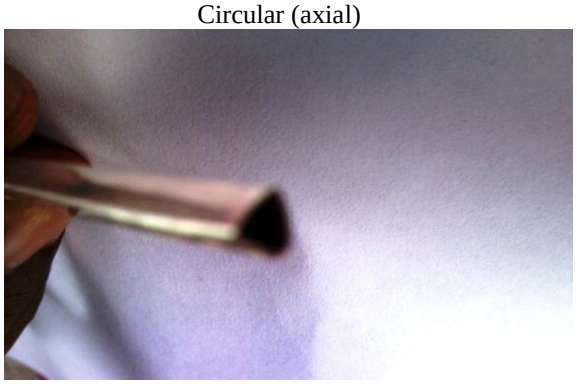

Triangular (lateral)

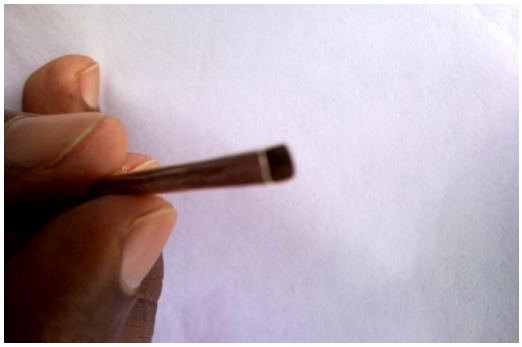

Square (lateral)

Convergent-Divergent (axial)

Convergent-Divergent (lateral)

TMMHP with K-type thermocouples

Sealed TMMHP after filling working liquid

TMMHP, horizontal

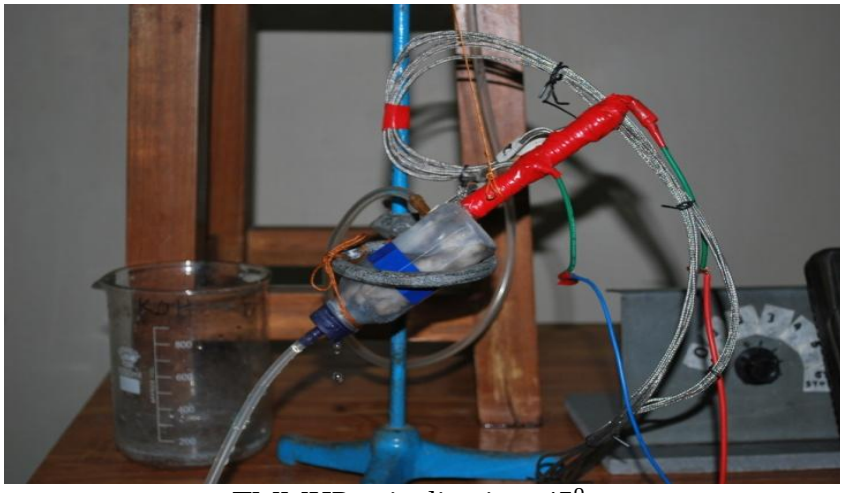

TMMHP at inclination, 45^{o}

TMMHP, vertical

3.1.4 Assembling the components of experimental set up

Table 3.1 through Table 3.4 provides the physical dimensions of the TMMHP. The TMMHPs used in this study have a common length of 150 mm and are based on mean 3.0 mm hydraulic diameter. These are made with 0.3 mm thick metal tube half of which is pure copper and the other half is pure silver. The copper-end is the evaporator section while the silver-end is the condenser. The lengths of the evaporator and adiabatic sections are of equal length of 45 mm each and the rest 60 mm is the condenser section. Thus, the evaporator and condenser are fully covered with copper and silver respectively while the adiabatic section is with both metals. The evaporator side is then welded to seal. Before preparing the heat pipes for experiment, those were purged out thoroughly with hot water, and then blown by hot air to become dry.

For wick, a steel mesh of 0.3 mm thickness with the equal length of TMMHP is wrapped around a mandrel and inserted into the tube so that the wick radially press fits in the inner wall of the tube. Five 1.1 mm holes are drilled on each tube according to the Fig. 3.2 to Fig. 3.5. Five K-type thermocouples are inserted to reach the vapor core and brazed with silver to know the internal working fluid's state. Then another five thermocouples are attached right beside the holes by quick fixing adhesive to measure the surface temperatures at those locations.

The condenser-end of the heat pipe is then plugged into one end of a capillary tube while the other end is attached with a vacuum pump. When pressure within the heat pipe goes well below the atmospheric pressure, and then is locked for a couple of minutes to reconfirm its air freeness. Then a pinch-clip is used to choke the capillary tube near the junction, and a slim syringe (Dispovan, 1 ml) filled with appropriate amount of working liquid, which is 100% (Fill Ratio) of the empty space of the evaporator, is injected into the capillary tube (see Table 3.5). Actually, the liquid is sucked into the capillary tube spontaneously because of having lower than atmospheric pressure within the tube. After filling, the condenser-end of the TMMHP is now pinched and sealed by brazing.

Table 3.5 Filling amount of Working Liquid for different TMMHP

TMMHP	Filling Amount
Circular cross section	0.50 ml
Triangular cross section	0.55 ml
Square cross section	0.55 ml
Convergent-Divergent (circular cross section)	0.60 ml

At the evaporator, a fire and electric shock proof tape is laid around and then SGW36 (Ni-Cr) electric heater wire having diameter of 0.28 mm (10Ω/m) is wound around at a closer pace possible without clinging to each other. To avoid the dispersion of heat produced by the heater in view to keep the heat input value significantly unaltered, the coil is insulated by the asbestos rope by many folds and is extended up to the end of adiabatic section. Finally, another strip of insulating tape is wrapped around to avoid getting soaked by the splash of water. Now the condenser-end of the TMMHP is wrapped up with cotton and inserted into a plastic container which has two outlets. Then the outlets are connected with flexible water tube – upper one is fitted with the valve of the coolant (water) reservoir and the lower one is dipped into an empty measuring bucket to collect the used coolant.

The whole setup is then mounted on a rig which is placed on a wooden table. Then the thermocouples are connected with a digital thermometer through a selector switch. The coolant reservoir is filled with the supplied water which is placed above the level of TMMHP. To produce the variable heat input for the heat pipe, a Variac is introduced, which is then monitored by one ammeter and one precision voltmeter to record the current and voltage simultaneously.

3.2 Test procedures

Since the study of TMMHP follows an experimental heat transfer method, hence measuring the heat generated in heat source, temperatures developed at various

locations of the tube and coolant flow-rate over the condenser is essential. These values can be directly measured using different equipment (i.e. volt meters, ammeters, thermometers etc.). On the other hand, the thermodynamic properties like pressure change developed within the heat pipe at different sections for using different working fluids and their densities, must need consultations with the engineering handbooks and data-bank of chemical companies. (i.e. CRC Handbook, Perry's Chemical Engineers' Handbook, Wikipedia, Dow Chemicals, Methanex, etc.).

3.2.1 Test parameters

Table 3.6 provides the list of test parameters pertinent to the experimental subjects.

Table 3.6 Summary of the test parameters

Parameters	Subjects and Conditions
Types of cross sections	Circular, triangular, square and convergent-divergent (circular)
Types of working liquids	Water and low boiling point fluids (ethanol, methanol and iso-propanol)
Inclination angles	Horizontal, 45^{o} and vertical
Mode of condensate return	Stainless steel mesh made wick

At first the coolant flow is opened to run through the condenser end to ensure that the condenser jacket is soaked and fully immersed in water. Then the Variac is connected with the AC power source to produce controlled heat by the heater. The power range is chosen from 2W to 16W which produces different heat flux ranges are provided in the Table 3.7. These heat fluxes simulate the generated heat in a laptop computer processor and similar electronic equipment [6]. It can be noted, before wrapping the heater coil, its red-hot power limit is checked and found to be 24W. Thus, the upper limit of 16W is quite safe for the experimental purposes. Initially, the TMMHP is inclined at 0^{o} (horizontally), and the time and temperature at the evaporator

are recorded until the system reaches steady state. The experiment is continued by keeping the setup at 45^{o} and 90^{o} (vertically) with evaporator uphill position. To attain steady state, a minimum coolant flow rate of 400 ml/min or 70 ml/s has been found to be reasonable to find the used coolant temperature equal to ambient temperature. Although the initial steady-state for 2W is achieved not until ten minutes; however, the subsequent steady-states takes only less than two minutes.

Table 3.7 Heat fluxes applied to different TMMHP

TMMHP	Heat Flux (kW/m^2)
Circular	4.7 - 37.7
Triangular	3.7 - 29.6
Square	3.1 - 24.7
Convergent-Divergent	1.9 - 15.1

3.2.2 Calibration of the measuring equipment

The electrical equipment, i.e. ammeter, voltmeter as well as the thermocouples and digital thermometer, are calibrated which is presented in Appendix C. A detailed analysis regarding the uncertainties within the equipment, measurements and results is carried out, which cumulatively is 8.90% with 95% confidence level, and the details are appended in Appendix D.

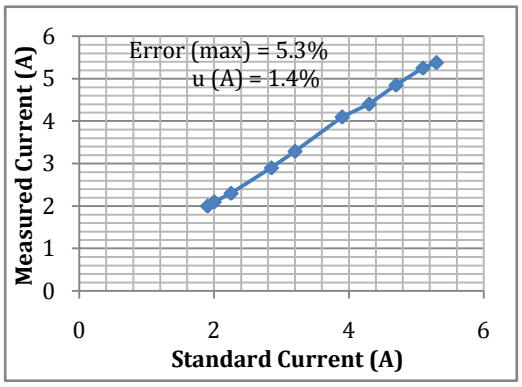

Figure 3.6 Uncertainty in Ammeter

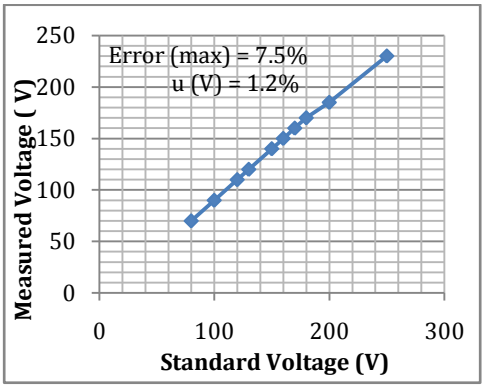

Figure 3.7 Uncertainty in Voltmeter

Fig. 3.6 indicates the error propagates linearly in measuring current which authenticates the well functioning of the equipment. Fig. 3.7 indicates errors in voltmeter are high

because of instability of the power supply. However, the error propagates linearly that approves of the dependability of the equipment.

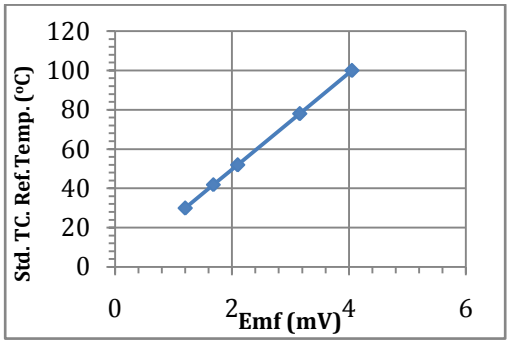

Figure 3.8 Std. TC. Ref. Temp. vs. Emf

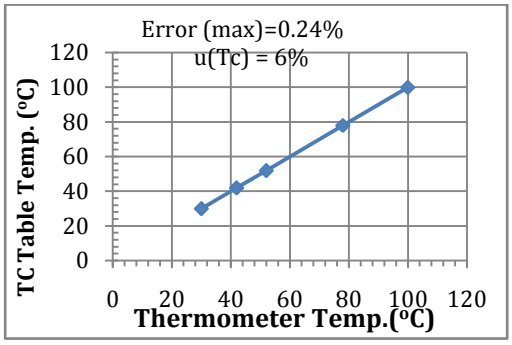

Figure 3.9 Uncertainty in using thermocouple (K-Type)

Good linearity of emf to measured (St. TC) temperature in Fig. 3.8 validates Fig. 3.9, from which the uncertainty in K-type thermocouple is calculated.

3.2.3 Validation of the experimental setup with known results [25]

To validate the present experimental setup and results, four experiments are carried out in the IUT Lab with a dissimilar setup following the test procedures applied to TMMHP. The setup contained a circular SMMHP made with copper which was tested by the experimenters Hossain et al. [25] for ethanol, methanol and acetone, and operated at 30^o, 50^o, 70^o and 90^o angles with the heat inputs of 0.61W, 1.56W, 3.67W, and 8.71W. Out of three fluids, ethanol is selected as the working fluid for the validation test. The specifications of the setup are given in Table 3.8.

Table 3.8 Specifications of the experimental setup to be examined

Test Parameters	Dimensions (mm)
Outer diameter of the tube, d_o	2.0
Hydraulic diameter of the tube, d_h	1.8
Length of heat pipe, L	150
Length of evaporator section, L_e	50
Length of adiabatic section, L_a	30
Length of condenser section, L_c	70

All the data collected from the validation experiments are appended in Appendix A-2. The values of overall heat transfer coefficient, *U*, extracted from the source [25] are compared with those found from the validation experiment, which are within the proximity of 93% of TMMHP. Similarly, the thermal resistances, *R*, are also compared and found to be within 95% of the known values.

The variation of overall heat transfer coefficient, *U*, at different inclinations are shown in the following figures, Fig.3.10 (a-d). In the legendry of the plots, H represents Hossain et al [25] and I for Iqbal (author).

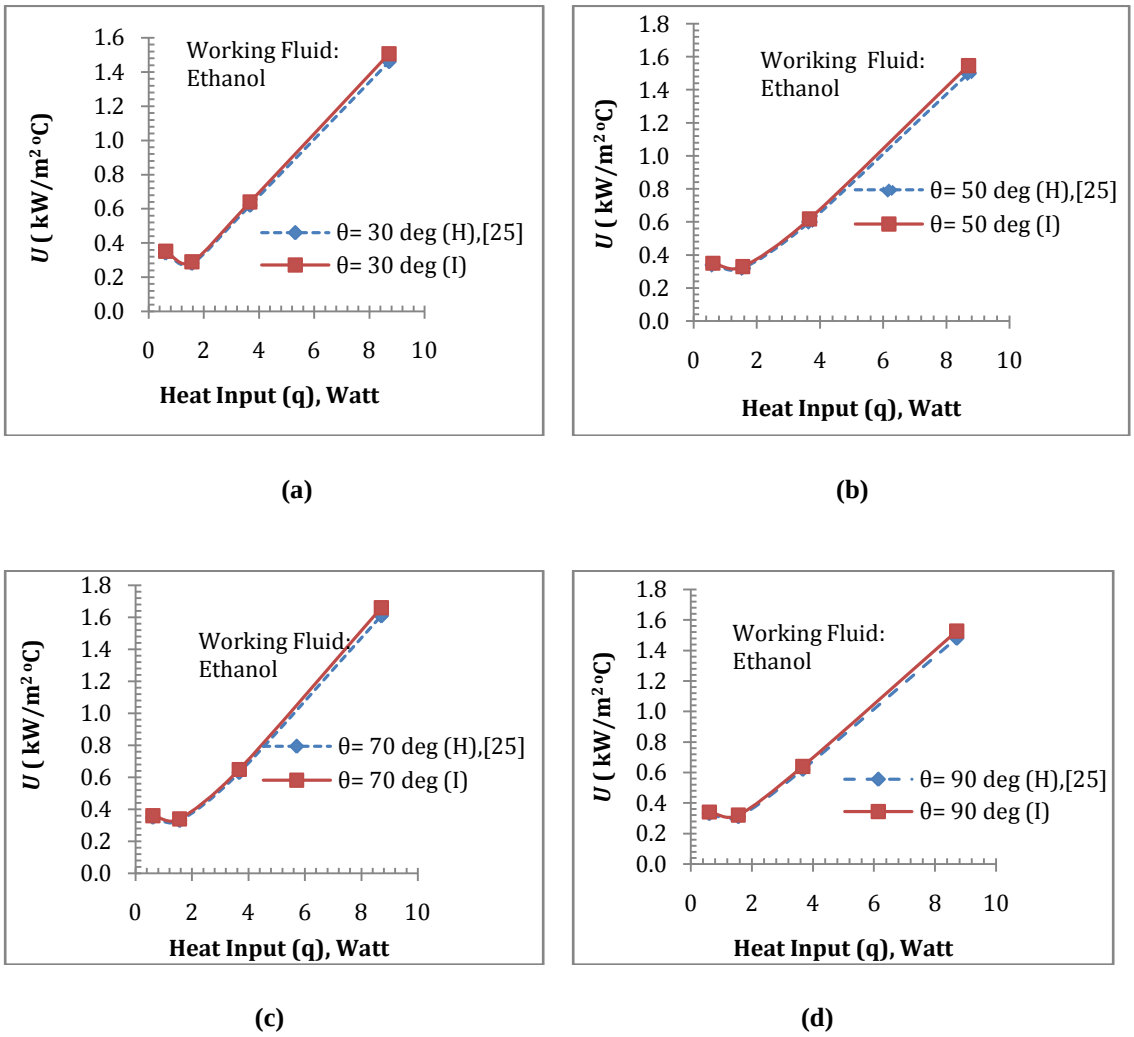

Figure 3.10 (a-d) Variation of *U* at different heat inputs and inclinations

The following figures, Fig. 3.11-13, indicate the comparison of overall heat transfer coefficient (U) and thermal resistance (R) against different parameters.

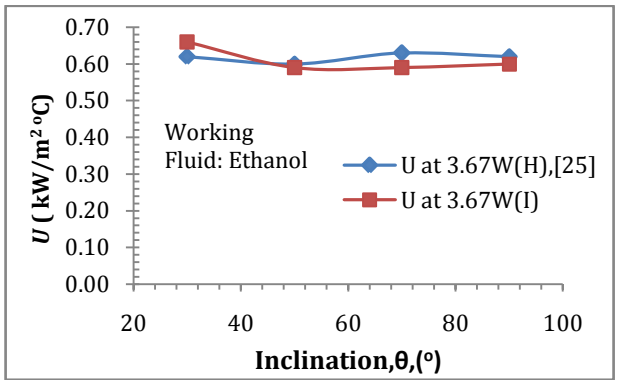

Figure 3.11 Comparison of U at different inclinations

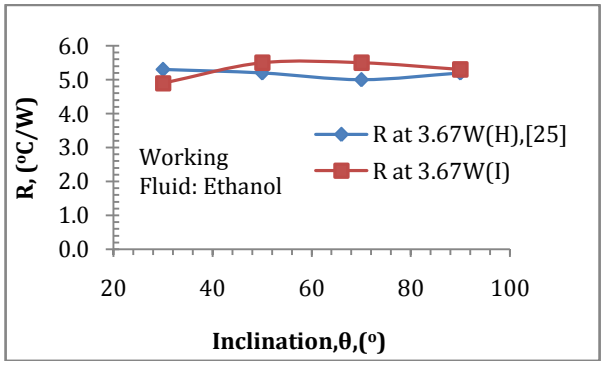

Figure 3.12 Comparison of R at different inclinations

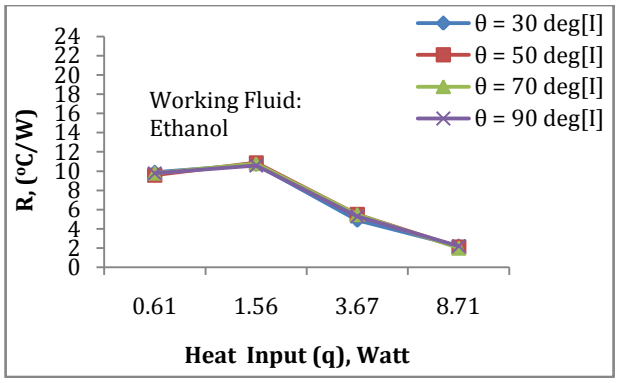

Figure 3.13 Comparison of R at different heat inputs and inclinations

3.3 General distribution of the experiments

Thermal performances of TMMHPs are studied in four subsections of the experiment. Those subsections are as follows:

I. Study of two-metal (Cu-Ag) micro heat pipe of **circular** cross section using different working liquids of low boiling point.
II. Study of two-metal (Cu-Ag) micro heat pipe of **triangular** cross section using different working liquids of low boiling point [29].
III. Study of two-metal (Cu-Ag) micro heat pipe of **square** cross section using different working liquids of low boiling point [30].
IV. Study of two-metal (Cu-Ag) micro heat pipe of **convergent-divergent** of circular cross section using different working liquids of low boiling point.

Chapter 4

Results and Discussions

The collected data acquired from forty eight experiments using four sets of experimental setup are appended in Appendix A–1. Next, those are reduced to the useful results using the equations mentioned in Appendix – B with the help of the tables presented in Appendix – E. Now, the results are thoroughly discussed and presented both individually and summarily in the following sections.

4.1 Study of two-metal (Cu-Ag) micro heat pipe of circular cross section using different working liquids of low boiling point

Using collected data in this investigation various curves are plotted as shown from Fig. 4.1.1 to Fig. 4.1.20. Fig. 4.1.1 shows time required for reaching steady state temperature for different working fluids. It is found that water takes the least time out of four while the other three takes approximately the same period of delayed time. Ethanol and iso-propanol are almost entwined in terms of temperature rise as well as attaining steady-state condition – this may occur because of their proximity of boiling points (BP). On the other hand, methanol takes the longest time to reach but at a higher temperature range than the other three. It is observable that not only the methanol's boiling point is low but also is its flash point. Methanol's flash point is only 11 ^{o} C which is 5.6 degrees less than that of ethanol. This indicates the earlier boiling and condensation of methanol than other fluids, which becomes chaotic within the narrow space of the micro heat pipe. Consequently, methanol takes longer period of time to reach thermal equilibrium thus to attend steady state than that of others. Therefore, the heat capacity of a fluid not only depends on its thermophysical properties (i.e. density, SG etc.) but also on its chemical bonding (i.e. hydrogen bonding). The trends of temperature rises at the evaporator section for using different fluids in TMMHP are

shown in Fig. 4.1.2 where the curve for methanol is overshadowed by the curve of iso-propanol.

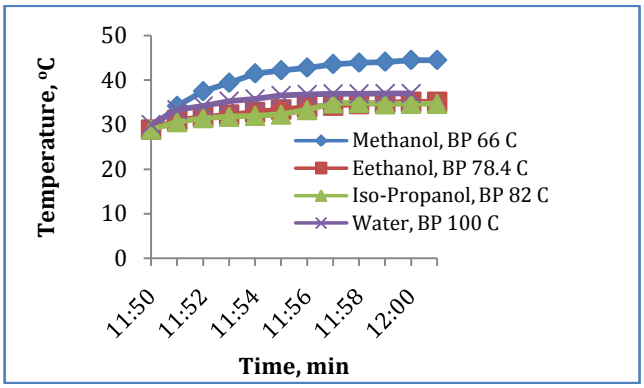

Figure 4.1.1 Time required for reaching steady-state of different fluids

However, water's character is specifically non-linear. This may happen because of the three are organic compounds and have similar chemical bonding, and the water as an inorganic compound is made up from hydrogen and oxygen's covalent bond. Thus it supports the conception that the heat capacity of a fluid is not simply based on

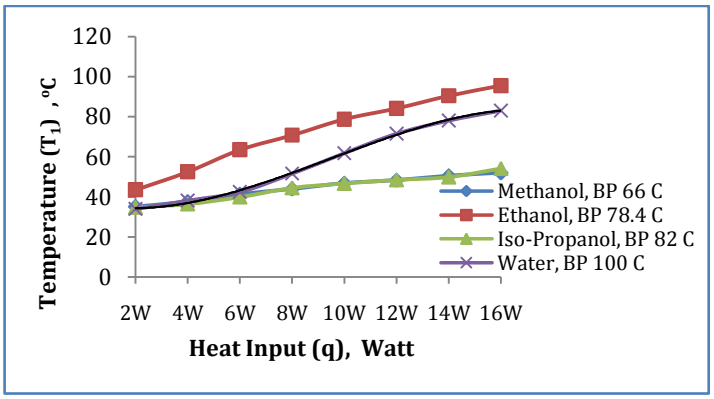

Figure 4.1.2 Rise of fluid temp. vs. heat input at the evaporator

thermophysical property (i.e. density,oiling point, SG etc.) rather mainly on its bonding.

4.1.1 Evaporator as a super heater

Distributions of temperatures along the length of the TMMHP for different working fluids, for different heat inputs, and also for different inclinations are shown from Fig. 4.1.3 (a) to 4.1.10 (b). It is observed from these figures that in each case of fluid used in TMMHP, there is a temperature rise in the evaporator from T_1 to T_2.

Annamalai A. S. *et al.* [44] has reasoned that "In the evaporator zone heat is supplied by an electric coil and the coil surface area density is very high in the middle of the evaporator portion and hence the temperature of the vapor in the middle of the evaporator is high". Author here disagrees with Annamalai that there should be no reason to windup the heater coil densely in the middle of the evaporator rather wrapping must be uniformly done so the produced heat flux remains constant throughout the evaporator. Based on this work and the work of Mahmood [6] and Sreenivasa [36], the working fluid should be filled only equal to or less than the empty space (vapor core) of the evaporator of the heat pipe. However, a lot more space in the heat pipe is still vacant to travel during operation. Soon after the MHP goes on operation, boiling starts at the beginning of the heat pipe – part of the fluid evaporates – that leaves a significant room empty within the evaporator which is fully wrapped up by the heater coil. Therefore, when the saturated vapor advances, it continuously receives heat from that part of heater to become superheated, and then it enters the adiabatic section. That's why we notice the temperature rise at point $T_{2,}$ hence this end of the evaporator act as a *super heater*.

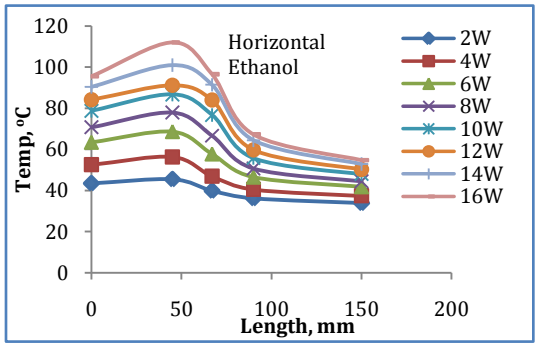

Figure 4.1.3 (a) Fluid temp. distribution along the TMMHP

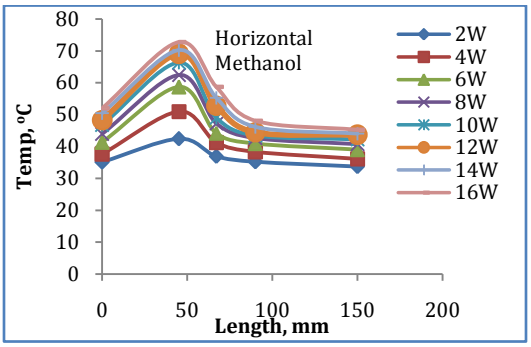

Figure 4.1.3 (b) Fluid temp. distribution along the TMMHP

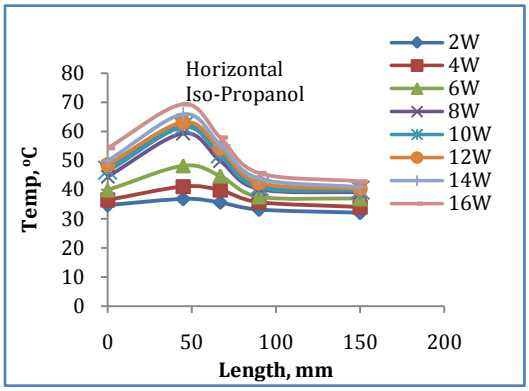

Figure 4.1.3 (c) Fluid temp. distribution along the TMMHP

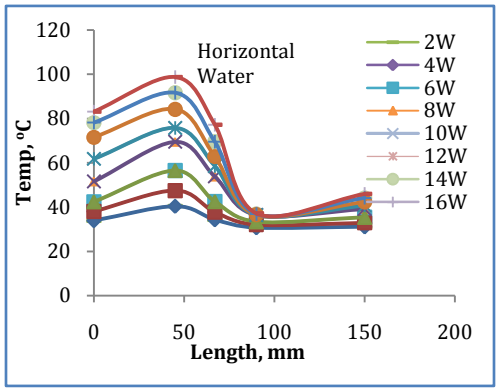

Figure 4.1.3 (d) Fluid temp. distribution along the TMMHP

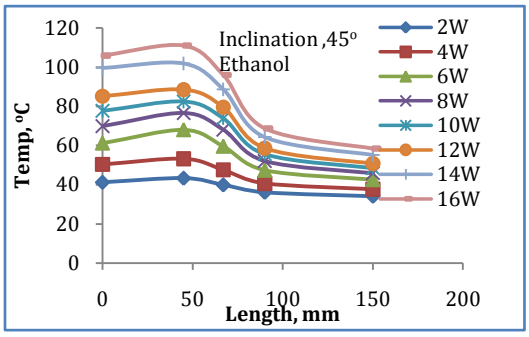

Figure 4.1.4 (a) Fluid temp. distribution along the TMMHP

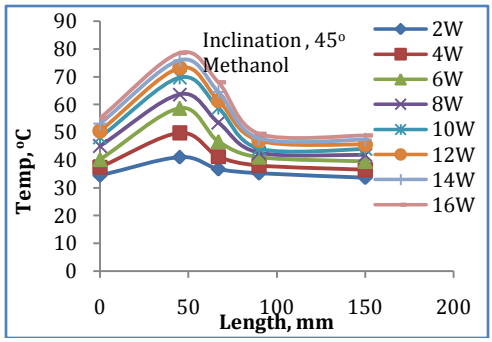

Figure 4.1.4 (b) Fluid temp. distribution along the TMMHP

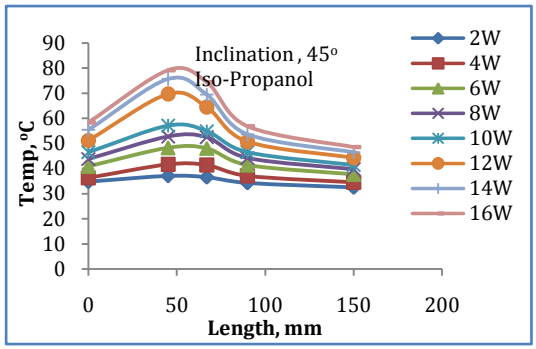

Figure 4.1.4 (c) Fluid temp. distribution along the TMMHP

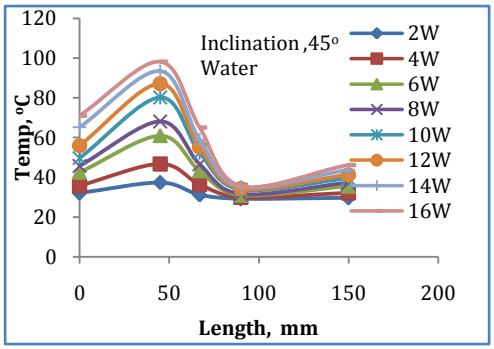

Figure 4.1.4 (d) Fluid temp. distribution along the TMMHP

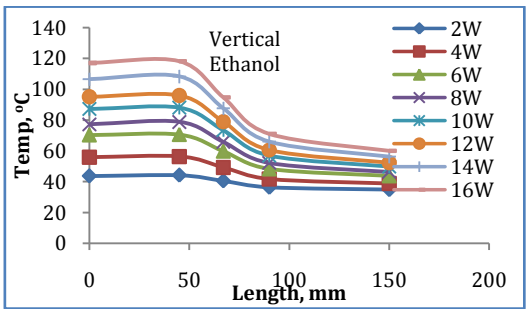

Figure 4.1.5 (a) Fluid temp. distribution along the TMMHP

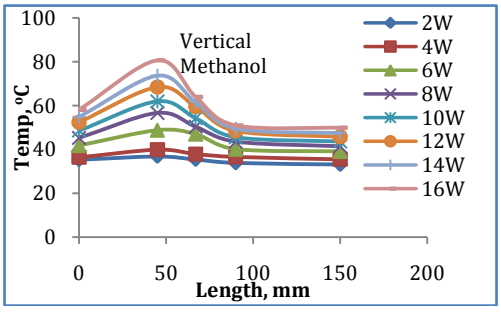

Figure 4.1.5 (b) Fluid temp. distribution along the TMMHP

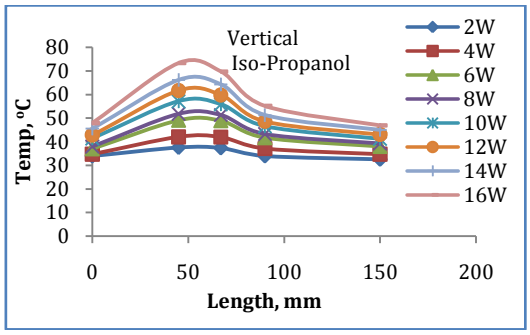

Figure 4.1.5 (c) Fluid temp. distribution along the TMMHP

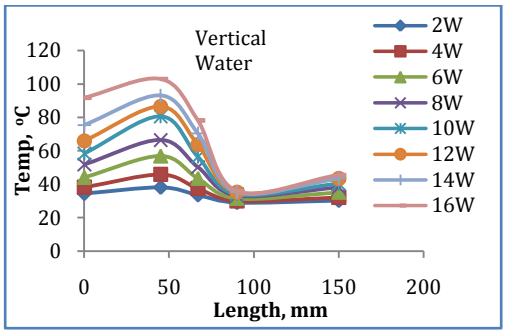

Figure 4.1.5 (d) Fluid temp. distribution along the TMMHP

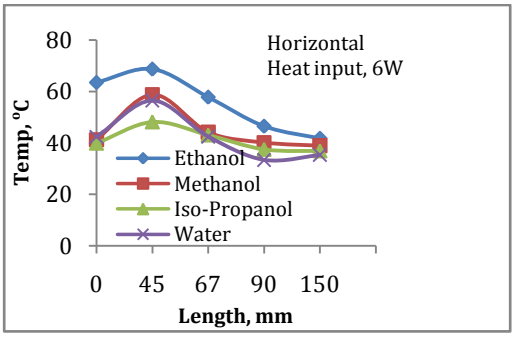

Figure 4.1.6 (a) Temp. distribn. along TMMHP of diff. fluids

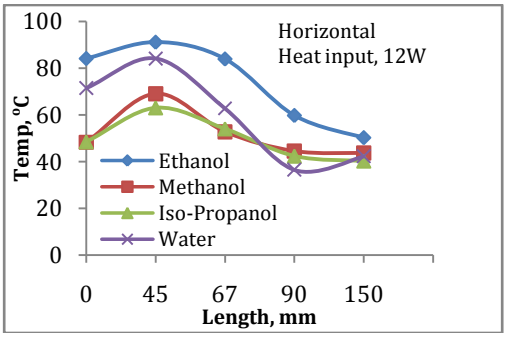

Figure 4.1.6 (b) Temp. distribn. along TMMHP of diff. fluids

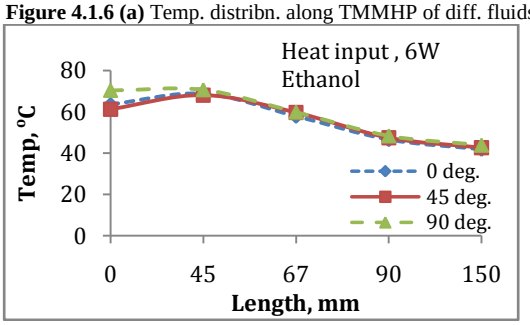

Figure 4.1.7 (a) Temp. distribn. along TMMHP at diff. inclns.

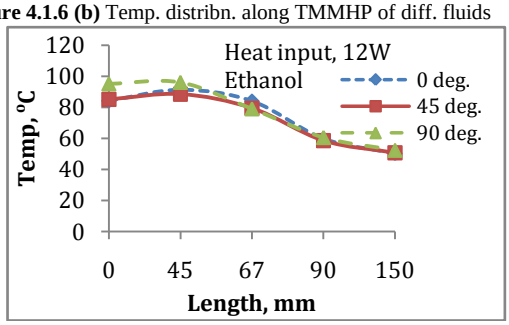

Figure 4.1.7 (b) Temp. distribn. along TMMHP at diff. inclns.

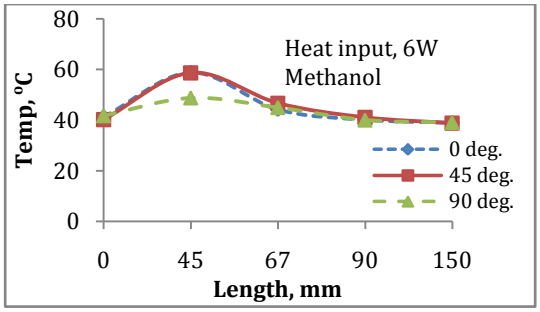

Figure 4.1.8 (a) Temp. distribn. along TMMHP at diff. inclns.

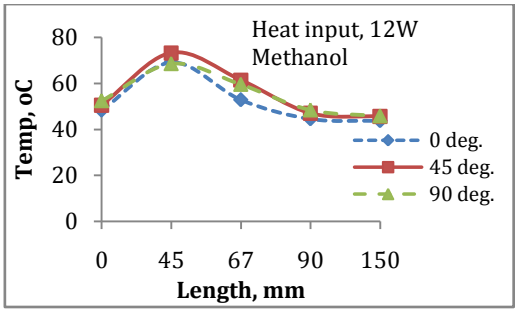

Figure 4.1.8 (b) Temp. distribn. along TMMHP at diff. inclns.

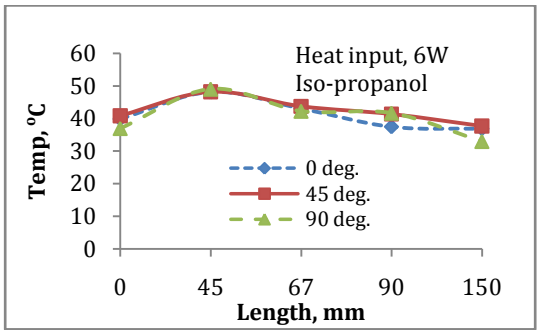

Figure 4.1.9 (a) Temp. distribn. along TMMHP at diff. inclns.

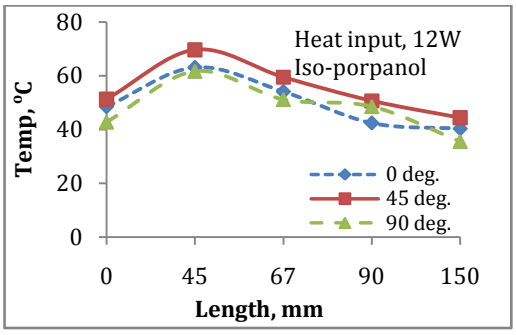

Figure4.1.9 (b) Temp. distribn. along TMMHP at diff. inclns.

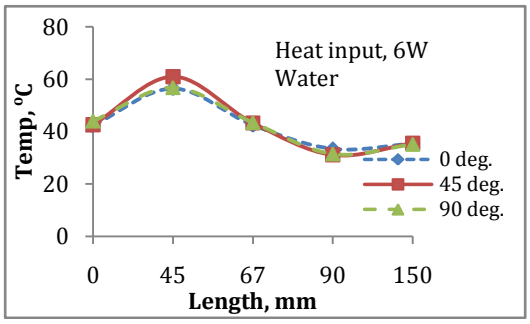

Figure 4.1.10 (a) Temp. distribn. along TMMHP at diff. inclns.

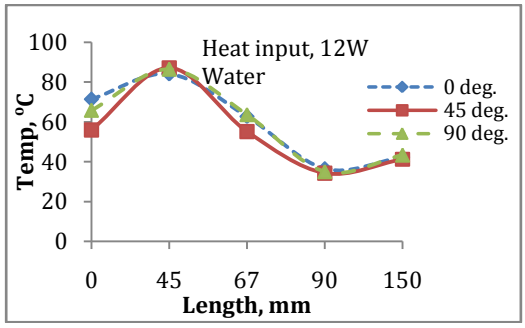

Figure 4.1.10 (b) Temp. distribn. along TMMHP at diff. inclns.

Regarding the change of temperature in the evaporator, a comparative relationship between the fluids in the TMMHP and in the SMMHP [6] is shown in Fig. 4.1.11. Temperature rise for methanol is found to be higher than those of other three fluids. It is obvious that the boiling points of the fluids play an important role in superheating – the high the boiling point, the complex the function. On the other hand, in the case of SMMHP [6, 36] the trend is negative which indicates no superheating effect present in it. Apparently, it may occur due to single metal of single thermal conductivity.

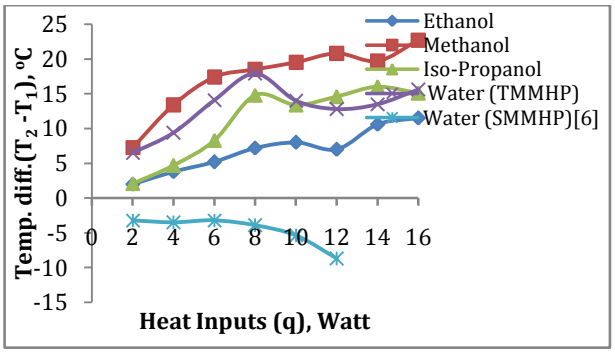

Figure 4.1.11 Comparison of temp. diff. (T_2-T_1) of TMMHP of diff. fluids with the SMMHP [6], horizontal

It is noticed that the temperature rise of all fluids are maintaining their own tracks with an almost certain pace. Methanol has given the highest rise while ethanol the minimum. However, the lowest rise of temperature of ethanol may be explained as its earliest evaporation and speedy escaping the evaporation chamber due to pressure rise.

Fig. 4.1.12 indicates that water is condensed within the smallest temperature range because of the highest specific heat (c_p) and latent heat. Considering this, methanol should have possessed the largest range, but it is found that ethanol has got the highest range. Thus it is proved again that the heat capacity of a liquid is not only depended on its physical property but also on its chemical property (i.e. structural bonding). While being condensed, the internal working fluids were experiencing negative temperature gradient within the condenser, but the water is an exception with a positive gradient as shown in Fig. 4.1.13. This behavior of water is due to the impact of the saturated liquid at the end of condenser. The advancing water vapor from the adiabatic section towards the condensation port (T_4) creates high pressure on the saturated liquid constantly that accelerates the liquid particles of heavy momentum to hit the other end of the heat pipe.

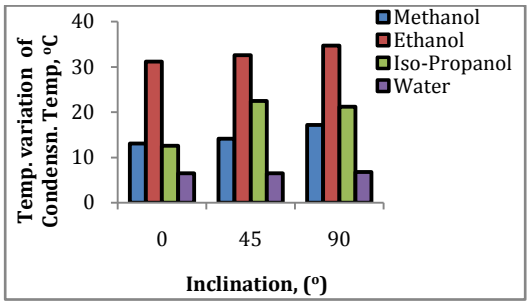

Figure 4.1.12 Temp. variation of condensn. temp. ($T_{4,16W}$ - $T_{4,2W}$) of diff.fluids for diff. heat inputs to TMMHP at diff. inclns.

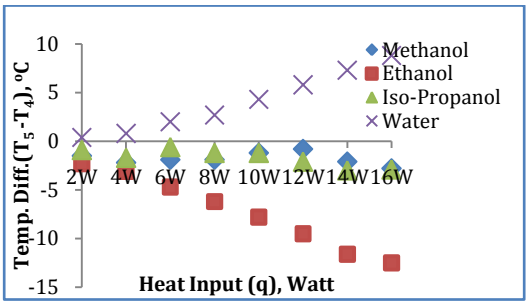

Figure 4.1.13 Comparison of condensn . temp. (T_5-T_4) range of diff. fluids for increasing heat inputs to TMMHP, horizontal

During this impact, the inherent kinetic energy of the liquid is converted to heat, hence the temperature of the liquid increases. At the turning point, such a temperature increase of the liquid benefits the capillary action of the wick to drive back condensate even faster to the evaporator. A comparison of thermal performances between the single-metal and two-metal micro heat pipe is shown in the Table 4.1.1.

The efficiency of MHP is exhibited by its heat transfer capability at a lower temperature difference. A comparison between the TMMHP and SMMHP [6] of circular cross

section is shown in Fig. 4.1.14. As it is seen, the terminal temperature difference in TMMHP is only the fourth or even less than that of in SMMHP. This has become possible because of relatively higher conductivity of silver at the condenser port that accelerates the thermodynamic cycle of the working fluid within the heat pipe.

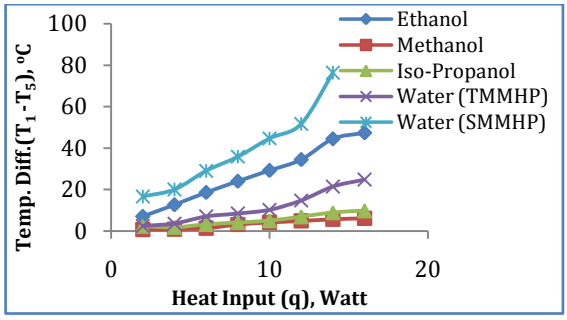

Figure 4.1.14 Comparison of terminal temp. diffs. (T_1 -T_5) of TMMHP with SMMHP [6] at 45^o

4.1.2 Comparison of *h* for water between TMMHP and SMMHP

In Fig. 4.1.15 and 4.1.16, *h* values of water in both SMMHP [6] and TMMHP for different inclinations can be compared. The *h* values in TMMHP are very high and sinusoidal throughout the heat input range while the *h* at SMMHP begins with very low values and increases slowly with the increasing heat input. In addition, the highest *h* value (0.75 kw/m^2.^{o}C) is recorded at vertically for SMMHP and 2.5 kw/m^2.^{o}C at 45^o for TMMHP. However, the trajectories at both SMMHP and TMMHP clearly indicate the limit of *h* with the increasing heat input. Since all the operating and test parameters remain the same at both single and two-metal micro heat pipe, the difference of heat conductivity as well as their designed orientation validates greater *h* values in TMMHP.

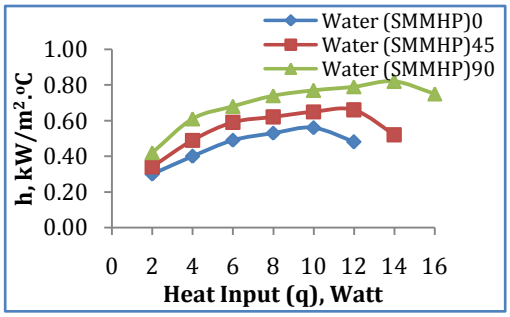

Figure 4.1.15 Convec. HT coeff. of water in SMMHP[6] diff.inclns.

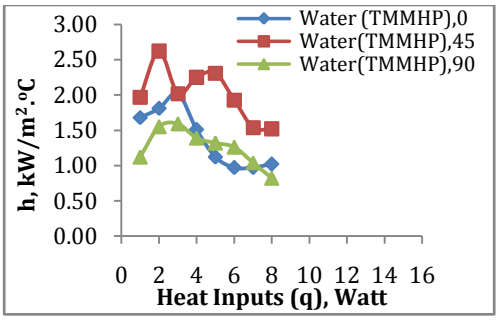

Figure 4.1.16 Convec. HT coeff.of water in TMMHP at at diff. inclns.

4.1.3 Comparison of *h* for four fluids in TMMHP

Fig. 4.1.17 (a), (b) and (c) show the values of heat transfer coefficient of different fluids at inclinations of horizontal, 45° and vertical. In each case methanol possesses the highest '*h*' (6.5 kW/m^2.°C) among all the fluids, and the highest value is attained at inclination 45°. Thus in respect to *h*, methanol is the most useful working fluid out of the four for circular cross section TMMHP. However, the sequence of '*h*' values for the four fluids remains the same at all three orientations.

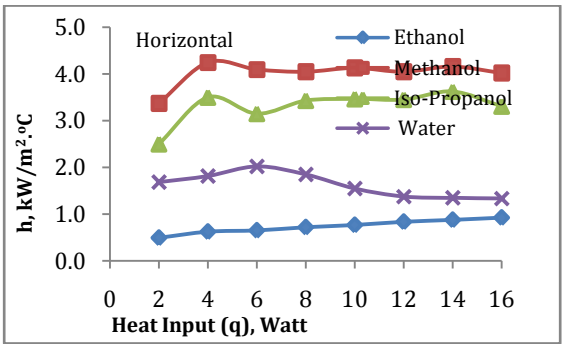

Figure 4.1.17 (a) Convec. coeff. vs. Heat input at TMMHP

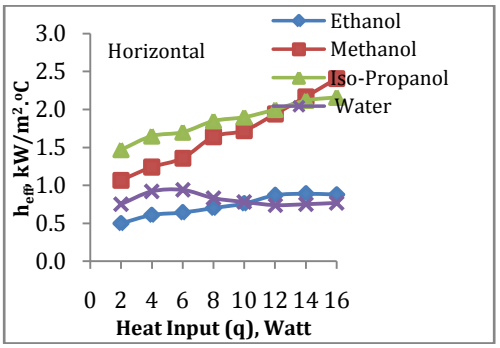

Figure 4.1.18 (a) Eff. convec.coeff. vs.Heat input at TMMHP

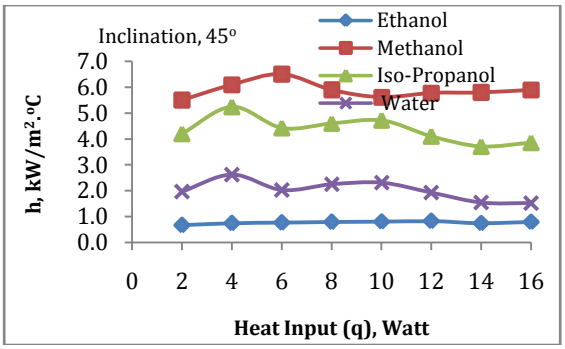

Figure 4.1.17 (b) Convec. coeff. vs. Heat input in TMMHP

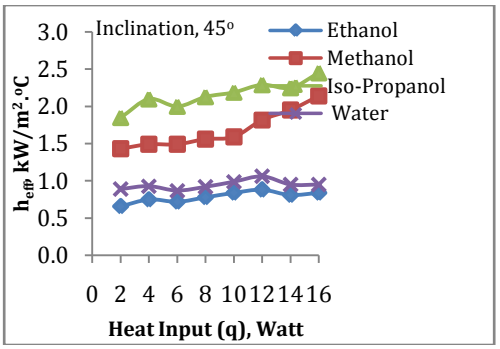

Figure 4.1.18 (b) Eff. convec.coeff. vs.Heat input atTMMHP

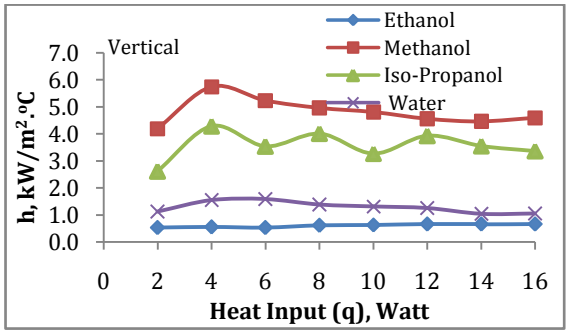

Figure 4.1.17 (c) Convec. coeff. vs. Heat input at TMMHP

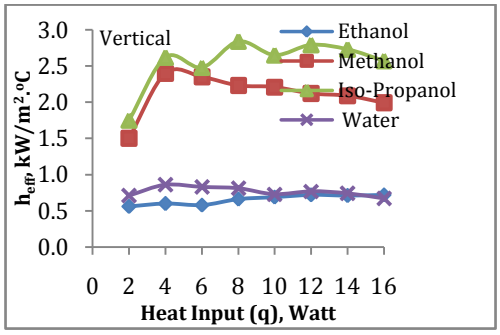

Figure 4.1.18 (c) Eff. convec.coeff. vs.Heat input at TMMHP

In Fig. 4.1.18, the sequential rise of h_{eff} of all four fluids in TMMHP at 45° is shown. Iso-propanol gains the highest value of h_{eff} whereas ethanol gives the lowest.

The h_{eff} is different from h because h_{eff} is based on the average temperature of both evaporator and condenser. Since the surface temperature of the TMMHP is depended on the heat input and heat rejection at the evaporator and condenser respectively, such extreme values of '*h'* become dependent only on the internal fluids' overall thermophysical properties. According to Newton's law of cooling, *h of a system with constant heat input and surface area gets the highest value for the smallest terminal temperature difference within the heat pipe and vice versa.* This correlation can be authenticated by comparing Fig. 4.1.14 and Fig.4.1.17 where methanol achieves the highest value of *h*. Consequently, at a small terminal temperature difference, the sharp decrease of pressure gradient leads to rapid condensation at the condenser port to increase the *h* value. As the vapor becomes liquid at the condenser, the density of the fluid therein goes many folds high. However, the *h* keeps no direct relationship with the density alone which reflects in both Fig. 4.1.17 and Fig.4.1.18. Rather it is found that *h is compositely related with the fluid's density, pressure drop and heat input.* This relationship can be expressed by $h = f(\rho(p(q)))$.

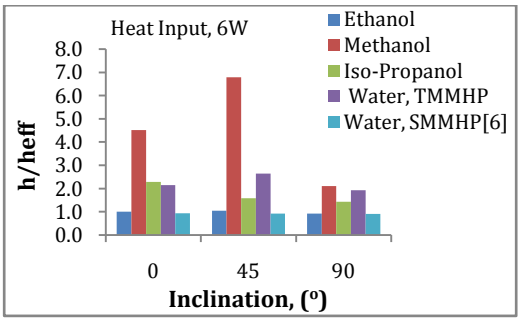

Figure 4.1.19(a) Comparison of h/h_{ef} between TMMHP and SMMHP [6]

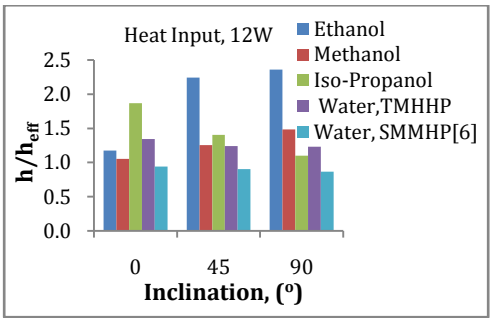

Figure 4.1.19(b) Comparison of h/h_{ef} between TMMHP and SMMHP [6]

In Fig. 4.1.19(a-b), all the fluids' dimensionless heat transfer coefficients are shown including the water's h/h_{eff} at single-metal micro heat pipe. The maximum value of methanol is seen at 45^{o} inclination at lower heat input (i.e.6W) because of its lowest boiling point (66 ^{o}C) which allows it to complete the boiling-condensation cycle faster than the other three liquids. On the other hand, it provides a mixed response at higher heat input (12W). However, the water's h/h_{eff} value at TMMHP is twice as high as that of at SMMHP [6]. Thus, the two different thermal conductivities at the two ports of the

TMMHP initiate the quicker heat removal than that of the SMMHP, hence improves the *h* so greatly.

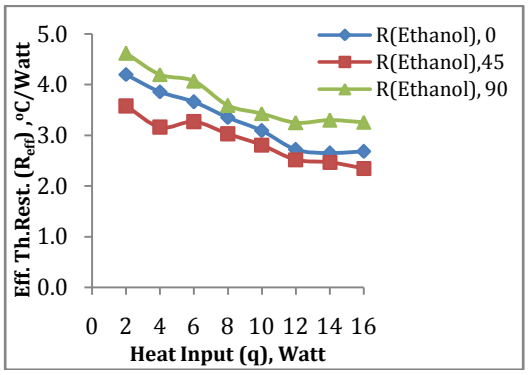

Figure 4.1.20 (a) Eff.Thermal Resistance Vs. Heat Input at TMMHP

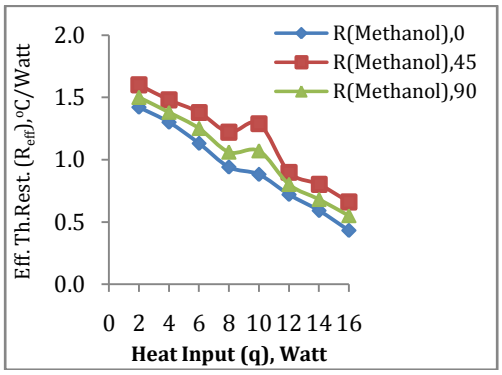

Figure 4.1.20 (b) Eff. Thermal Resistance Vs. Heat Input at TMMHP

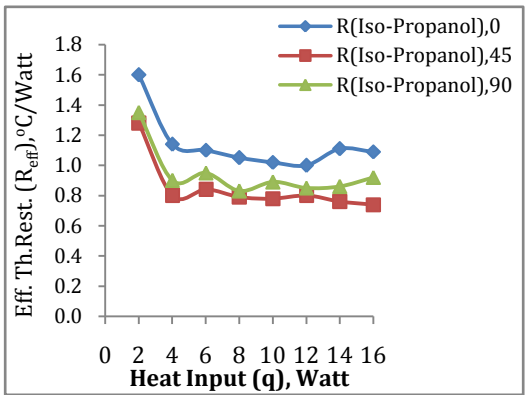

Figure 4.1.20 (c) Eff. Thermal Resistance vs. Heat Input at TMMHP

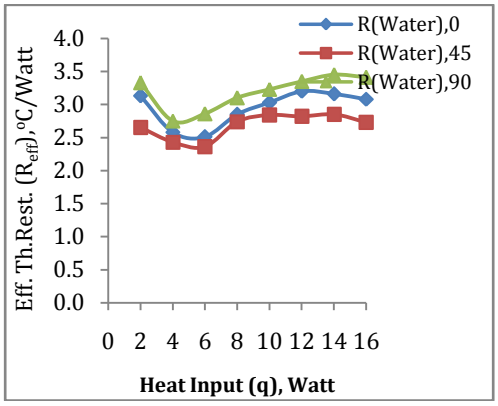

Figure 4.1.20 (d) Eff.Thermal Resistance vs. Heat Input at TMMHP

In Fig.4.1.20 (a-d), effective thermal resistances, R_{eff} are shown for all the working fluids used in the TMMHP. It is obvious that the orientation of the heat pipe plays an important role on maintaining the order of thermal resistance for particular fluid. However, except water three liquids are keeping almost the same lower trend of thermal resistance with the increasing heat input. This difference is occurred because of the two different kinds of fluids where water is covalent compound and other three are hydrocarbons. Having such difference in chemical structure, their thermophysical properties (i.e. density, specific heat etc.) also go different resulting thermal resistances. In all four cases, it is seen that like the heat transfer coefficient, thermal resistance also takes a turn as the heat input is increased to a moderately high value (i.e. 10W). Methanol is found to be of the lowest thermal resistance as 0.43 ^{o} C/Watt as it is in

congruence with the highest value of *h*. A comparison of thermal performance between single-metal (SMMHP) [6] and two-metal micro heat pipe (TMMHP) of same parameters is made in this study which is given in Table 4.1.1.

Table 4.1.1 Comparison of thermal performance between SMMHP [6] and TMMHP for water, circular

Sl. No.	Aspects of Comparison	SMMHP [6]	TMMHP	Remarks
1	Thermal conductivity (k)	Constant	Two different	Rate of heat removal is increased in TMMHP
2	Temp. variation of condensation temperature (water, horizontal)	Small 3.6 ^{o}C	Large 7.0 ^{o}C	Condensation takes place at higher temp. in TMMHP than in SMMHP
3	Overall temp. difference between two ends of MHP (water, horizontal)	41.2 ^{o}C	13.0^{o}C	In TMMHP is much smaller, thus enhances cyclic order and quick heat removal
4	Temp. gradient at condenser for water	Negative	Positive	Positivity at TMMHP improves capillary action
5	Time reqd. to complete cycle (water, horizontal)	2 min	1½ min	Because of thermal vacuum created in TMMHP
6	h/h_{eff} (water, horizontal)	0.93	1.82	*h* is very high at TMMHP
7	*h* (water, horizontal)	0.46 kW/m^2. ^{o}C	1.33 kW/m^2. ^{o}C	At TMMHP *h* reaches enormously high
8	*h* with respect to increasing Q	~Constant	increasing	Mean value of *h* is 3.5 times higher at TMMHP than that of SMMHP

4.2 Study of two-metal (Cu-Ag) micro heat pipe of triangular cross section using different working liquids of low boiling point [29]

Using recorded data in this investigation various curves are plotted as shown from Fig. 4.2.1 to Fig. 4.2.18. Fig.4.2.1 shows time required for reaching steady state temperature for different working fluids. It is found that ethanol takes the least time out of four while the other three delayed approximately the same period of time. Ethanol and iso-propanol are almost entwined in terms of temperature rise as well as attaining steady-state condition – this may occur because of their proximity of boiling points (BP). On the other hand, methanol and water took longer to reach but at a higher

temperature range than the other two. It is observable that although the methanol's boiling is low, still it took the same time period of water. This indicates the earlier boiling and condensation of methanol than other fluids, which becomes erratic within the narrow space of the micro heat pipe. Consequently, methanol takes longer period of time to reach thermal equilibrium thus to attain steady state than that of others. On the other hand, water takes the same time but at a higher temperature than the other three. Therefore, the heat capacity of a fluid not only depends on its thermophysical properties (i.e. density, SG etc.) but also on its chemical bonding (i.e. hydrogen bonding for water).

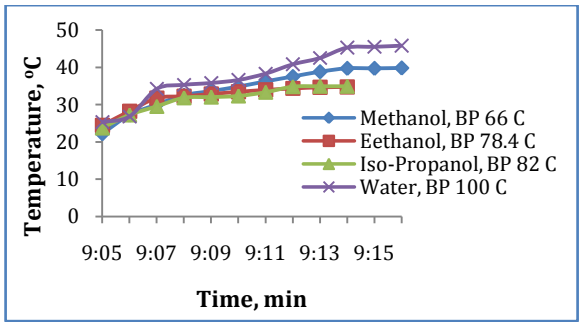

Figure 4.2.1 Time required for reaching steady-state of different fluids

The trends of temperature rises (meter reading minus the ambient, 25^{o}C) at the evaporator section for using different fluids in TMMHP are shown in Fig. 4.2.2. Other than water, all three are nonlinear. This may happen because the three fluids are organic compounds and have similar chemical bonding, and the water as an inorganic compound is made up from hydrogen and oxygen's covalent bond. Again it supports the conception that the heat capacity of a fluid is not simply based on thermophysical property (i.e. density, boiling point, SG etc.) rather mainly on its bonding.

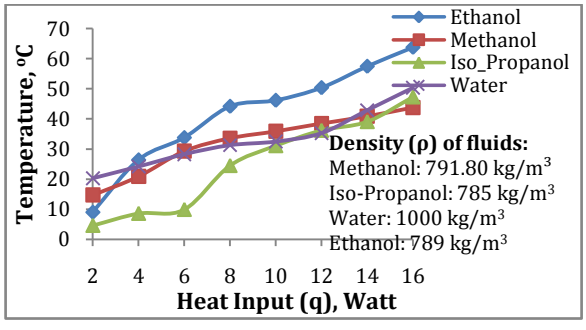

Figure 4.2.2 Rise of fluid temp. vs. heat input at the evaporator

4.2.1 Evaporator of TMMHP as a super heater

Distributions of temperatures along the length of the TMMHP for different working fluids, for different heat inputs, and also for different inclinations are shown from Fig. 4.2.3 (a) to 4.2.10 (b). It is observed from these figures that in each case of fluid used in TMMHP, there is a temperature rise in the evaporator from T_1 to T_2. Annamalai A. S. *et al.* [44] has reasoned that "In the evaporator zone heat is supplied by an electric coil and the coil surface area density is very high in the middle of the evaporator portion and hence the temperature of the vapor in the middle of the evaporator is high". Authors here disagree with Annamalai that there should be no reason to windup the heater coil densely in the middle of the evaporator rather wrapping must be uniformly done so the produced heat flux remains constant throughout the evaporator. Based on this work and the work of Mahmood [6] and Sreenivasa [36], the working fluid should be filled only equal to or less than the empty space (vapor core) of the evaporator of the heat pipe. However, a lot more space in the heat pipe is still vacant to travel during operation. Soon after the MHP goes into operation, boiling starts at the beginning of the heat pipe – part of the fluid evaporates – that leaves a significant room empty within the evaporator which is fully wrapped up by the heater coil. Therefore, when the saturated vapor advances, it continuously receives heat from that part of heater to become superheated, and then it enters the adiabatic section. That's why the temperature rise at point T_2 takes place; hence this end of the evaporator acts as a *super heater*.

Regarding the rise of temperature in the evaporator, a comparison between the fluids in the TMMHP is shown in Fig. 4.2.11 (a-c). At the initial steps, the trend for temperature rise for all the fluids are quite similar; however, they get scattered at moderately higher heat inputs (i.e. 12W). This may happen from the "dry out" situation meaning poor capillary pumping of condensate back to the evaporator that leads uniform heating of evaporator. It becomes obvious that the orientation of the TMMHP plays an important role in superheating quality of the fluids.

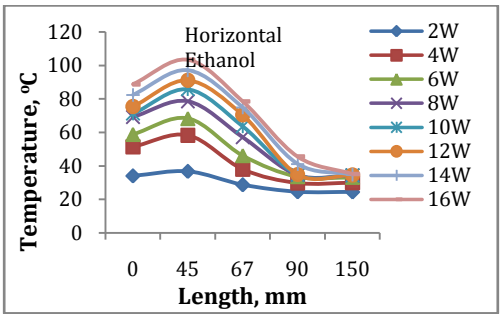

Figure 4.2.3 (a) Fluid temp. distribution along the TMMHP

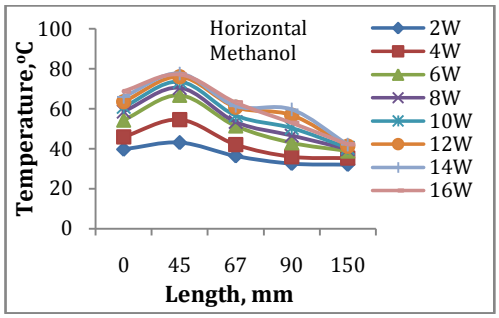

Figure 4.2.3 (b) Fluid temp. distribution along the TMMHP

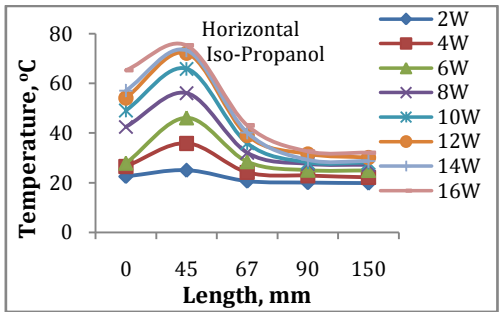

Figure 4.2.3 (c) Fluid temp. distribution along the TMMHP

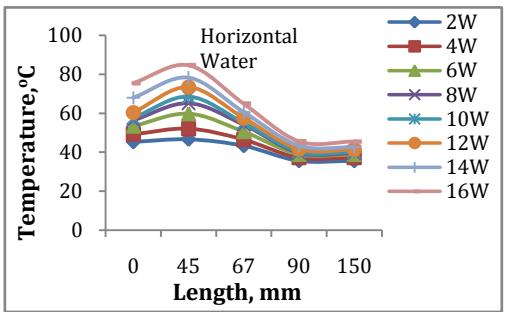

Figure 4.2.3 (d) Fluid temp. distribution along the TMMHP

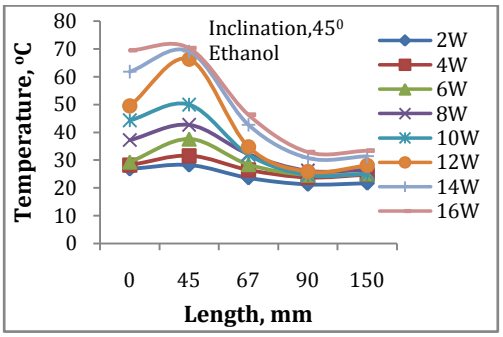

Figure 4.2.4 (a) Fluid temp. distribution along the TMMHP

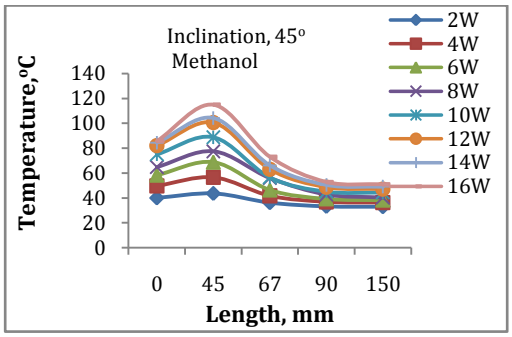

Figure 4.2.4 (b) Fluid temp. distribution along the TMMHP

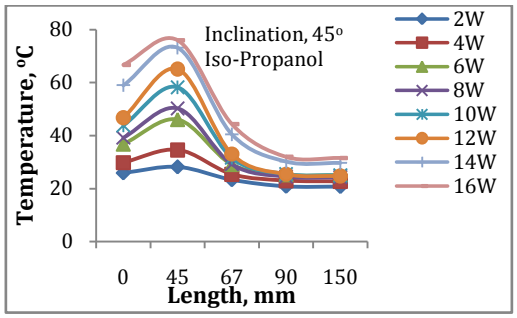

Figure 4.2.4 (c) Fluid temp. distribution along the TMMHP

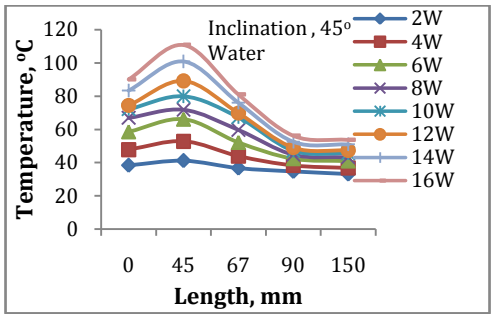

Figure 4.2.4 (d) Fluid temp. distribution along the TMMHP

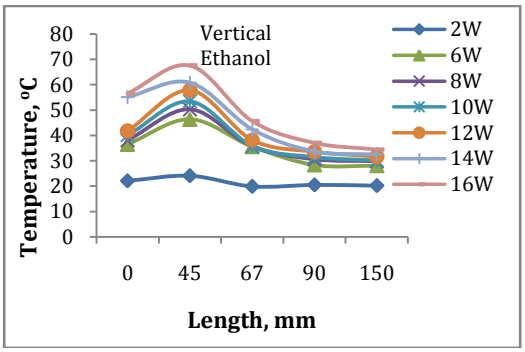

Figure 4.2.5 (a) Fluid temp. distribution along the TMMHP

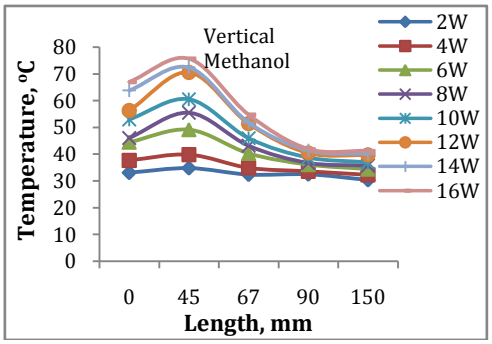

Figure 4.2.5 (b) Fluid temp. distribution along the TMMHP

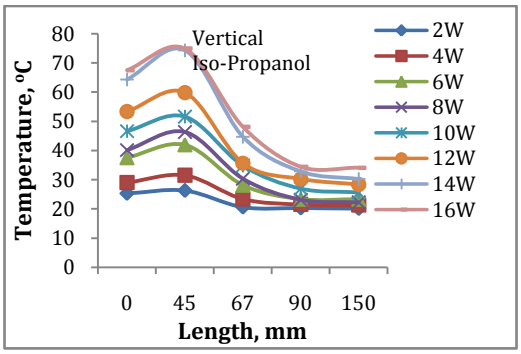

Figure 4.2.5 (c) Fluid temp. distribution along the TMMHP

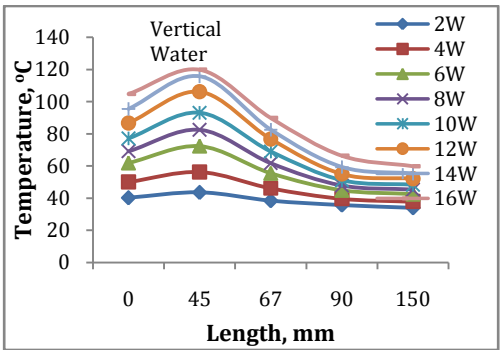

Figure 4.2.5 (d) Fluid temp. distribution along the TMMHP

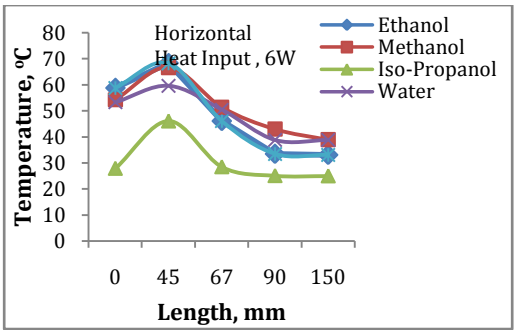

Figure 4.2.6 (a) Temp. distribn. along TMMHP of diff. fluids

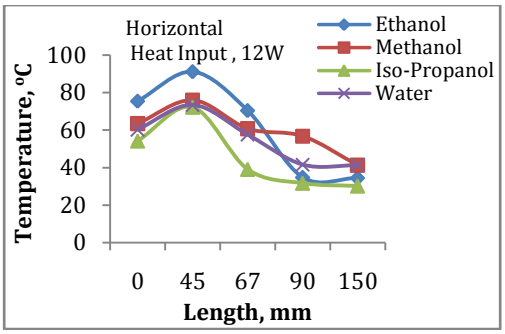

Figure 4.2.6 (b) Temp. distribn. along TMMHP of diff. fluids

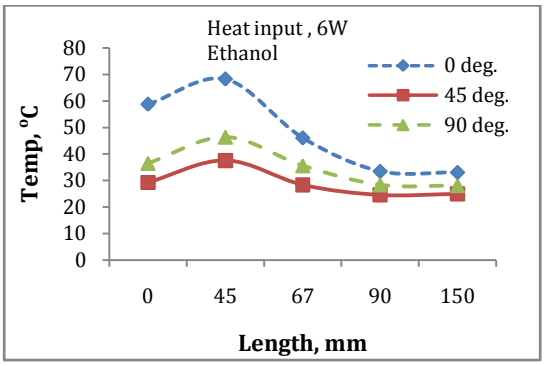

Figure 4.2.7 (a) Temp. distribn. along TMMHP at diff. inclns.

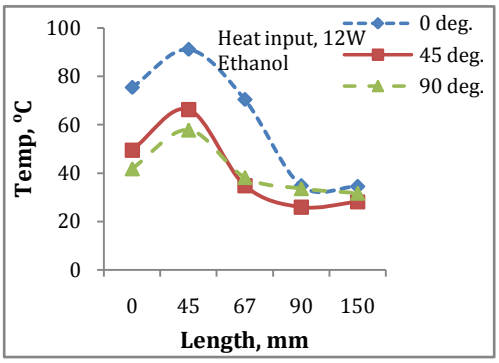

Figure 4.2.7 (b) Temp. distribn. along TMMHP at diff. inclns.

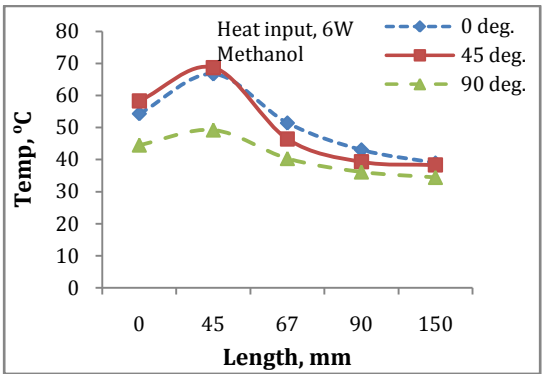

Figure 4.2.8 (a) Temp. distribn. along TMMHP at diff. inclns.

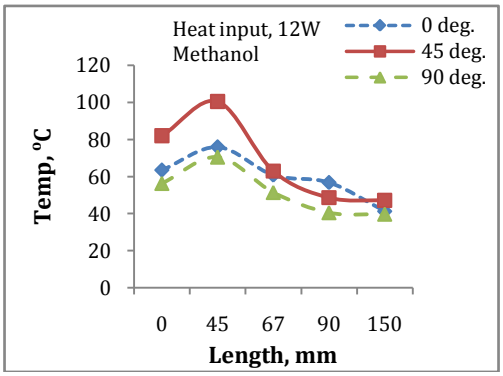

Figure 4.2.8 (b) Temp. distribn. along TMMHP at diff. inclns.

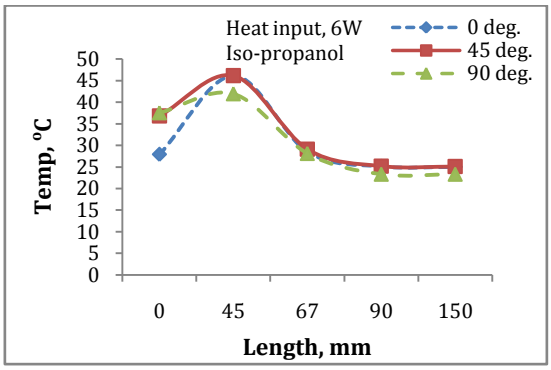

Figure 4.2.9 (a) Temp. distribn. along TMMHP at diff. inclns.

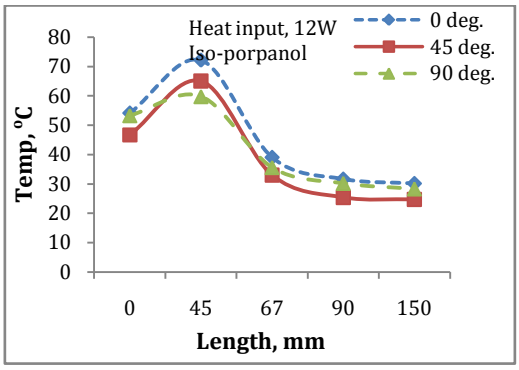

Figure 4.2.9 (b) Temp. distribn. along TMMHP at diff. inclns.

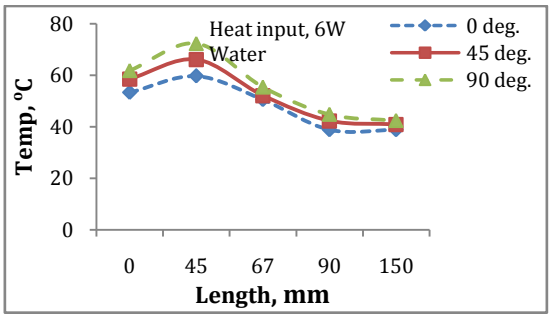

Figure 4.2.10 (a) Temp. distribn. along TMMHP at diff. inclns.

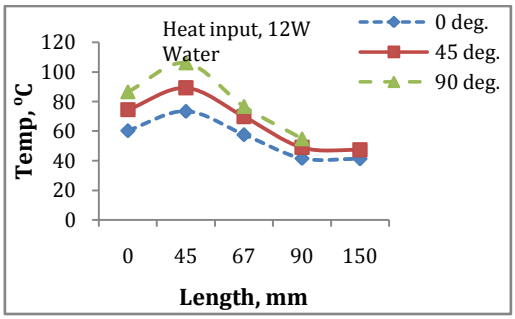

Figure 4.2.10 (b) Temp. distribn. along TMMHP at diff. inclns.

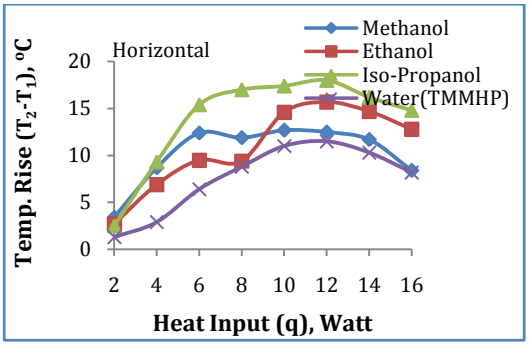

Figure 4.2.11 (a)

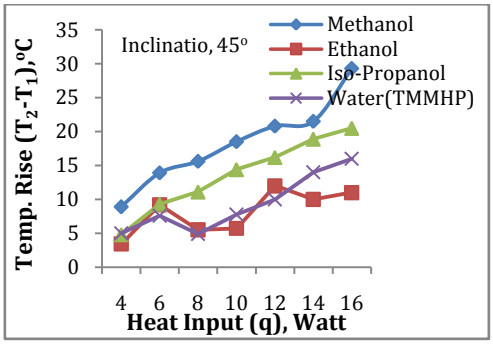

Figure 4.2.11 (b)

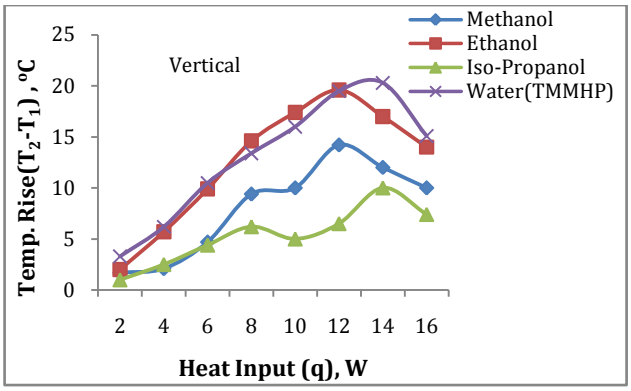

Figure 4.2.11(c)

Figure 4.2.11(a-c) Comparison of temp. rise (T_2-T_1) of diff. fluids in TMMHP at diff. incln s.

In Fig. 4.2.11, the temperature rise in the evaporator is shown which clarifies the importance of heat pipe orientation. Here, no particular fluid is dominating in any particular orientation. The geometry of the heat pipe may be the reason of such inconclusive result. Fig. 4.2.12 indicates that the fluids were condensed within the smallest temperature range at vertical position (90^o). It is noticeable that all the hydrocarbon's condensation temperature ranges are much lower than that of water. This may happen due to the slowest capillary action of water through the wick that takes longer time to travel from the condenser to evaporator.

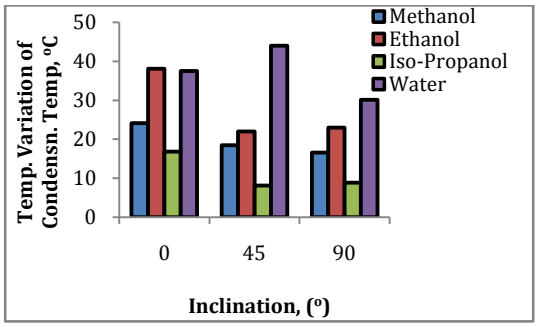

Figure 4.2.12 Temp. variation of condensn. temp. ($T_{4,16W}$ - $T_{4,2W}$) of diff.fluids for diff. heat inputs to TMMHP at diff. incls.

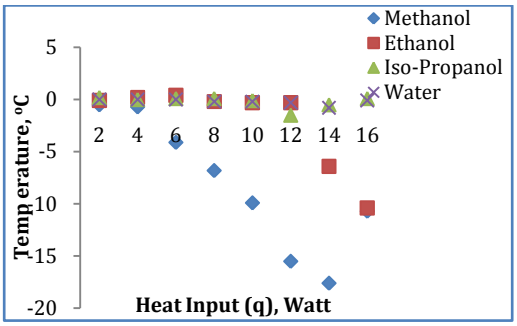

Figure 4.2.13 Comparison of condensn . temp. (T_5-T_4) range of diff. fluids for increasing heat inputs to TMMHP, horizontal

However, in all three inclinations, the values of *h* are maintaining the same sequence and order of magnitude. Capillary action of the water and hydro-carbons are quite different. As a result, the values for *h* of the three hydrocarbons are closely placed while the value of water is far away from them. Thus it is proved again that the heat capacity of a liquid is not only depended on its physical property but also on its chemical property (i.e. structural bonding).

While being condensed, the internal working fluids are experiencing negative temperature gradient within the condenser, but the water is an exception with a positive gradient as shown in Fig.4.2.13. This behavior of water is due to the impact of the saturated liquid at the end of condenser. The advancing water vapor from the adiabatic section towards the condensation port (T_4) creates high pressure on the saturated liquid constantly that accelerates the liquid particles of heavy momentum to hit the condenser port of the heat pipe. During this impact, the inherent kinetic energy of the liquid is converted to heat, hence the temperature of the liquid increases. At the turning point, such a temperature increase of the liquid benefits the capillary action of the wick to drive back condensate even faster to the evaporator.

The efficiency of MHP is evident by its heat transfer capability at a low temperature difference. A comparison of such terminal temperature difference among the fluids in the TMMHP is shown in Fig. 4.2.14. As it is seen, the lowest temperature difference is exhibited by methanol, and it may be possible because of its lowest boiling point.

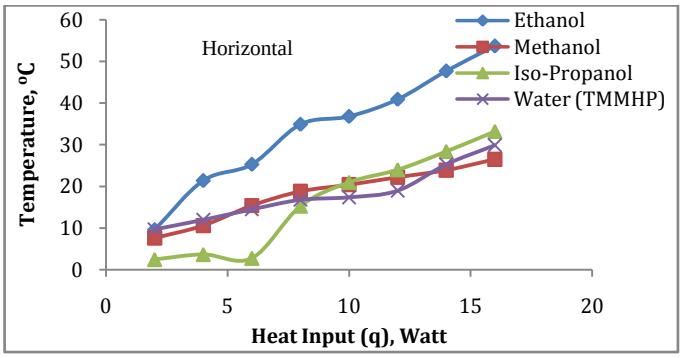

Figure 4.2.14 Comparison of terminal temp. diffs. (T_1 -T_5) in TMMHP

4.2.2 Comparison of *h* among four fluids in TMMHP

Fig. 4.2.15 (a), (b) and (c) show the values of heat transfer coefficient of different fluids at horizontal, inclination of 45^o and vertical positions. Except at horizontal position, ethanol possesses the highest '*h*' (3.3 kW/m^2.^{o}C) among all the fluids, and the highest value is attained at vertical position. Thus in respect to *h*, ethanol is the most valuable working fluid out of the four for triangular TMMHP. Since the surface temperature of the TMMHP is depended on the heat input and heat rejection at the evaporator and condenser respectively, such high values of '*h*' become dependent only on overall thermophysical properties of the internal fluid. In Fig.4.2.17, the sequential rises of *h* of all four fluids in TMMHP at different angles are shown. Except at horizontal, ethanol gains the highest value of *h* whereas water gains the lowest. According to Newton's law of cooling, *h of a system with constant heat input and surface area gets the highest value for the smallest terminal temperature difference within the heat pipe and vice versa.* This correlation can be authenticated by comparing Fig. 4.2.14 and Fig. 4.2.15(a) where water in TMMHP achieves the highest value of *h* although erroneously shown for iso-popanol. As a result, at a small terminal temperature difference, the sharp decrease of pressure gradient leads to rapid condensation at the condenser port to increase the *h* value. The calculated h_{eff} values of all the fluids, based on the average temperature of the evaporator and condenser, for different inclinations are shown in Fig. 4.2.16. It shows almost the same trend of *h* values of four fluids in Fig. 4.2.15. This similarity becomes possible for the well

managed heat input to the evaporator and heat rejection through the condenser section as well.

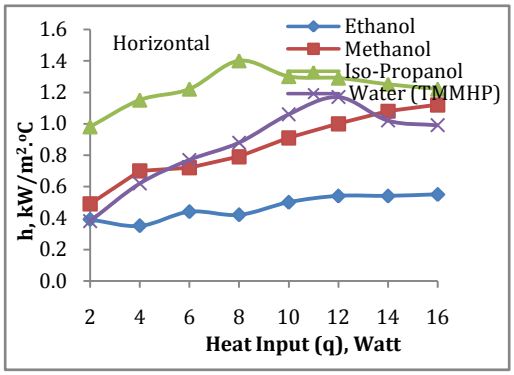

Figure 4.2.15 (a) Convec. coeff vs. Heat input atTMMHP

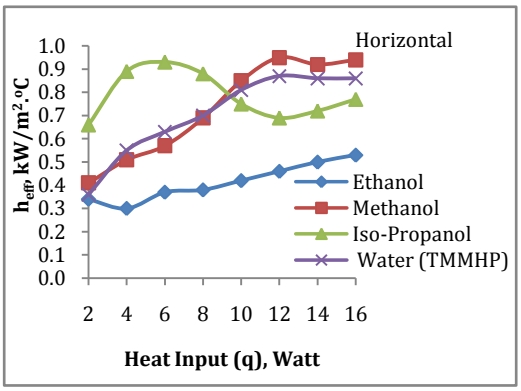

Figure 4.2.16 (a) Eff. convec.coeff. vs.Heat input at TMMHP

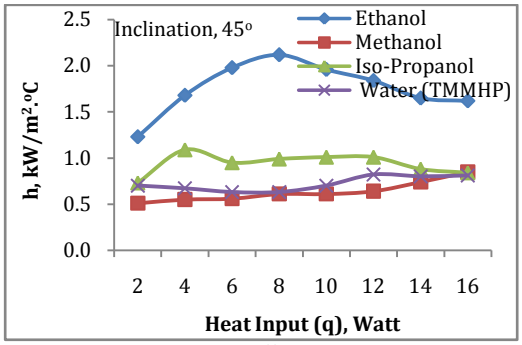

Figure 4.2.15(b) Convec. coeff. vs. Heat input at TMMHP

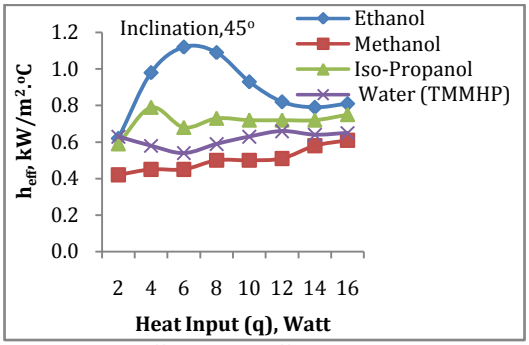

Figure 4.2.16 (b) Eff. convec. coeff. vs. Heat input at TMMHP

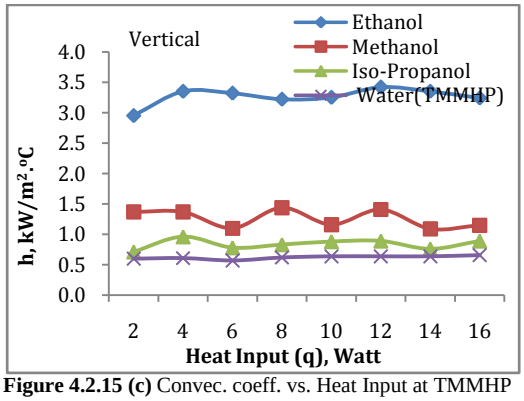

Figure 4.2.15 (c) Convec. coeff. vs. Heat Input at TMMHP

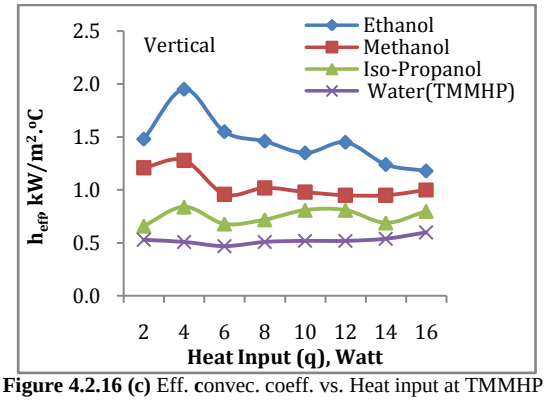

Figure 4.2.16 (c) Eff. convec. coeff. vs. Heat input at TMMHP

However, the discrepancies between the two results may arise from the adiabatic section which may not be fully thermo-proof. Density is a thermophysical property of a fluid. Therefore, when the vapor becomes liquid at the condenser; the density of the fluid therein goes many folds high. However, the *h* keeps no direct relationship with the density alone which reflects in both Fig. 4.2.15 and Fig. 4.2.16. Rather it is found that *h*

is compositely related with the fluid's density, pressure drop and heat input. This relationship can be expressed by $h = f(\rho(p(q)))$. In Fig. 4.2.17(a-b), all the fluids' dimensionless heat transfer coefficients are shown. The maximum value of dimensionless *h* for ethanol is seen at vertical position at 12W, which is quite in match with its *h* value (Fig.4.2.15 c).

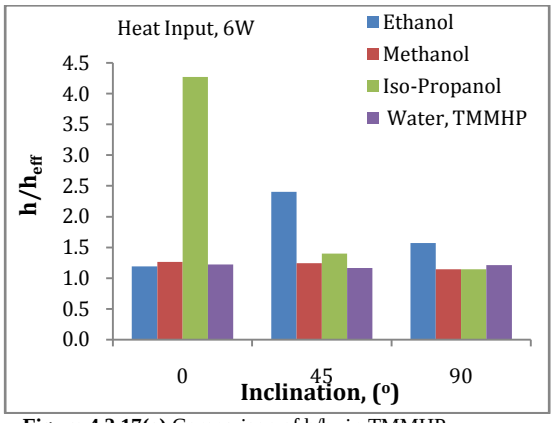

Figure 4.2.17(a) Comparison of h/h_{ef} in TMMHP

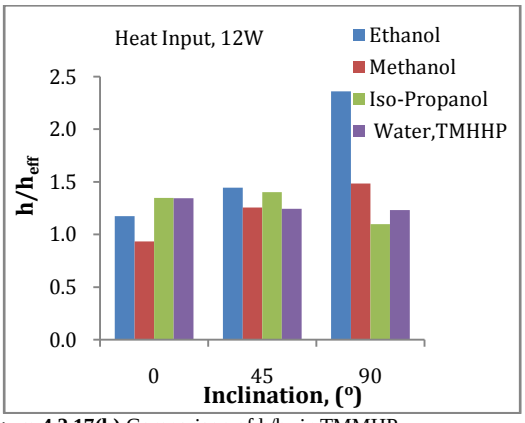

Figure 4.2.17(b) Comparison of h/h_{ef} in TMMHP

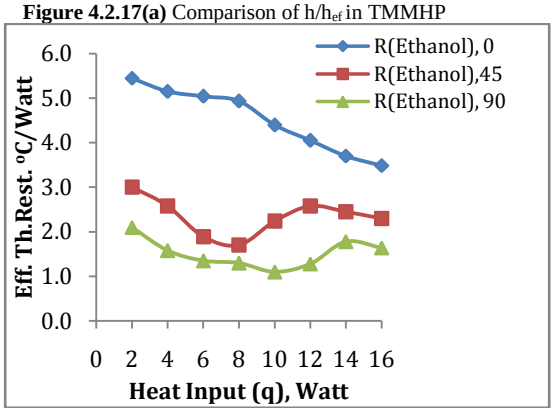

Figure 4.2.18 (a) Eff.Thermal Resistance vs. Heat Input at TMMHP

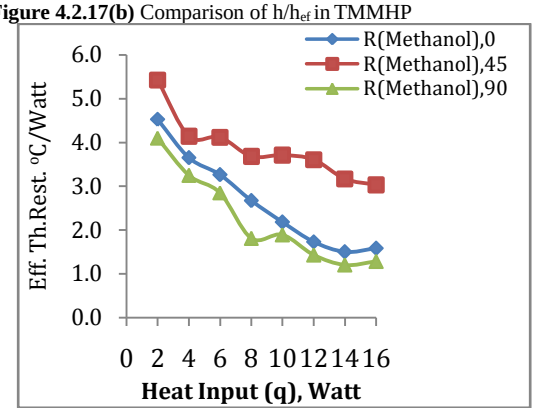

Figure 4.2.18 (b) Eff.Thermal Resistance vs. Heat Input at TMMHP

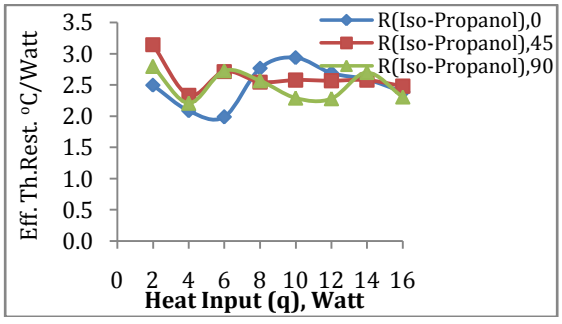

Figure 4.2.18 (c) Eff.Thermal Resistance vs. Heat Input at TMMHP

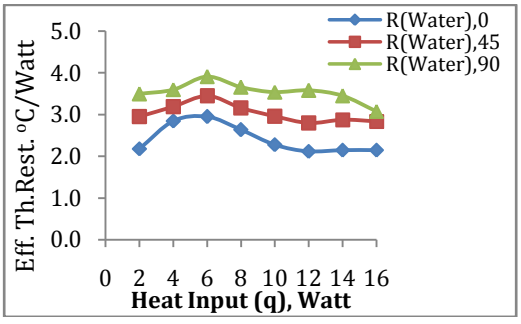

Figure 4.2.18 (d) Eff.Thermal Resistance vs. HeatIinput at TMMHP

Fig. 4.2.18 (a-d) shows the effective thermal resistance, R_{eff} , of all four fluids. It shows that methanol possess the highest resistance while ethanol does the lowest. Although, ethanol experiences very high resistance at horizontal position at lower heat inputs, but at 45^{o} and vertical positions show the lowest out of all four. However, on average effective thermal resistance, water provides the highest resistance comparing with others which also occurred at the previous experiment on triangular cross section. Thus, it is proved again that the thermal behavior of covalent compound and hydrocarbons cannot be estimated from the thermophysical properties alone.

4.3 Study of two-metal (Cu-Ag) micro heat pipe of square cross section using different working liquids of low boiling point [30]

Using collected data in this investigation various curves are plotted as shown from Fig. 4.3.1 to Fig. 4.3.18. Fig.4.3.1 shows time required for reaching steady state temperature for different working fluids. It is found that ethanol takes the least time out of four while the other three takes approximately the same period of time. Ethanol and iso-propanol advances parallel in terms of temperature rise as well as attaining steady-state condition – this may occur because of their proximity of boiling points. On the other hand, methanol and water took longer to reach but at a higher temperature range than the other two. It is observable that although the methanol's boiling point is low, still it takes the same time period of water. This indicates the earlier boiling and condensation of methanol than other fluids, which becomes chaotic within the narrow space of the micro heat pipe. Consequently, methanol takes longer time to reach thermal equilibrium thus to attend steady state than that of others. On the other hand, water takes the same time but at a higher temperature than the other three. Therefore, the heat capacity of a fluid not only depends on its thermophysical properties (i.e. density, SG etc.) but also on its chemical bonding (i.e. hydrogen bonding for water).

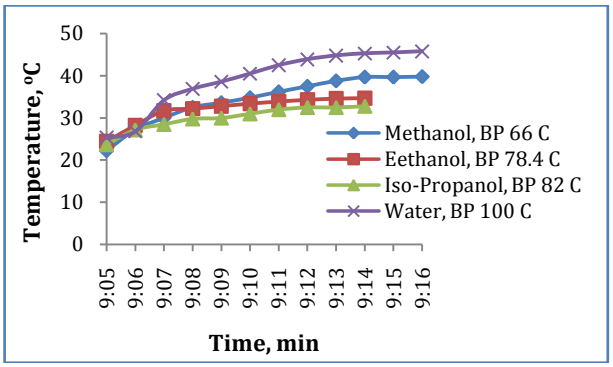

Figure 4.3.1 Time required for reaching steady-state of different fluids

The trends of temperature rises (meter reading minus the ambient, 25^{o}C) at the evaporator section for using different fluids in TMMHP are shown in Fig. 4.3.2. Other than water, all three are nonlinear. This may happen because the three are organic compounds and have similar chemical bonding, and the water as an inorganic compound is made up from hydrogen and oxygen's covalent bond. Again it supports the conception that the heat capacity of a fluid is not simply based on thermophysical property (i.e. density, boiling point, SG etc.) rather mainly on its bonding.

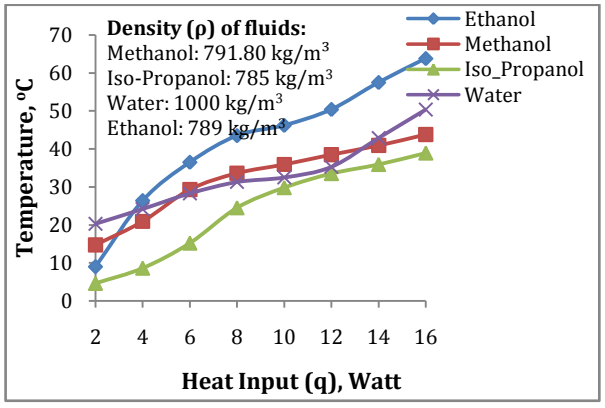

Figure 4.3.2 Rise of fluid temp. vs. heat input at the evaporator

4.3.1 Evaporator of TMMHP as a super heater

Distributions of temperatures along the length of the TMMHP for different working fluids, for different heat inputs, and also for different inclinations are shown from Fig. 4.3.3 (a) to 4.3.10 (b). It is observed from these figures that in each case of fluid used in TMMHP, there is a temperature rise in the evaporator from T_1 to T_2.

Annamalai A. S. et al. [44] has reasoned that "In the evaporator zone heat is supplied by an electric coil and the coil surface area density is very high in the middle of the evaporator portion and hence the temperature of the vapor in the middle of the evaporator is high". Authors here disagree with Annamalai that there should be no reason to windup the heater coil densely in the middle of the evaporator rather wrapping must be uniformly done so the produced heat flux remains constant throughout the evaporator. Based on this work and the work of Mahmood [6] and Sreenivasa [36], the working fluid should be filled only equal to or less than the empty space (vapor core) of the evaporator of the heat pipe. However, a lot more space in the heat pipe is still vacant to travel during operation. Soon after the MHP goes on operation, boiling starts at the beginning of the heat pipe – part of the fluid evaporates – that leaves a significant room empty within the evaporator which is fully wrapped up by the heater coil. Therefore, when the saturated vapor advances, it continuously receives heat from that part of heater to become superheated, and then it enters the adiabatic section. That's why we notice the temperature rise at point $T_{2,}$ hence this end of the evaporator acts as a *super heater*.

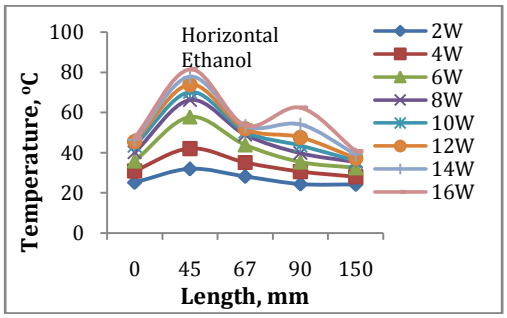

Figure 4.3.3 (a) Fluid temp. distribution along the TMMHP

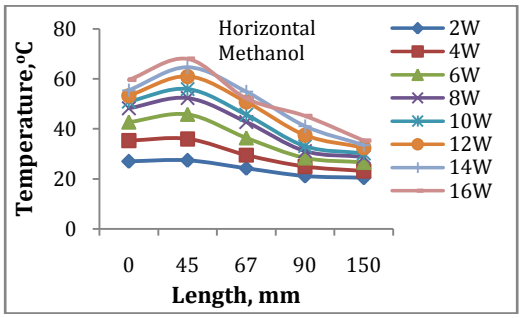

Figure 4.3.3 (b) Fluid temp. distribution along the TMMHP

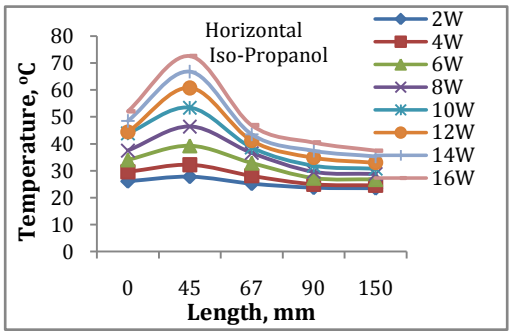

Figure 4.3.3(c) Fluid temp. distribution along the TMMHP

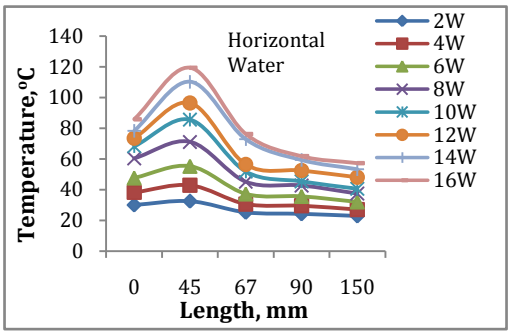

Figure 4.3.3 (d) Fluid temp. distribution along the TMMHP

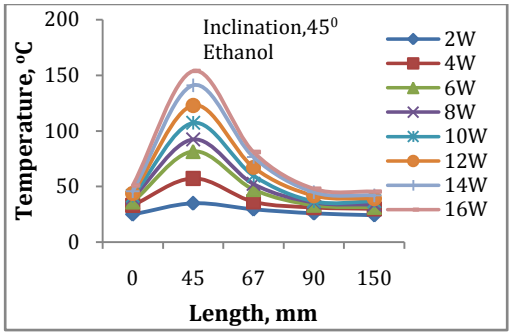

Figure 4.3.4 (a) Fluid temp. distribution along the TMMHP

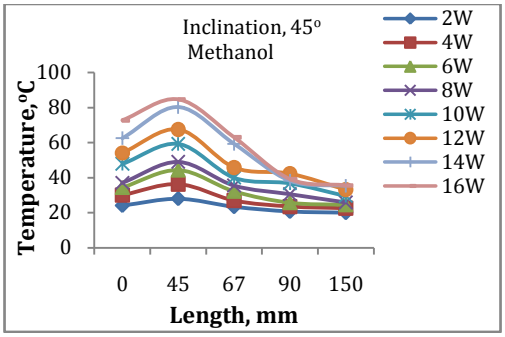

Figure 4.3.4 (b) Fluid temp. distribution along the TMMHP

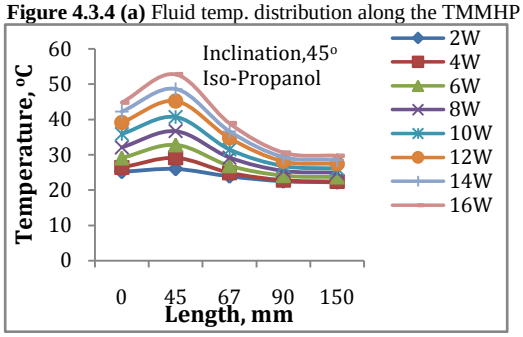

Figure 4.3.4 (c) Fluid temp. distribution along the TMMHP

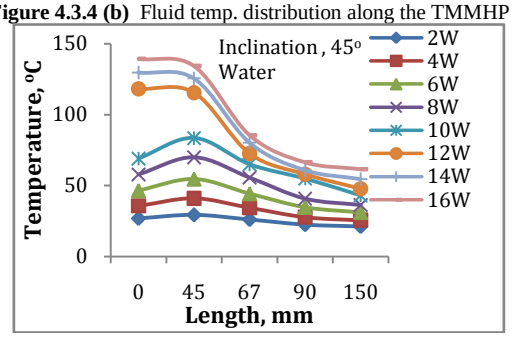

Figure 4.3.4 (d) Fluid temp. distribution along the TMMHP

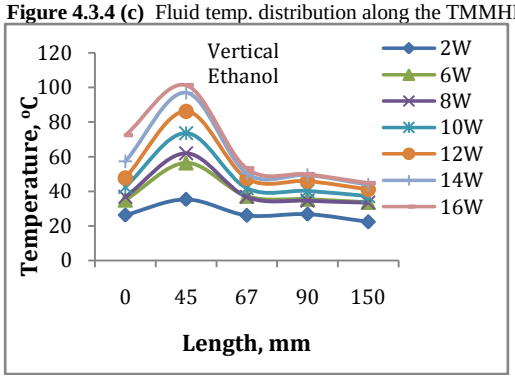

Figure 4.3.5 (a) Fluid temp. distribution along the TMMHP

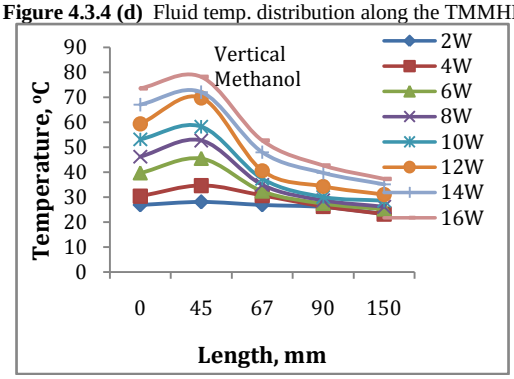

Figure 4.3.5 (b) Fluid temp. distribution along the TMMHP

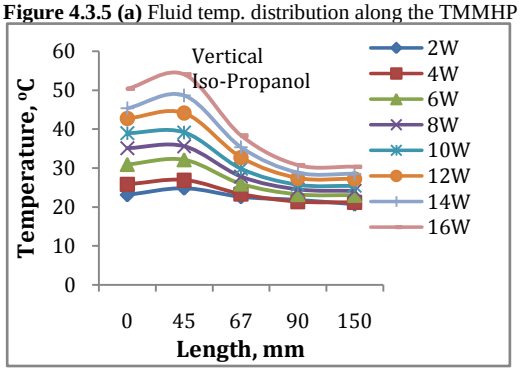

Figure 4.3.5 (c) Fluid temp. distribution along the TMMHP

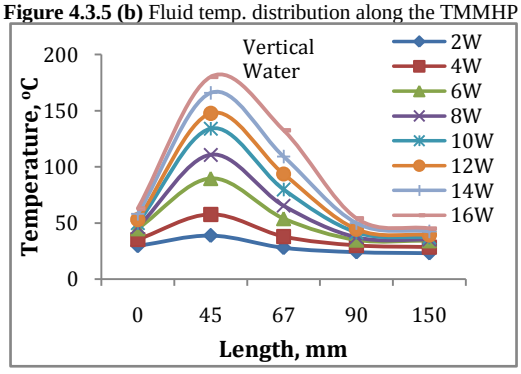

Figure 4.3.5 (d) Fluid temp. distribution along the TMMHP

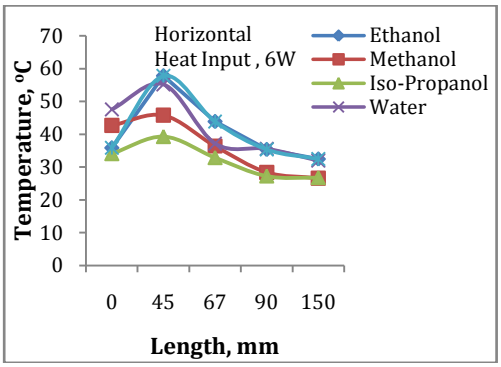

Figure 4.3.6(a) Temp. distribn. along TMMHP of diff. fluids

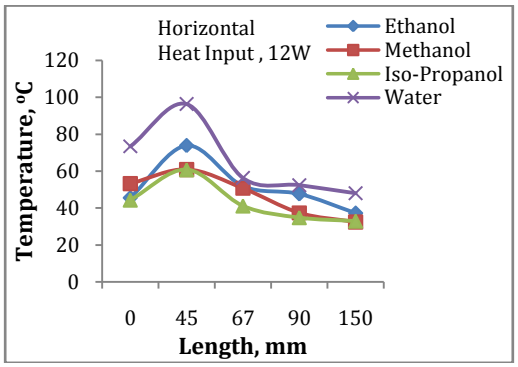

Figure 4.3.6 (b) Temp. distribn. along TMMHP of diff. fluids

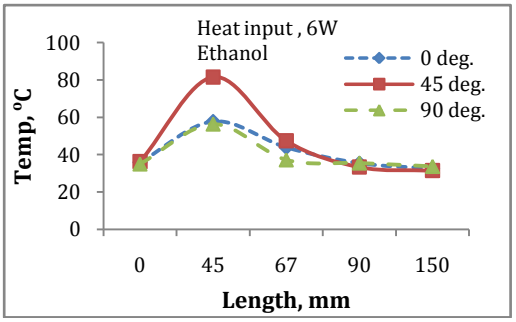

Figure 4.3.7 (a) Temp. distribn. along TMMHP at diff. inclns.

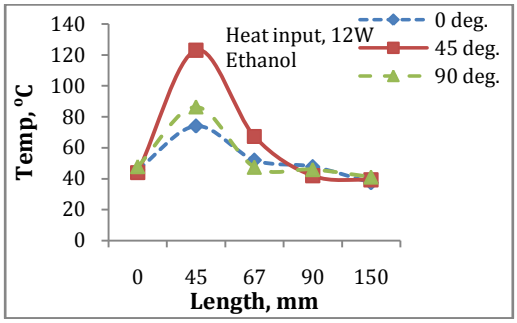

Figure 4.3.7 (b) Temp. distribn. along TMMHP at diff. inclns.

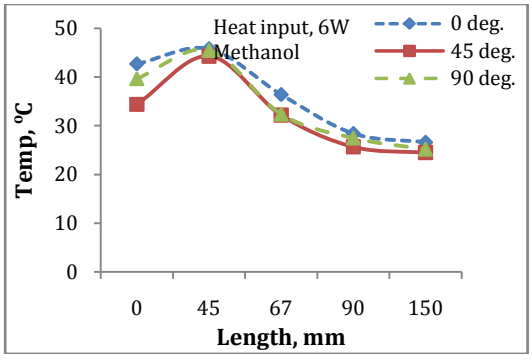

Figure 4.3.8 (a) Temp. distribn. along TMMHP at diff. inclns.

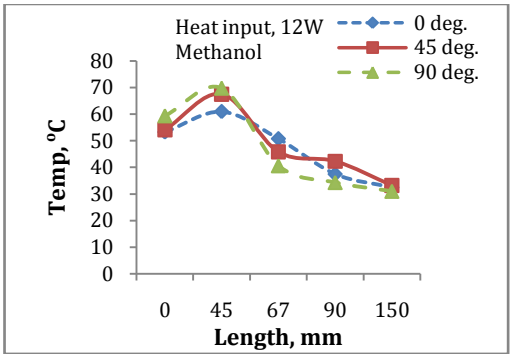

Figure 4.3.8 (b) Temp. distribn. along TMMHP at diff. inclns.

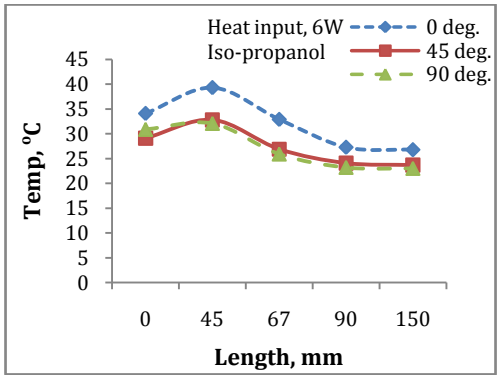

Figure 4.3.9 (a) Temp. distribn. along TMMHP at diff. inclns.

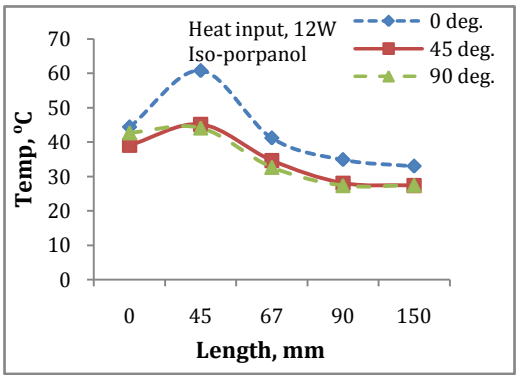

Figure 4.3.9 (b) Temp. distribn. along TMMHP at diff. inclns.

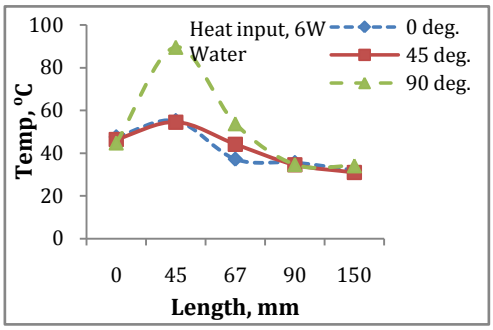

Figure 4.3.10 (a) Temp. distribn. along TMMHP at diff. inclns.

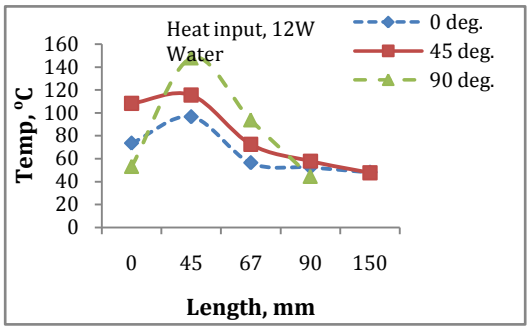

Figure 4.3.10 (b) Temp. distribn. along TMMHP at diff. inclns.

Regarding the rise of temperature in the evaporator, a comparative relationship among the fluids in the TMMHP is shown in Fig. 4.3.11 (a-c). The trend for temperature rise for all the hydrocarbons is quite similar all along the heat pipe. It becomes obvious that the orientation of the TMMHP plays an important role in superheating quality of the fluids.

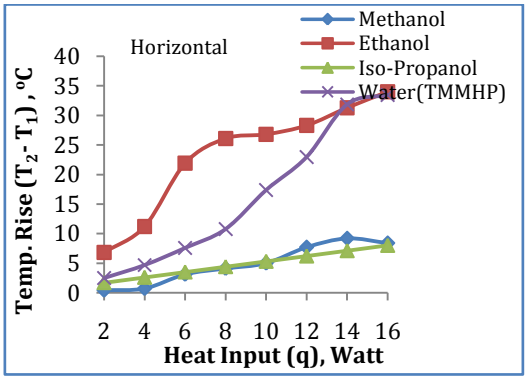

Figure 4.3.11 (a)

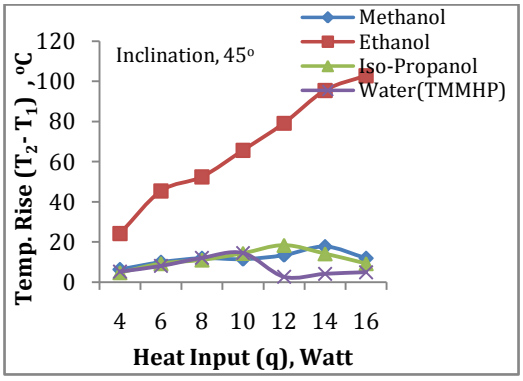

Figure 4.3.11 (b)

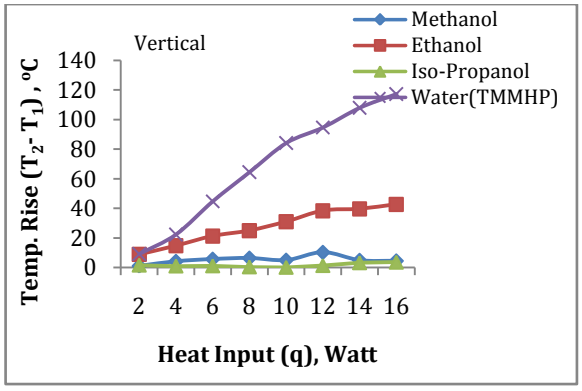

Figure 4.3.11(c)

Figure 4.3.11 (a-c). Comparison of temp. rise (T_2-T_1) in TMMHP between diff. fluids at diff. inclinations

Fig.4.3.12 indicates that water is condensed within the highest temperature band because of the highest specific heat (C_p) while the iso-propanol becomes the lowest. However, the sequence of the condensation of the fluids remains the same in all three different inclinations.

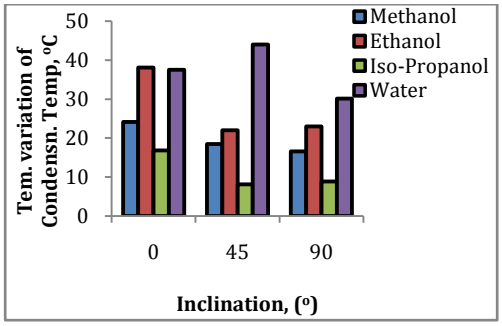

Figure 4.3.12 Temp. variation of condensn. temp. ($T_{4,16W}$ - $T_{4,2W}$) of diff.fluids for diff. heat inputs applied to TMMHP at diff.inclins.

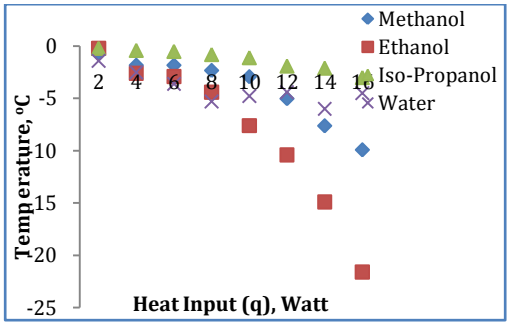

Figure 4.3.13. Comparison of condensn . temp. (T_5-T_4) range of diff. fluids for increasing heat inputs to TMMHP, horizontal

At vertical position, the values are significantly low because of possible "dry out" situation. Capillary action of the water and hydro-carbons are quite different. As a result, the values of the three hydrocarbons are closely placed while the value of water is higher from them. Thus it is proved again that the heat capacity of a liquid not only depends on its physical property but also on its chemical property (i.e. structural bonding). While being condensed, the internal working fluids were experiencing negative temperature gradient within the condenser as shown in Fig. 4.3.13. It is noticeable that the sequence of negativity of the fluids within the condenser is just the opposite of that in the evaporator (Fig. 4.3.11).

The efficiency of MHP is highlighted by its heat transfer capability at a lower temperature difference. A comparison of the temperature difference in the TMMHP is shown in Fig. 5.3.14. It is seen that the terminal temperature difference of ethanol is the lowest at here in TMMHP. Since all other test parameters remain the same as the previous experiment (i.e. triangular), then only the dissimilar parameter of square geometry may be the reason for it.

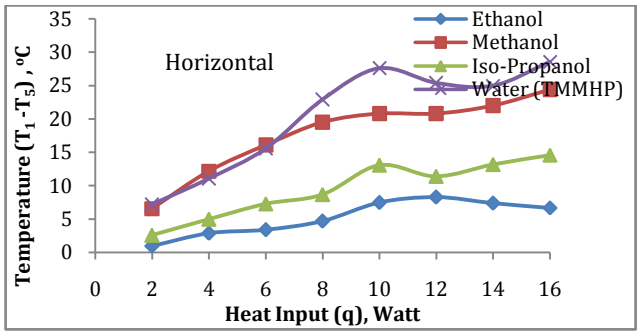

Figure 4.3.14 Comparison of terminal temp. diffs. (T_1 -T_5) in TMMHP

4.3.2 Comparison of *h* among four fluids in TMMHP

Fig. 4.3.15 (a), (b) and (c) show the values of heat transfer coefficient of different fluids at horizontal, inclination of 45^o and vertical positions. Ethanol gives the highest '*h'* (2.7 kW/m^2.^{o}C) among all the fluids, and the highest value is attained at horizontal position. Thus in respect to *h*, ethanol is the most useful working fluid out of the four for square TMMHP. Since the surface temperature of the TMMHP is depended on the heat input and heat rejection at the evaporator and condenser respectively, such high values of '*h'* become dependent only on the internal fluids' overall thermophysical properties. Ethanol gains the highest value of '*h'* whereas water gives the lowest. According to Newton's law of cooling, *h of a system with constant heat input and surface area gets the highest value for the smallest terminal temperature difference within the heat pipe and vice versa.* This correlation can be authenticated by comparing Fig. 4.3.14 and Fig. 4.3.16 where ethanol in TMMHP achieves the highest value of *h*. Consequently, at a small terminal temperature difference, the sharp decrease of pressure gradient leads to rapid condensation at the condenser port to increase the *h* value. The calculated h_{eff} values of all the fluids, based on the average temperature of the evaporator and condenser, for different inclinations are shown in Fig. 4.3.16 (a-c). Effective heat transfer coefficients are different from the overall ones in case of all fluids. As it is noticed, in all three orientations, iso-propanol shows the highest h_{eff}. However, the discrepancies between the two results may arise from the adiabatic section which may not be fully thermo-proof. Density is a thermophysical property of a fluid. Therefore, when the vapor becomes liquid at the condenser; the density of the

fluid therein goes many folds high. However, the *h* keeps no direct relationship with the density alone which reflects in both Fig. 4.3.15 and Fig. 4.3.16.

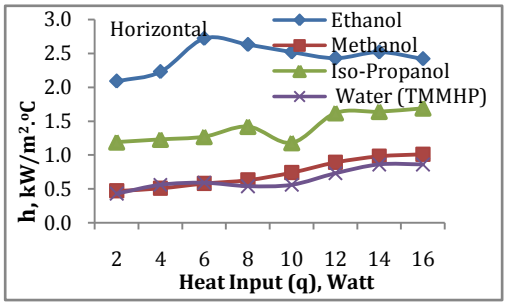

Figure 4.3.15 (a) Convec. coeff. vs. Heat input at TMMHP

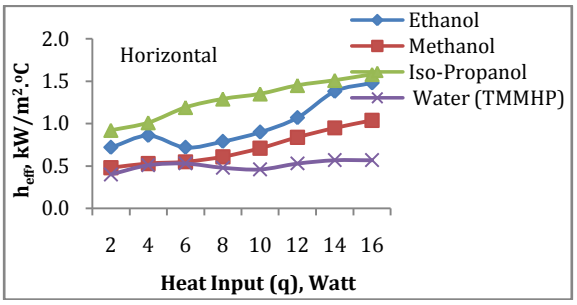

Figure 4.3.16 (a) Eff. convec.coeff. vs.Heat input at TMMHP

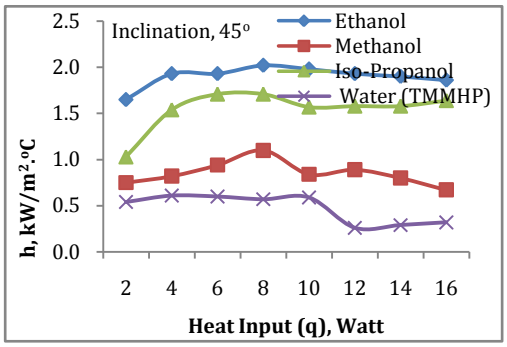

Figure 4.3.15 (b) Convec. coeff. vs. Heat input at TMMHP

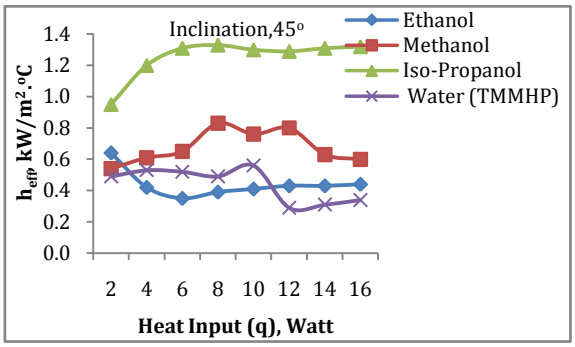

Figure 4.3.16 (b) Eff. convec. coeff. vs. Heat input at TMMHP

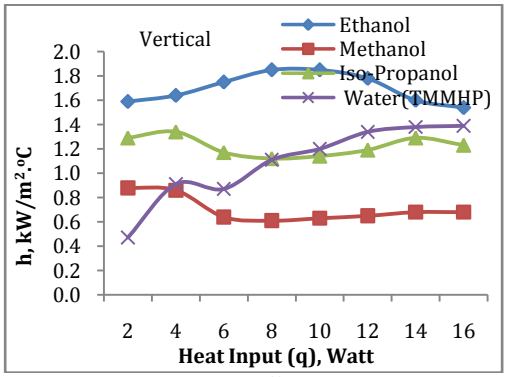

Figure 4.3.15 (c) Convec. coeff. vs. Heat input at TMMHP

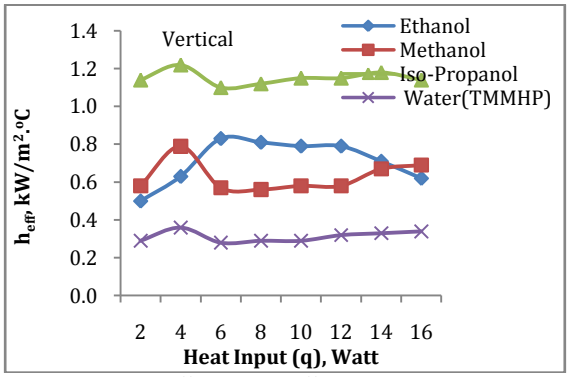

Figure 4.3.16 (c) Eff. convec. coeff. vs. Heat input at TMMHP

Rather it is found that *h is compositely related with the fluid's density, pressure drop and heat input.* This relationship can be expressed by $h = f(\rho(p(q)))$. In Fig. 4.3.17(a-b), all the fluids' dimensionless heat transfer coefficients, h/h_{eff}, are shown. The maximum value of ethanol is seen both at vertical position which is quite in match with its *h* value (Fig. 4.3.15c).

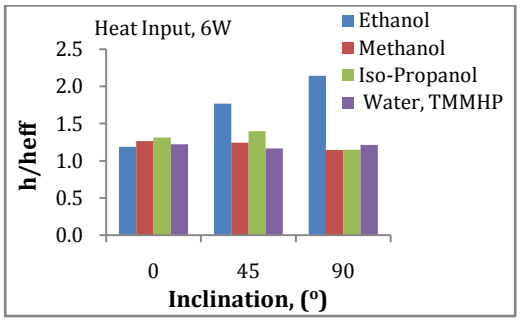

Figure 4.3.17(a) Comparison of h/h_{ef} in TMMHP

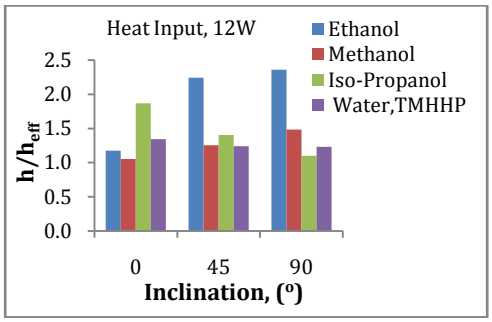

Figure 4.3.17(b) Comparison of h/h_{ef} in TMMHP

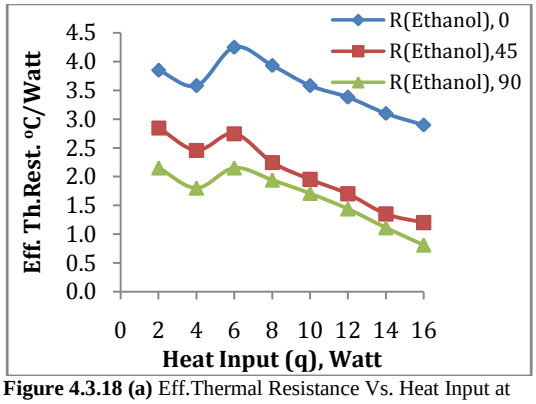

Figure 4.3.18 (a) Eff.Thermal Resistance Vs. Heat Input at TMMHP

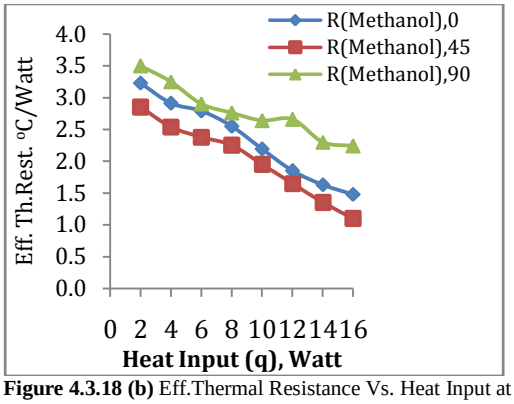

Figure 4.3.18 (b) Eff.Thermal Resistance Vs. Heat Input at TMMHP

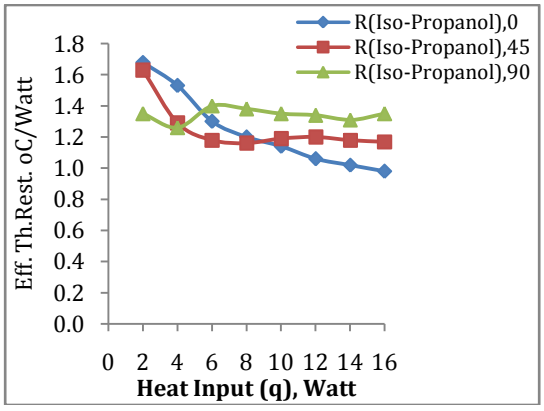

Figure 4.3.18 (c) Eff.Thermal Resistance Vs. Heat Input at TMMHP

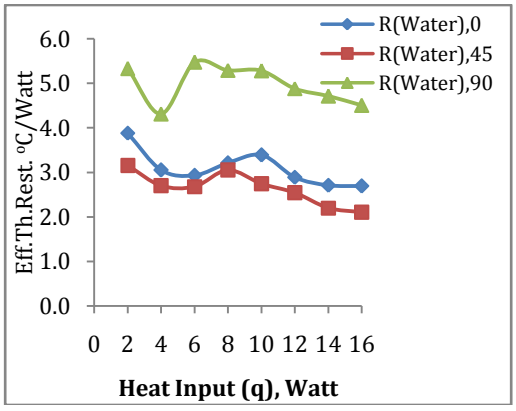

Figure 4.3.18 (d) Eff. Thermal Resistance Vs. Heat Input at TMMHP

Effective thermal resistance, R_{eff}, for four fluids in TMMHPs are shown in Fig. 4.3.18(a-d). R_{eff} for iso-propanol is bit lower than that of ethanol; because R_{eff} is calculated based on the average temperature of both evaporator and condenser. Although this is may be contradictory; but the values of h_{eff} shown in Fig. 4.3.16 (a-c) where iso-propanol keeps the highest value is in good matching with the values shown in Fig. 4.3.18 (c). However, the highest thermal resistance is shown by the water in all three inclinations. Again, the heat transfer behavior between organic and inorganic

compounds cannot be estimated only from their thermophysical properties; the chemical bonding energy also plays an important role.

4.4 Study of two-metal (Cu-Ag) micro heat pipe of convergent-divergent cross section using different working liquids of low boiling point

Using collected data in this investigation various curves are plotted as shown from Fig. 4.4.1 to Fig. 4.4.18. Fig. 4.4.1 shows time required for reaching steady state temperature for different working fluids. It is found that ethanol takes the least time out of four while the other three takes approximately the same belated period of time. Methanol and iso-propanol are almost overlapped in terms of temperature rise as well as attaining steady-state condition – this may occur because of their proximity of boiling points (BP). On the other hand, water took longer to reach the BP but at a higher temperature range than the other three. It is observed that although the methanol's boiling point is low, still it took the same time period of iso-propanol. This indicates the earlier boiling and condensation of methanol and iso-propanol than other two, which becomes chaotic within the narrow space of the micro heat pipe. Consequently, methanol takes longer period of time to reach thermal equilibrium thus to attend steady state than that of other two hydrocarbons. However, water takes the same time but at a higher temperature than the other three because of water's higher latent heat. Therefore, the heat capacity of a fluid not only depends on its thermophysical properties (i.e. density, SG etc.) but also on its chemical bonding (i.e. hydrogen bonding for water).

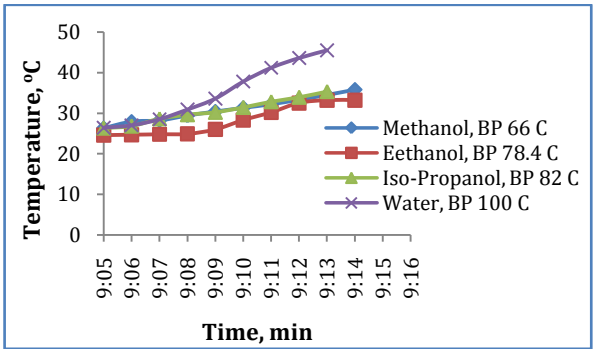

Figure 4.4.1 Time required for reaching steady-state of different fluids

The trends of temperature rises (meter reading minus the ambient, 25^{o}C) at the evaporator section for using different fluids in TMMHP are shown in Fig. 4.4.2. Other than water, all three are nonlinear. This may happen because the three are organic compounds and have similar chemical bonding, and the water as an inorganic compound is made up from hydrogen and oxygen's covalent bond. Again it supports the conception that the heat capacity of a fluid is not simply based on thermophysical property (i.e. density, boiling point, SG etc.) rather mainly on its bonding.

4.4.1 Evaporator of TMMHP as a super heater

Distributions of temperatures along the length of the TMMHP for different working fluids, for different heat inputs, and also for different inclinations are shown from Fig. 4.4.3 (a) to 4.4.10 (b). It is observed from these figures that in each case of fluid used in TMMHP,

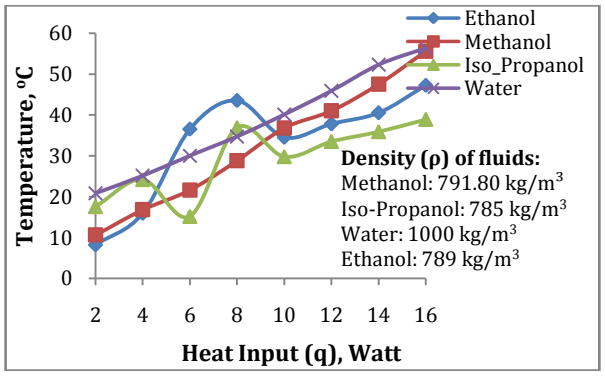

Figure 4.4.2 Rise of fluid temp. vs. heat input at the evaporator

there is a temperature rise in the evaporator from T_1 to T_2. Annamalai A. S. et al. [44] has reasoned that "In the evaporator zone heat is supplied by an electric coil and the coil surface area density is very high in the middle of the evaporator portion and hence the temperature of the vapor in the middle of the evaporator is high". Authors here disagree with Annamalai that there should be no reason to windup the heater coil densely in the middle of the evaporator rather wrapping must be uniformly done so the produced heat flux remains constant throughout the evaporator. Based on this work and the work of Mahmood [6] and Sreenivasa [36], the working liquid should be filled only equal to or less than the empty space (vapor core) of the evaporator of the heat pipe. However, a lot

more space in the heat pipe is still vacant to travel during operation. Soon after the MHP goes into operation, boiling starts at the beginning of the heat pipe – part of the fluid evaporates – that leaves a significant room empty within the evaporator which is fully wrapped up by the heater coil. Therefore, when the saturated vapor advances, it continuously receives heat from that part of heater to become superheated, and then it enters the adiabatic section. That's why we notice the temperature rise at point $T_{2,}$ hence this end of the evaporator act as a *super heater*. Regarding the rise of temperature in the evaporator, a comparative relationship between the fluids in the TMMHP is shown in Fig. 4.4.11 (a-c). At the initial steps, the trend for temperature rise for all the fluids are quite similar at horizontal position; however, they get dispersed at moderately higher heat inputs (i.e. 12W) as the heat pipe is raised to 45^{o} and 90^{o}. This may happen from the "dry out" situation meaning poor capillary pumping of condensate back to the evaporator that leads uniform heating of evaporator. It becomes obvious that the orientation of the TMMHP plays an important role in superheating quality of the fluids.

4.4.2 Condenser of TMMHP as an exothermic port

It is also noticeable from Fig. 4.4.3 to Fig. 4.4.10; there is a rise of temperature of the condensate within the condenser section of the TMMHP. Its convergent-divergent geometry creates a variable pressure gradient throughout the heat pipe that results in a quick pressure drop at the condenser port. Thus the inherent kinetic energy of the condensate increases the terminal temperature which improves the heat transfer of the system. Such an increase of the liquid's temperature also enhances the capillary action which speeds up the rate of evaporation-condensation cycle.

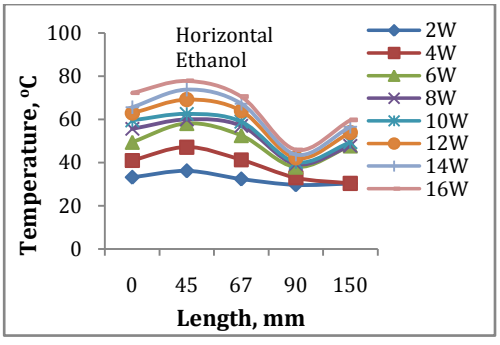

Figure 4.4.3 (a) Fluid temp. distribution along the TMMHP

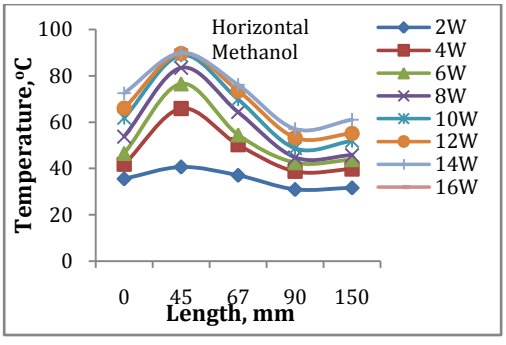

Figure 4.4.3 (b) Fluid temp. distribution along the TMMHP

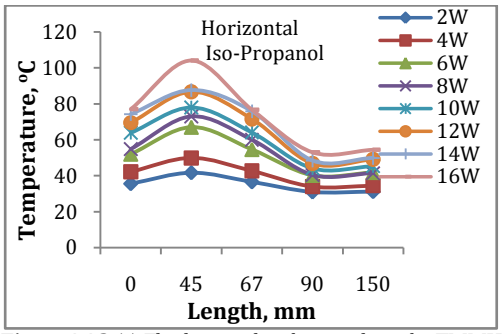

Figure 4.4.3 (c) Fluid temp. distribution along the TMMHP

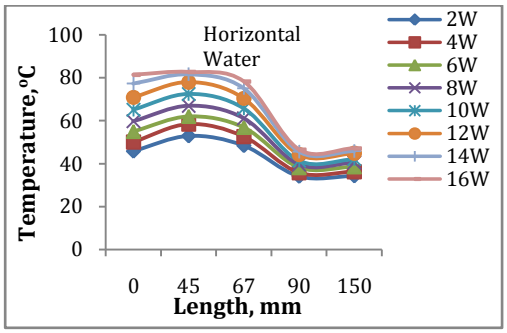

Figure 4.4.3 (d) Fluid temp. distribution along the TMMHP

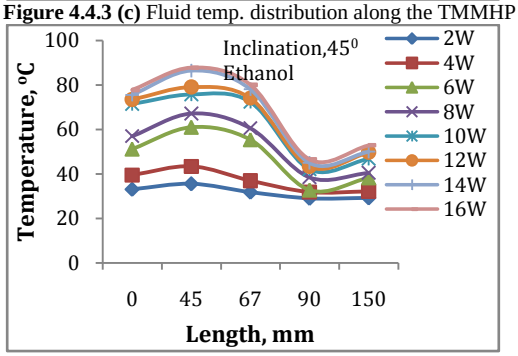

Figure 4.4.4 (a) Fluid temp. distribution along the TMMHP

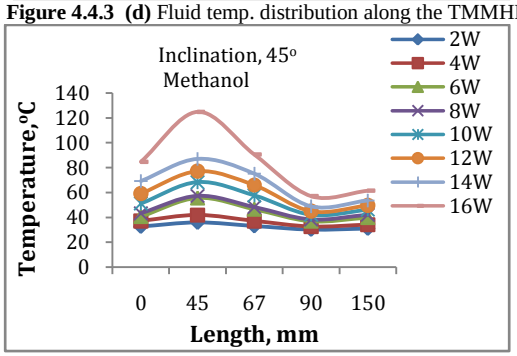

Figure 4.4.4 (b) Fluid temp. distribution along the TMMHP

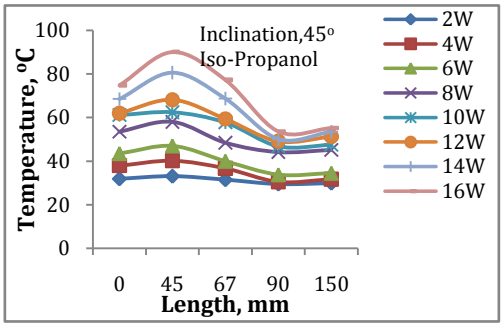

Figure 4.4.4 (c) Fluid temp. distribution along the TMMHP

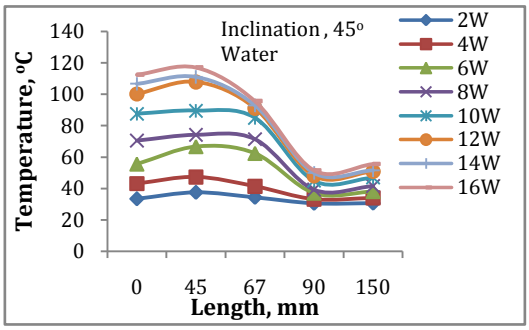

Figure 4.4.4 (d) Fluid temp. distribution along the TMMHP

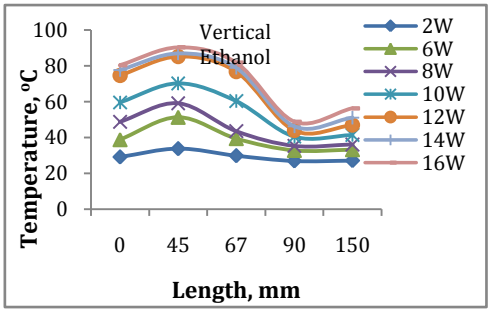

Figure 4.4.5 (a) Fluid temp. distribution along the TMMHP

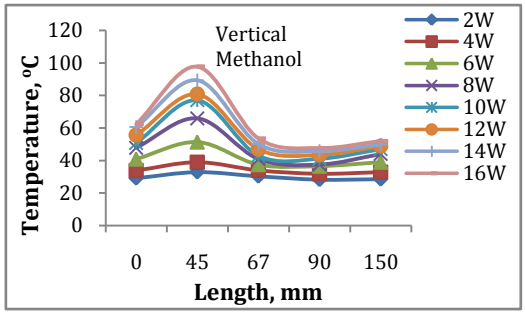

Figure 4.4.5 (b) Fluid temp. distribution along the TMMHP

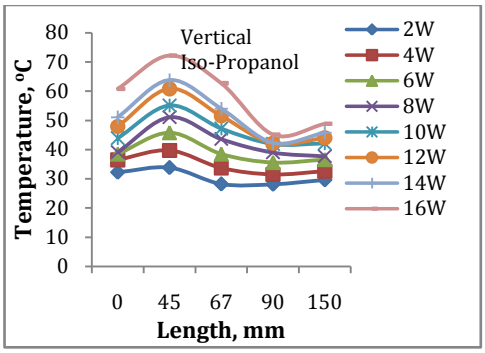

Figure 4.4.5 (c) Fluid temp. distribution along the TMMHP

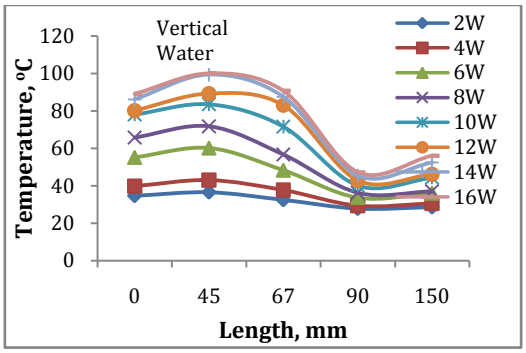

Figure 4.4.5 (d) Fluid temp. distribution along the TMMHP

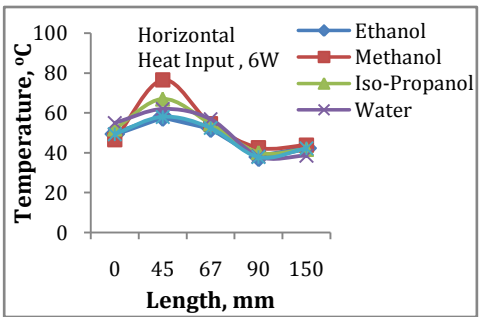

Figure 4.4.6 (a) Temp. distribn. along TMMHP of diff. fluids

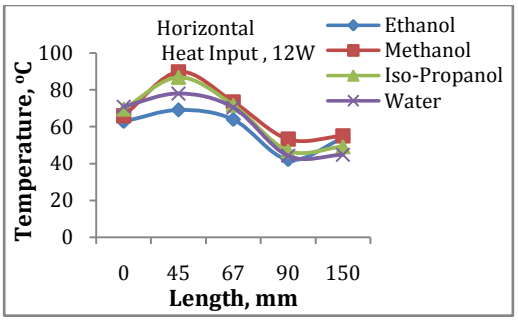

Figure 4.4.6 (b) Temp. distribn. along TMMHP of diff. fluids

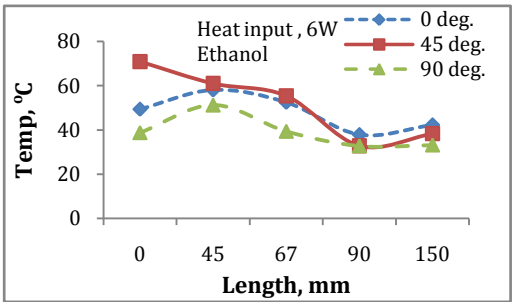

Figure 4.4.7 (a) Temp. distribn. along TMMHP at diff. inclns.

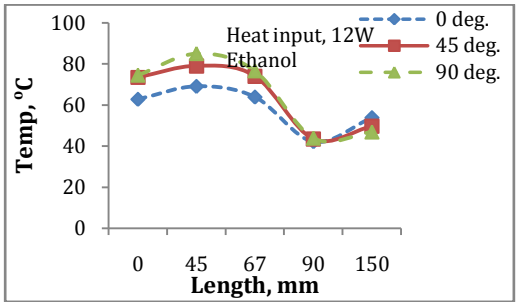

Figure 4.4.7 (b) Temp. distribn. along TMMHP at diff. inclns.

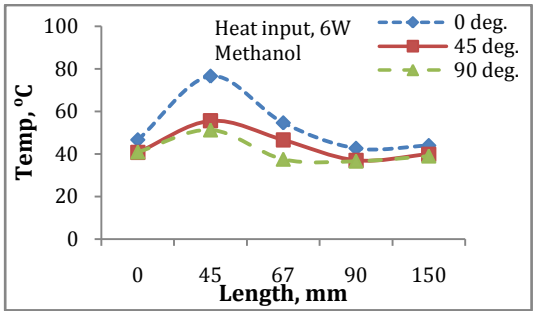

Figure 4.4.8 (a) Temp. distribn. along TMMHP at diff. inclns

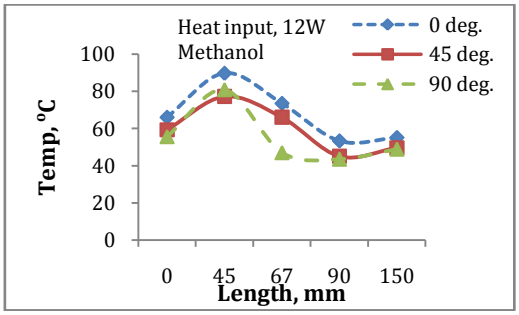

Figure 4.4.8 (b) Temp. distribn. along TMMHP at diff. inclns.

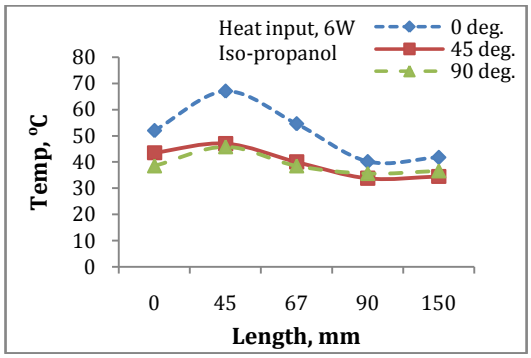

Figure 4.4.9 (a) Temp. distribn. along TMMHP at diff. inclns.

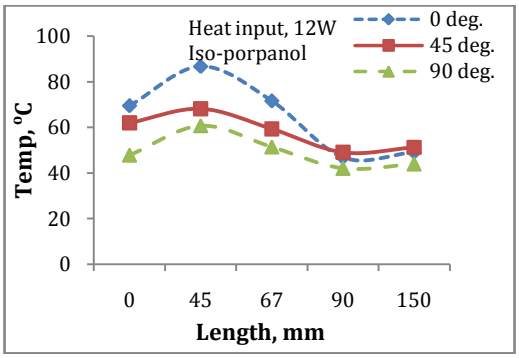

Figure 4.4.9 (b) Temp. distribn. along TMMHP at diff. inclns

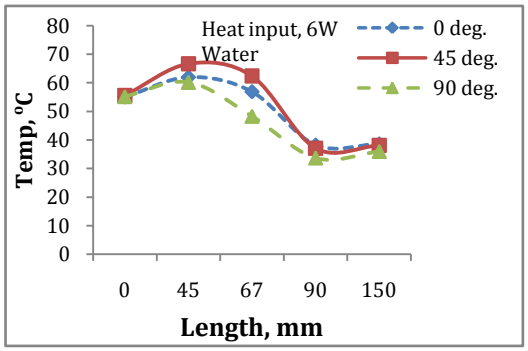

Figure 4.4.10 (a) Temp. distribn. along TMMHP at diff. inclns.

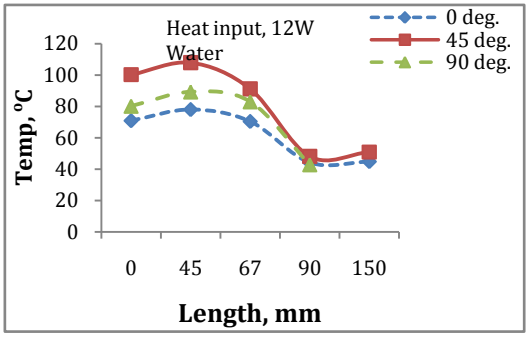

Figure 4.4.10 (b) Temp. distribn. along TMMHP at diff. inclns.

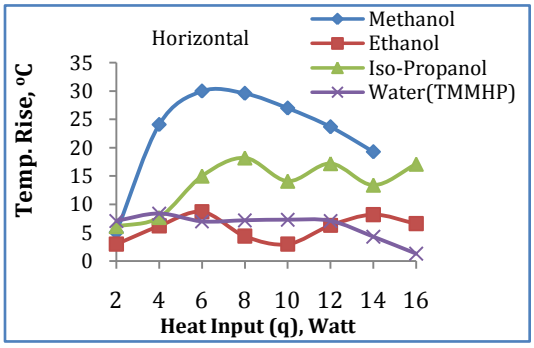

Figure 4.4.11 (a)

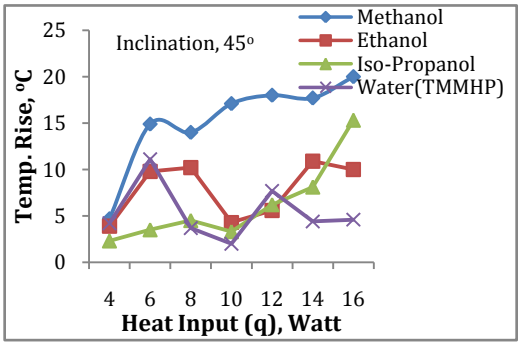

Figure 4.4.11 (b)

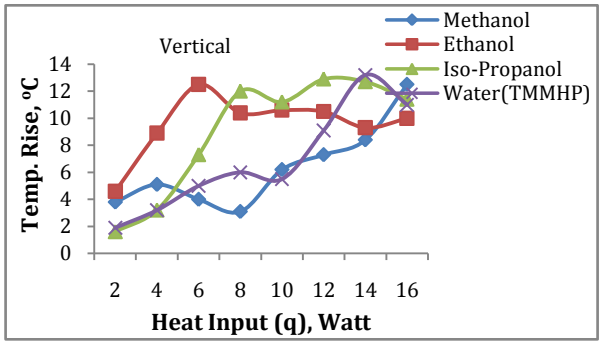

Figure 4.4.11(c)

Figure 4.4.11(a-c) Comparison of temp. rise (T_2-T_1) in TMMHP of diff. fluids at diff. inclins.

Fig. 4.4.12 indicates that apparently methanol is condensed within the highest temperature range while water was condensed within the lowest. Such two different temperature ranges were identified because of their lower and higher boiling point respectively. On the other hand, the sequence of temperature ranges remains increasing for ethanol in all orientations.

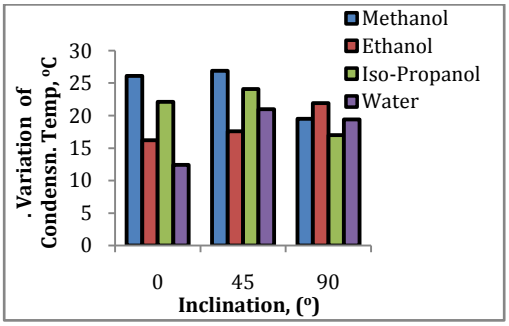

Figure 4.4.12 Variation of condensn. temp. ($T_{4,16W}$ - $T_{4,2W}$) of diff.fluids for diff. heat inputs to TMMHP at diff. inclns.

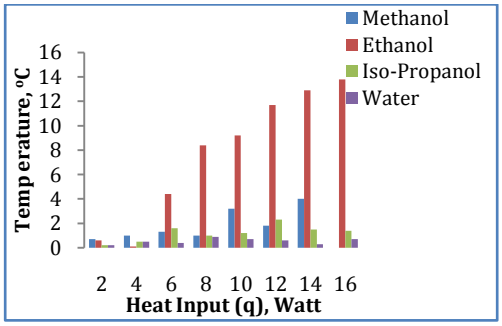

Figure 4.4.13 Comparison of condensn . temp. (T_5-T_4) range of diff. fluids for increasing heat inputs to TMMHP, horizontal

However, at vertical position, the values are scattered because of possible "dry out" situation. Capillary action of the water and hydro-carbons are quite different. As a result, the values of the three hydrocarbons are closely placed while the value of water is a bit apart from them. Thus it is proved again that the heat capacity of a liquid is not only depended on its physical property but also on its chemical property (i.e. structural bonding).

The positive gradient at the condenser of convergent-divergent TMMHP is due to sudden pressure drop within its divergent condenser shown in Fig. 4.4.13. During this pressure fall, the inherent kinetic energy of the liquid is converted to heat, hence the temperature of the liquid increases. At the turning point, such a temperature increase of the liquid benefits the capillary action of the wick to drive back condensate even faster to the evaporator.

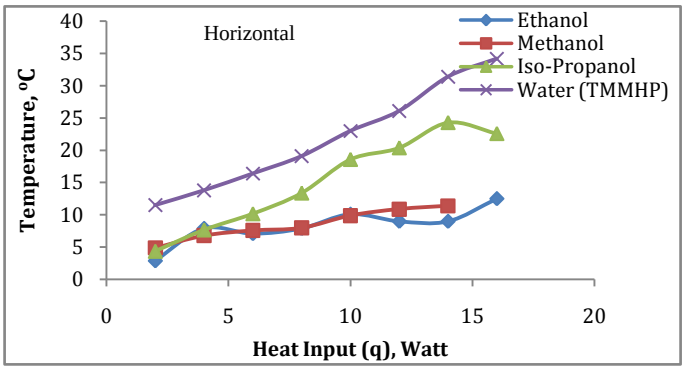

Figure 4.4.14 Comparison of terminal temp. diffs. (T_1 -T_5) in TMMHP

Thermal performance of heat pipe is measured by *h* which in turn depends on terminal temperature difference. In Fig. 4.4.14, the range of terminal temperature differences for four fluids are shown where water exhibits the highest and methanol does the lowest. These differences are basically for the higher and lower boiling point of the two fluids.

4.4.3 Comparison of *h* among four fluids in TMMHP

Fig. 4.4.15 (a-c) shows the values of heat transfer coefficient of different fluids at horizontal, inclinations of 45^o and vertical positions. In all orientations, methanol possesses the highest '*h*' among all the fluids, and the highest value (1.7 kW/m^2.^{o}C) is attained at inclination vertical position. Thus in respect of *h*, methanol is the most suitable working liquid out of the four for convergent-divergent TMMHP. Since the surface temperature of the TMMHP is depended on the heat input and heat rejection at the evaporator and condenser respectively, such high values of '*h*' become dependent only on overall thermophysical properties of the internal fluid. In Fig. 4.4.15, the sequential rises of *h* of all four fluids in TMMHP at different angles are shown. In all cases, methanol gives the highest value of *h* whereas the lowest values are not for a particular fluid. According to Newton's law of cooling, *h of a system with constant heat input and surface area gets the highest value for the smallest terminal temperature difference within the heat pipe and vice versa.* This correlation can be authenticated by comparing Fig. 4.4.14 and Fig. 4.4.15 where methanol in TMMHP achieves the highest value of *h*. Consequently, at a small terminal temperature difference, the sharp decrease of pressure gradient leads to rapid condensation at the condenser port to increase the *h*

value. The calculated h_{eff} values of all the fluids, based on the average temperature of the evaporator and condenser, for different inclinations are shown in Fig. 4.4.16. It shows that the water and three hydrocarbons are not producing the same pattern of h – all are nonlinear. Again it is proved that the value of h for any liquid is not only depended on its thermophysical properties but also on its chemical bond.

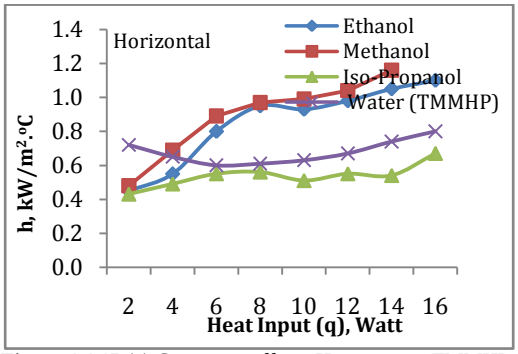

Figure 4.4.15 (a) Convec. coeff. vs. Heat input at TMMHP

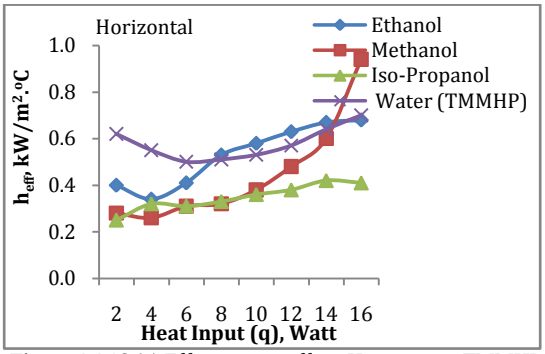

Figure 4.4.16 (a) Eff. convec.coeff. vs.Heat input at TMMHP

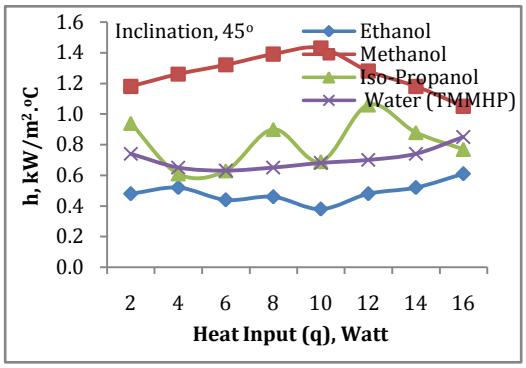

Figure 4.4.15 (b) Convec. coeff. vs. Heat input at TMMHP

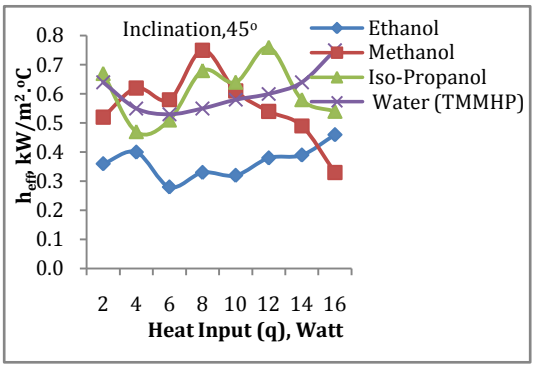

Figure 4. 4.16 (b) Eff. convec. coeff. vs. Heat input at TMMHP

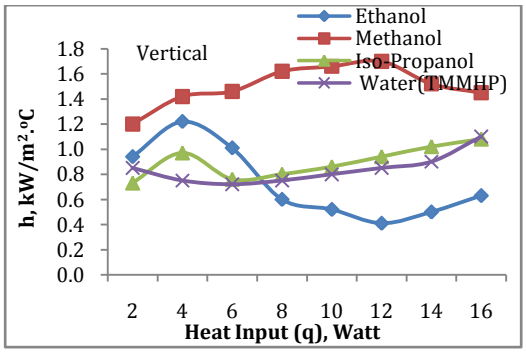

Figure 4.4.15 (c) Convec. coeff. vs. Heat input at TMMHP

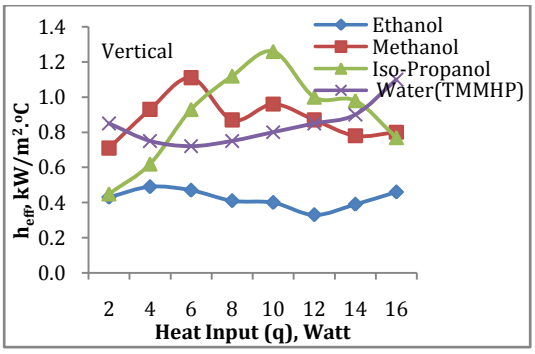

Figure 4. 4.16 (c) Eff. convec. coeff. vs. Heat input at TMMHP

Density is a thermophysical property of a fluid. Therefore, when the vapor becomes liquid at the condenser; the density of the fluid therein goes many folds high. Nevertheless, *h* keeps no direct relationship with the density alone which reflects in both Fig. 4.4.15 and Fig. 4.4.16. Rather it is found that *h is compositely related with the fluid's density, pressure drop and heat input.* This relationship can be expressed by $h = f(\rho(p(q)))$. Then the authors have developed the common dimensionless correlations from this relationship for all the data presented later in this chapter. In Fig. 4.4.17(a-b), all the fluids' dimensionless heat transfer coefficients are shown. The maximum value of dimensionless *h* for methanol is seen both at 45^{o} for 6W which is quite in match with its *h* value at Fig.4.4.15 b. However, a little deviation at vertical for methanol indicates the experimental error that spikes up the value of iso-propanol.

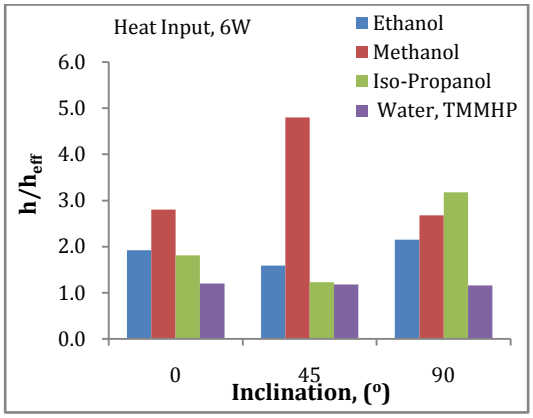

Figure 4.4.17(a) Comparison of h/h_{ef} in TMMHP

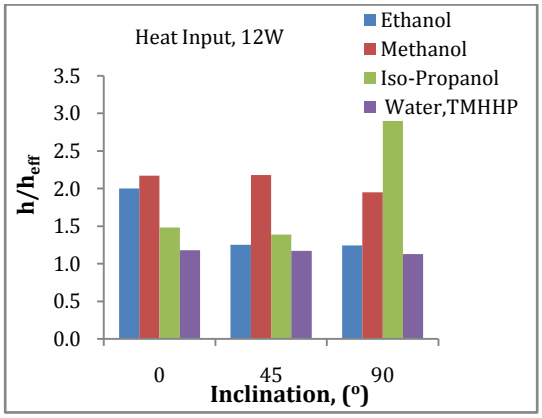

Figure 4.4.17(b) Comparison of h/h_{ef} in TMMHP

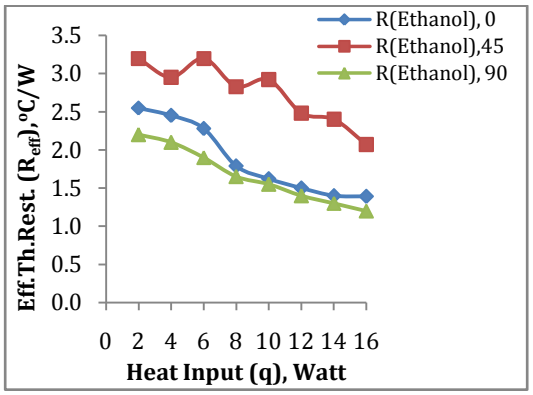

Figure 4.4.18(a) Eff. Thermal Resistance vs. Heat Input at TMMHP

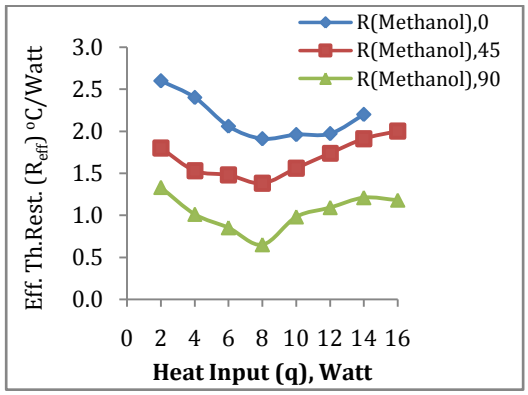

Figure 4.4.18 (b) Eff. Thermal Resistance vs. Heat Input at TMMHP

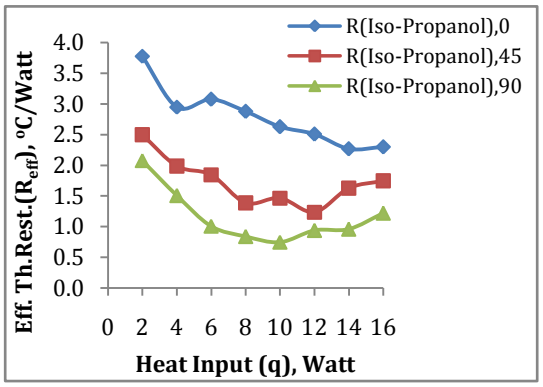

Figure 4.4.18 (c) Eff. Thermal Resistance Vs. Heat Input at TMMHP

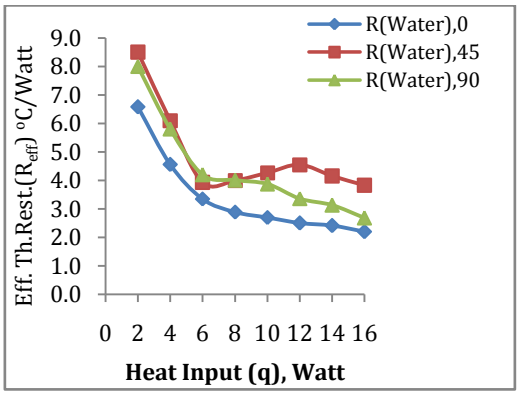

Figure 4.4.18 (d) Eff. Thermal Resistance Vs. Heat input at TMMHP

In Fig. 4.4.18 (a-d), the effect of thermal resistances for all four fluids is shown. Except water, the rest three fluids keep almost the same pattern of resistance in the convergent-divergent TMMHP with respect to heat input. Again, the reason can be the difference of their chemical bonding – water is covalent compound and the other three are hydrocarbons. However, a variation of resistance in different fluids is obvious according to the inclination of the heat pipe. It is seen, as the heat input increases to the moderately higher value (i.e. 10W) the resistance goes higher in all four cases and in all inclinations. Since all other parameters are fixed, the geometry of the micro heat pipe is causing this upper trend. Still there are some irregularities between the heat input intervals; those are because of "dry out" situation in the evaporator. It is noticed, the time required for completing the evaporation-condensation cycle is very low in the convergent-divergent TMMHP; the capillary pumping of the wick is not enough for the liquid to reach the evaporator. In case of water, by comparing Fig.4.4.16 for h_{eff} and Fig. 4.4.18d for R_{eff}, it is seen the trend of the curves is almost alike. In respect to the heat input, it can be deduced that such decreasing-increasing path is maintained by the internal variability of the conductivity of the two different metals (Cu-Ag). In addition, the convergent-divergent geometry of the TMMHP; this also guides the variability of pressure that induces variation of heat transfer. However, methanol has the lowest thermal resistance 0.65 ^{o} C/Watt out of four fluids used in this study.

4.5 Summary of the experiments and results of thermal performances of two-metal (Cu-Ag) micro heat pipes (TMMHP)

In this study the thermophysical properties (i.e. temperature, pressure, density etc.) of ethanol, methanol, iso-propanol and water have been deployed in the relevant engineering equations to check each fluid's thermal performances in the TMMHP of all four cross sections in three orientations. All the experimental data were recorded when the system attained steady state. Summary of the test parameters and field variables are listed below.

1. All four sets of experiments are done keeping the same heat inputs (2W-16W) to each TMMHP evaporator.
2. Over the range of heat inputs, each system's thermal responses, i.e. temperature rise as well as the temperature gradient at the evaporator, are recorded.
3. In each heat input, the variation of fluids pressure, temperature and densities are checked.
4. The modes of heat transfer into and out of the TMMHP are recorded and explained.
5. To verify the heat transfer capability of a TMMHP, terminal temperature differences are recorded at each heat input.
6. To observe the inclination effect on TMMHP, each experimental set up is placed in three different angles (horizontal, 45^{o} and vertical).
7. In each case, thermal performances are measured by determining both overall heat transfer coefficient and effective heat transfer coefficient.
8. To verify the calculated heat transfer coefficient, the individual effective thermal resistance is calculated and cross-checked.
9. Finally, all the experimental data are correlated to develop an equation of dimensionless coefficients.

The experimental data (3,820 nos.) are correlated for which the graphical representation is shown below.

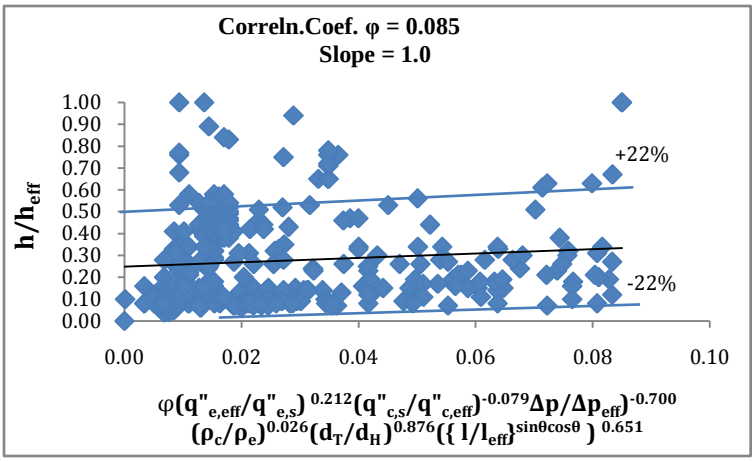

Figure 4.5.1 Graphical representation of the correlation of TMMHP (all four cross sections)

In dimensionless correlation for all four cross sections of TMMHP:

$$\frac{h}{h_{eff}} = 0.085\left(\frac{q"_{e,eff}}{q"_{e,s}}\right)^{0.212}\left(\frac{q"_{c,s}}{q"_{c,eff}}\right)^{-0.079}\left(\frac{\Delta P}{\Delta P_{eff}}\right)^{-0.700}\left(\frac{\rho_c}{\rho_e}\right)^{0.026}\left(\frac{d_T}{d_H}\right)^{0.876}\left(\left\{\frac{l}{l_{eff}}\right\}^{sin\theta cos\theta}\right)^{0.651}$$

Graphical representation of all the correlated data for all four cross sections is shown in Fig. 4.5.1, and 96% of them are found to be within ±22% range of the regression line.

Chapter 5

Correlations

A dimensionless correlation is developed which includes all the data collected from the experiment. As it is mentioned earlier and showed in the graphs, few common relations are found between heat transfer coefficient and other field variables. These common relations can be shown mathematically as $\boldsymbol{h = f(\rho(p(q)))}$. To correlate all the experimental data on four different fluids, the dimensionless heat transfer coefficient $\frac{h}{h_{eff}}$ is chosen, which is the ratio of heat transfer coefficient to effective heat transfer coefficient of working fluid. The h is based on terminal temperature differences of the fluid within the TMMHP, while the h_{eff} is based on the difference between average temperatures of the fluid of the evaporator and condenser section.

(i) h increases as the heat input q increases within the evaporator:

$$\left(\frac{h}{h_{eff}}\right) \propto \left(\frac{q_{e,eff}}{q_{e,s}}\right)$$

$$ln\left(\frac{h}{h_{eff}}\right) \propto ln\left(\frac{q_{e,eff}}{q_{e,s}}\right)$$

$$Or,\ ln\left(\frac{h}{h_{eff}}\right) = n_1 ln\left(\frac{q_{e,eff}}{q_{e,s}}\right) \qquad Or,\quad ln\left(\frac{h}{h_{eff}}\right) = ln\left[\left(\frac{q_{e,eff}}{q_{e,s}}\right)^{n_1}\right] \text{ which leads to}$$

$$\left(\frac{h}{h_{eff}}\right) = \left(\frac{q_{e,eff}}{q_{e,s}}\right)^{n_1} \ldots\ldots\ldots\ldots (5.1)$$

where $q_{e,s}$ is the heatflux in through the evaporator (Cu, k= 398 W/m.K) section received from the heat source, and $q_{e,eff}$ is the heatflux calculated from the difference of the average temperature at the outer (surface) and inner wall (vapor) of evaporator using heat conduction equation. n_1 is the slope or proportionality constant of the equation.

(ii) h increases as the heat rejection q increases at the condenser:

$$\left(\frac{h}{h_{eff}}\right) \propto \left(\frac{q_{c,s}}{q_{c,eff}}\right)$$

$$Or, ln\left(\frac{h}{h_{eff}}\right) \propto ln\left(\frac{q_{c,s}}{q_{c,eff}}\right)$$

$$Or, \left(ln\frac{h}{h_{eff}}\right) = n_2 ln\left(\frac{q_{c,s}}{q_{c,eff}}\right)$$

$$Or, \left(ln\frac{h}{h_{eff}}\right) = \left[ln\left(\frac{q_{c,s}}{q_{c,eff}}\right)^{n_2}\right]$$

$$Or, \frac{h}{h_{eff}} = \left(\frac{q_{c,s}}{q_{c,eff}}\right)^{n_2} \ldots\ldots\ldots\ldots (5.2)$$

where $q_{c,s}$ is the heatflux calculated from the coolant's temperature difference at the condenser surface using the energy equation $q_{c,s} = \dot{m}c_{p,w}(T_{w,c} - T_{w,\infty})/A_C$,while the q_{eff} is calculated from the temperature difference between inner (condensate) and outer wall (surface)of the condenser (Ag, k = 428 W/m.K) section using heat conduction equation.

(iii) h increases as the pressure drop increases within the evaporator:

$$\left(\frac{h}{h_{eff}}\right) \propto \left(\frac{\Delta P}{\Delta P_{eff}}\right) \quad Or, \; ln\left(\frac{h}{h_{eff}}\right) \propto ln\left(\frac{\Delta P}{\Delta P_{eff}}\right)$$

$$Or, ln\left(\frac{h}{h_{eff}}\right) = n_3 ln\left(\frac{\Delta P}{\Delta P_{eff}}\right)$$

$$Or, \left(ln\frac{h}{h_{eff}}\right) = \left[ln\left(\frac{\Delta P}{\Delta P_{eff}}\right)^{n_3}\right]$$

$$Or, \frac{h}{h_{eff}} = \left(\frac{\Delta P}{\Delta P_{eff}}\right)^{n_3} \ldots\ldots\ldots\ldots (5.3)$$

where ΔP is calculated from the pressure difference of to ends of the TMMHP, in this case, at T_1 and T_5 which is called overall pressure difference. And the ΔP_{eff} is the average pressure difference at two average temperatures: one is the average pressure in evaporator at its average evaporation temperature, and the other one is also the average pressure in condenser at its average condensing temperature.

(iv)) h increases as the density of the fluid increases or vice versa:

$$\left(\frac{h}{h_{eff}}\right) \propto \left(\frac{\rho_c}{\rho_e}\right) \qquad or, \qquad ln\left(\frac{h}{h_{eff}}\right) = n_4 ln\left(\frac{\rho_c}{\rho_e}\right)$$

$$Or, \left(ln\frac{h}{h_{eff}}\right) = \left[ln\left(\frac{\rho_c}{\rho_e}\right)^{n_4}\right]$$

$$Or, \frac{h}{h_{eff}} = \left(\frac{\rho_c}{\rho_e}\right)^{n_4} \ldots\ldots\ldots\ldots\ldots (5.4)$$

where ρ_c and ρ_e are the densities at the condenser and evaporator respectively.
Furthermore, the heat transfer coefficient also increases with the wetted surface perimeter as well as with the orientation of TMMHP.

(v) h increases as the ratio of profile height to hydraulic diameter, $\left(\frac{d_T}{d_H}\right)$, increases:

$$\left(\frac{h}{h_{eff}}\right) \propto \left(\frac{d_T}{d_H}\right)$$

$$ln\left(\frac{h}{h_{eff}}\right) \propto ln\left(\frac{d_T}{d_H}\right)$$

$$Or, ln\left(\frac{h}{h_{eff}}\right) = n_5 ln\left(\frac{d_T}{d_H}\right) \qquad Or, \quad ln\left(\frac{h}{h_{eff}}\right) = ln\left[\left(\frac{d_T}{d_H}\right)^{n_5}\right] \text{ which leads to}$$

$$\left(\frac{h}{h_{eff}}\right) = \left(\frac{d_T}{d_H}\right)^{n_5} \ldots\ldots\ldots\ldots\ldots (5.5)$$

In case of TMMHP, n_5 is found to be equal to the inverse of its base, or $\frac{d_H}{d_T}$ for the respective cross section.

(vi) h increases as the ratio of $\left\{\frac{l}{l_{eff}}\right\}^{sin\theta cos\theta}$ where θ is the inclination of the heat pipe:

$$\left(\frac{h}{h_{eff}}\right) \propto \left(\left\{\frac{l}{l_{eff}}\right\}^{sin\theta cos\theta}\right)$$

$$ln\left(\frac{h}{h_{eff}}\right) \propto ln\left(\left\{\frac{l}{l_{eff}}\right\}^{sin\theta cos\theta}\right)$$

$$Or,\ ln\left(\frac{h}{h_{eff}}\right) = n_6 ln\left(\left\{\frac{l}{l_{eff}}\right\}^{sin\theta cos\theta}\right) \quad Or, \quad ln\left(\frac{h}{h_{eff}}\right) = ln\left[\left(\left\{\frac{l}{l_{eff}}\right\}^{sin\theta cos\theta}\right)^{n_6}\right] \text{ which leads to}$$

$$\left(\frac{h}{h_{eff}}\right) = \left(\left\{\frac{l}{l_{eff}}\right\}^{sin\theta cos\theta}\right)^{n_6} \ldots\ldots\ldots\ldots\ldots (5.6)$$

Thus, to obtain the dimensionless correlation we can superpose the above six equations, from *eqn. 5.1 to eqn. 5.6*, to acquire a single equation.

$$\left(\frac{h}{h_{eff}}\right) = \varphi\left[\left(\frac{q_{e,eff}}{q_{e,s}}\right)^{n_1}\left(\frac{q_{c,s}}{q_{c,eff}}\right)^{n_2}\left(\frac{\Delta P}{\Delta P_{eff}}\right)^{n_3}\left(\frac{\rho_c}{\rho_e}\right)^{n_4}\left(\frac{d_T}{d_H}\right)^{n_5}\left(\left\{\frac{l}{l_{eff}}\right\}^{sin\theta cos\theta}\right)^{n_6}\right]$$

where φ is the constant of proportionality.

For the sake of simplicity of calculation, the above correlation components will be represented as follows:

$$\left(\frac{h}{h_{eff}}\right) = \boldsymbol{h},\ \left(\frac{q_{e,eff}}{q_{e,s}}\right)^{n_1} = \boldsymbol{qe^{n_1}},\ \left(\frac{q_{c,s}}{q_{c,eff}}\right)^{n_2} = \boldsymbol{qc^{n_2}},\ \left(\frac{\Delta P}{\Delta P_{eff}}\right)^{\boldsymbol{n_3}} = \Delta \boldsymbol{p^{n_3}},$$

$$\left(\frac{\rho_c}{\rho_e}\right)^{n_4} = \boldsymbol{\rho^{n_4}},\qquad \left(\frac{d_T}{d_H}\right)^{n_5} = \boldsymbol{d^{n_5}},\ \left(\left\{\frac{l}{l_{eff}}\right\}^{sin\theta cos\theta}\right)^{n_6} = \boldsymbol{l^{n_6}}$$

Using the Excel of Microsoft Office 2007, the constants are calculated and installed into the correlations which are presented in the following sections.

The summarized correlation for all experimental data is presented in the next section.

5.1 Summarized data correlation for the study of two-metal (Cu-Ag) micro heat pipes (TMMHP) of all four cross sections

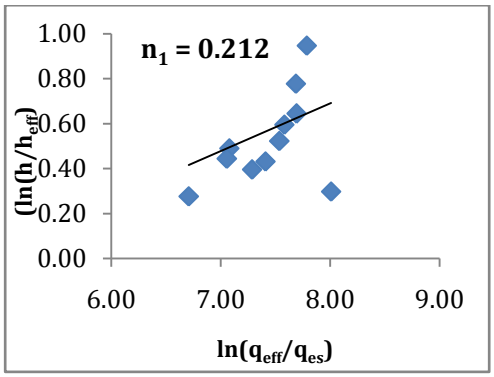

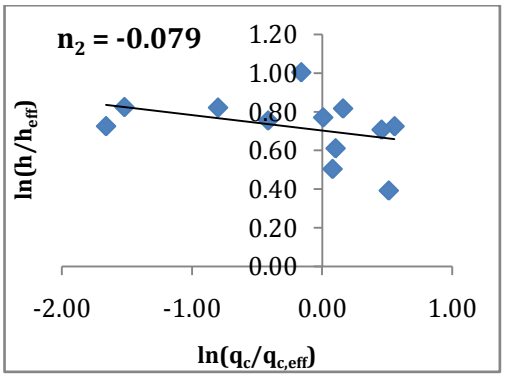

Figure 5.1.1 Determination of the exponent factor 'n_1' **Figure 5.1.2** Determination of the exponent factor 'n_2'

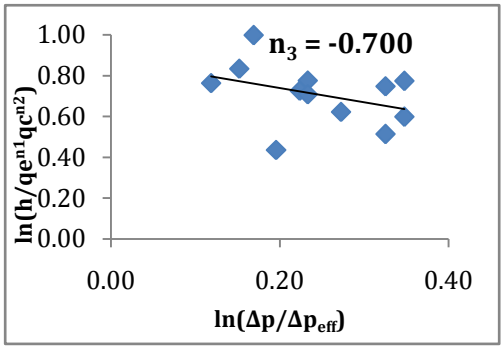

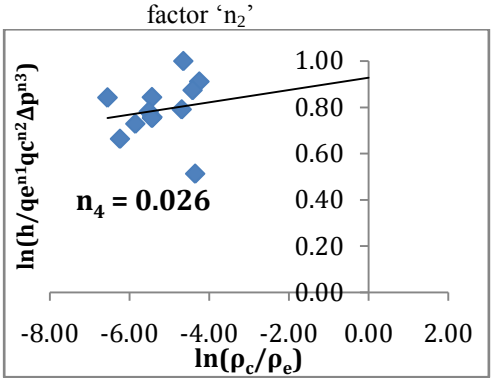

Figure 5.1.3 Determination of the exponent factor 'n_3' **Figure 5.1.4** Determination of the exponent factor 'n_4'

$(d_T/d_H)^{\wedge}\, d_H/d_T \Rightarrow n_5 = 0.876$

Figure 5.1.5 Determination of the exponent factor 'n_5'

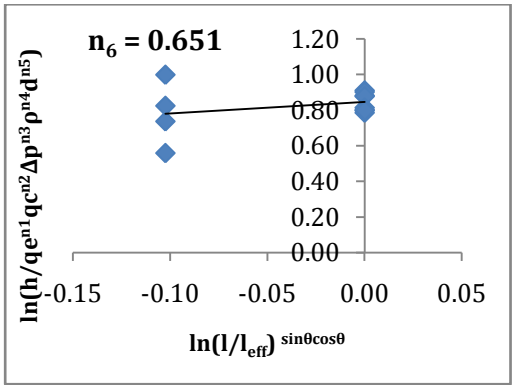

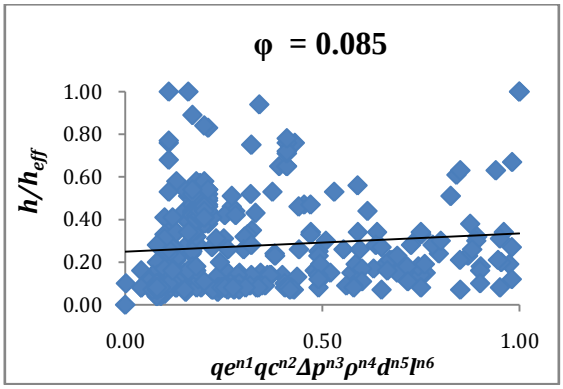

Figure 5.1.6 Determination of the exponent factor 'n_6' **Figure 5.1.7** Determination of the corrln. coeff. **'φ'**

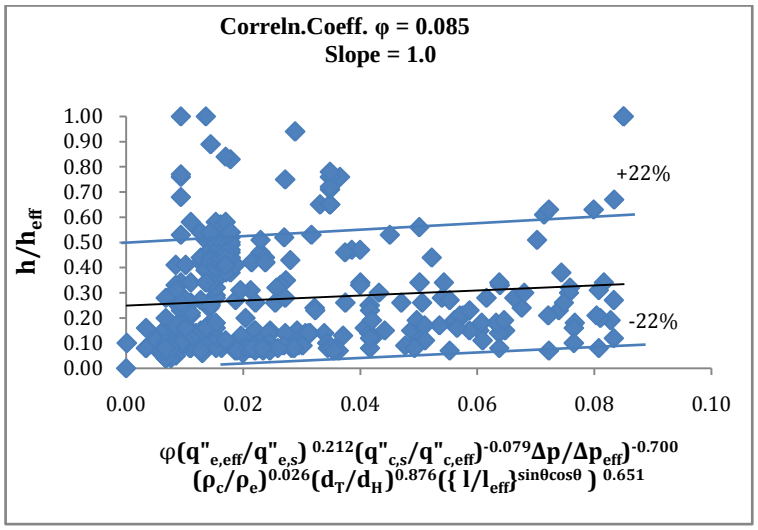

Figure 5.1.8 Graphical representation of the correlation of TMMHP (all four cross sections)

In dimensionless correlation for all four cross sections of TMMHP:

$$\frac{h}{h_{eff}} = 0.085\left(\frac{q"_{e,eff}}{q"_{e,s}}\right)^{0.212}\left(\frac{q"_{c,s}}{q"_{c,eff}}\right)^{-0.079}\left(\frac{\Delta P}{\Delta P_{eff}}\right)^{-0.700}\left(\frac{\rho_c}{\rho_e}\right)^{0.026}\left(\frac{d_T}{d_H}\right)^{0.876}\left(\left\{\frac{l}{l_{eff}}\right\}^{sin\theta cos\theta}\right)^{0.651}$$

Graphical representation of all the correlated data for all four cross sections is shown in Fig. 5.1.8, and 96% of them are found to be within ±22% range of the regression line.

Chapter 6

Conclusions and Future Suggestions

The experiments are conducted on heat pipes of four different cross sections with four different fluids in three orientations (horizontal, 45^o and vertical) which total forty eight experiments. In addition to that, four more experiments are conducted for the validation of the present experimental method. The analyses of the outputs are concluded below.

Circular

Out of four working liquids, *methanol* (organic) is found to be of the highest *h* of 6.5 $kW/m^2.^oC$ at 45^o inclination for the heat input of 6W. Apparently, methanol possesses the highest density and its heat capacity and boiling point are the lowest out of three hydrocarbons. However, its opponent, water (inorganic) has got higher values for all properties than those of three hydrocarbons. Even though water holds the highest latent heat, it could not provide the highest *h*. It may happen because of geometrical effect that supports the heat convection by hydrocarbons even better. Out of three orientations, TMMHP at 45^o produces the highest value of *h* for all four fluids. Capillary action in transporting the condensate to the evaporator may be helpful for methanol than any other fluids since the condensate has to crawl against the gravitation in its course. And in case of 45^o, the capillary resistance is less than vertical orientation.

Triangular

Out of four working liquids, *Ethanol* (organic) is found to provide the highest *h* of 3.3 $kW/m^2.^oC$ at vertical position for the heat input of 12W. Comparing to the case of circular tube, only the orientation of the setup is in common which may dismiss the possibility for methanol to provide the highest *h*. In addition, the triangular geometry may have an added advantage for capillary motion of more viscous ethanol than methanol.

Square

Out of four working fluids, *ethanol* is again found to provide the highest *h* of 2.7 kW/m^2.^{o}C at horizontal position for the heat input of 6W. Comparing to triangular case, ethanol is showing the best results in square cross section. One obvious thing is, the increasing number of fillet radius in square one than the triangular one. This kind of fillet radius is proven to be better carrier of condensate as it has been found in literature survey.

Convergent-Divergent

Out of four working fluids, *methanol* is found to provide the highest *h* of 1.7 kW/m^2.^{o}C at 45^o inclination for the heat input of 12W. Comparing with the previous three geometries, circular cross section is the closest ally of conv-div. tube. Therefore, it may be suggested that the circular or related geometry is the best for methanol as working liquid. However, the highest *h* of 6.5 kW/m^2.^{o}C given by methanol produced in the circular cross section at 45^o inclination for the heat input of 6W.

To validate the method used in TMMHP experiments, validation experiments [25] on dissimilar setup are conducted. The values of overall heat transfer coefficient produced from the validation experiments also authenticate the present experimental results of TMMHP with the proximity of 93%.

It can be concluded that the heat transfer coefficient, *h*, of a working liquid is a complex issue that cannot be described simply by one test parameter. Rather, it is a combined effect of the geometry, physical and chemical properties and orientation of the heat pipe. However, in an only comparable case of water as working liquid used in circular cross section SMMHP[6], the circular TMMHP produces the *h* (1.33 kW/m^2.^{o}C) as high as three times as that (0.46 kW/m^2.^{o}C) of SMMHP[6].

However, to improve the heat pipe performances following works are suggested for further study on TMMHP.

I. Instead of two-metal (Cu-Ag), a series of metal of different heat conductivity can be tried. In this way, the two-different-conductivities will take the form of variable-conductivity. The temperature gradient will be higher in this approach.

II. By changing material of the wick from SS mesh to sintered metal powder or any fibrous material, and its arrangement, i.e. embedding to the inner wall of the tube to centrally placed braid also can be tested.

III. Azeotrope can be used as working liquid as it may add or subtract some properties to the working liquid than its singular condition which may have some positive effects on heat transfer coefficient.

IV. Heavy water or deuterium may be considered as working liquid, because of the high boiling point which will possess high latent heat of evaporation. However, its radiation nature may be a concern in its application.

V. Detailed study on improving capillary action by investigating the temperature, roughness or porosity effect of the wick may also be attempted.

VI. Entropy generation within the heat pipe can be estimated to measure the irreversibility of the MHP that may misrepresent the transfer of actual heat content within a system.

References

1. Peterson, G. P., 1994, “An Introduction to Heat Pipes--Modeling, testing and applications”, John Wiley & Sons, Inc.

2. Peterson, G. P., Duncan, A. B., Ahmed, A. S., Mallik, A. K. and Weichold, M. H., 1991, "Experimental investigation of micro heat pipes in silicon wafers," presented at Winter Annual Meeting of the American Society of Mechanical Engineers, Dec 1-6, 1991, Atlanta, GA, USA.

3. http://www.lightstreamphotonics.com/images/tech_orangecontainer_small.png, Accessed in November 29, 2011.

4. Widah Saied, “Fundamentals of Heat Pipes”, (Faghri, 1995) http://www.seminarprojects.com/Thread-fundamentals-of-heat-pipes, Accessed in November November 30, 2011.

5. Faghri, A., 1995, “Heat Pipe Science and Technology”. US: Taylor &Francis, pp. 221–264.

6. Mahmood, S. L., 2007, “Experimental Investigation on Micro Heat Pipes of Different Cross-sections having same Hydraulic Diameter”, MS Thesis, Islamic University of Technology, OIC, Bangladesh.

7. http://www.thermalfluidscentral.org/encyclopedia/index.php/Heat_pipes, Accessed in November 15, 2011.

8. Senthilkumar, R., Vaidyanathan, S. and Sivaraman, B., 2010, “Study of heat pipe performance using an aqueous solution of n-Butanol”, Indian Journal of Science and Technology, Vol. 3 No. 6.

9. Cotter, T. P., 1984, “ Principles and Prospects for Micro Heat Pipes”, Proc. of 5th International Heat Pipe Conference, Japan.

10. Peterson, G.P.,1994, “An Introduction to Heat Pipes”, Wiley-Interscience Publication, New York, USA, pp. 44–117.

11. Mahmood, L. S., Akhanda, M. A, R., 2008, “Experimental study on the performance limitation of micro heat pipes of non circular cross-sections”, Thermal Science, vol. 12.

12. Zafiropoulos, E. P. and Dialynas, E. N., 2004,”Reliability and cost optimization of electronic devices considering the component failure rate uncertainty. Reliability Engineering & System Safety”, 84(3):271–284.

13. Lall, P. , Pecht, M. and Hakim, E. B., 1995, “Characterization of functional temperature and microelectronic reliability”. Microelectronics and Reliability, 35(3):377– 402.

14. Dalaroz´ee, G.,1999, “Introduction to reliability. Microelectronic Engineering”, 49(1-2):3–10.

15. Salmela, O., 2005, “The effect of introducing increased-reliability-risk electronic components into 3rd generation telecommunications systems”, Reliability Engineering & System Safety, 89(2):208–218.

16. Vasiliev, L.L., 2008, **“**Micro and miniature heat pipes – Electronic component coolers”, Applied Thermal Engineering, Volume 28, Issue 4, Pages 266-273.

17. Nadgauda, O. S., 2006,“Fabrication, Filling, Sealing and Testing of Micro Heat Pipes”, M.S. Thesis, Auburn University, Alabama, USA.

18. Gerner, B. B. F. M, Henderson, H.T. and Ramadas, P., 1993, "Silicon-Water Micro Heat Pipes".

19. Ali, A., Dehoff, R., and Grubb, K., 1999,”Advanced Heat Pipe Thermal Solutions For Higher Power Notebook Computers”.

20. Chi, “Heat Pipe Theory and Practice”, 1976, McGraw-Hill, New York, USA.

21. Peng, X. F., Wang, B. X., Peterson, G. P. and Ma, H. B., 1995, “Experimental investigation of heat transfer in flat plates with rectangular micro channels”, International Journal of Heat and Mass Transfer, 38(1):127–137.

22. Wang, C.Y. , Groll, M., Osler, S. R. and Tu, C. J., 1994, “Porous medium model for two-phase flow in mini channels with applications to micro heat pipes”, Heat Recovery Systems &CHP, 14(4):377–389.

23. Chen, Y. et al, 2008, “Condensation in Microchannels”’, Taylor & Francis Group, LLC, Nanoscale and Microscale Thermophysical Engineering, 12: 117–143.

24. Moon, S H., Hwang, G., Ko, S. C. Youn, Kim**,** T., 2004**,** “Experimental study on the thermal performance of micro-heat pipe with cross-section of polygon”, Microelectronics Reliability Volume 44, Issue 2, Pages 315-321.

25. Hossain, R.A., Chowdhuri, M.A.K, Feroz, C. M., 2010,“Design, Fabrication and Experimental Study of Heat Transfer Characteristics of a Micro Heat

Pipe",Jordan Journal of Mechanical and Industrial Engineering, Volume 4, Number 5, Pages 531- 542.

26. Kang, S.W., Tsai, S.H. and Chen**,** H.C., 2002**,"** Fabrication and test of radial grooved micro heat pipes", Applied Thermal Engineering, Volume 22, Issue 14, Pages 1559-1568.

27. Moon, S.H., Hwang, G., Ko, S.C., Kim, Y.T., 2004, "Experimental study on the thermal performance of micro-heat pipe with cross-section of polygon", Microelectronics Reliability, Vol.44, 315–321.

28. Kimura, Y., Nakamura, Y., Sotani J. and Katsuta, M.,"Steady and Transient Heat Transfer Characteristics of Flat Micro Heat pipe", www.furukawa.co.jp/review/fr027/fr27_02.pdf, August 17, 2011.

29. Iqbal, KMN S. and Akhanda, M. A. R., 2014,"Study of Two-metal (Cu-Ag) Micro Heat Pipe of Triangular Cross Section Using Different Working Fluids of Low Boiling Point", SYLWAN.English Edition, 158(6): 229-248.

30. Iqbal, KMN S. and Akhanda, M. A. R., 2014, "Study of two-metal (Cu-Ag) micro heat pipe of square cross section using different working liquids of low boiling point", American Journal of Mechanical Engineering,Vol. 2, Issue.3.

31. Khrustalev, D. and Faghri, A., 1994, "Thermal Analysis of a Micro Heat Pipe," J. Heat Transfer, Vol. 116, pp. 189-198.

32. Khrustalev, D. and Faghri, A., 1995, "Thermal Characteristics of Conventional and Flat Miniature Axially Grooved Heat Pipes," Journal of Heat Transfer, Vol. 117, pp. 1048-1054.

33. Le Berre, Pandraud, M. G., Morfouli, P. and Lallemand, M., 2006, "The performance of micro heat pipes measured by integrated sensors", Journal of Micromechanics and Microengineering, 16:1047–1050.

34. Oshman, Y. Li, C. Lee, R. Y., Peterson, G.P. Bright, V.M., 2011, "The Development of Polymer-Based Flat Heat Pipes", Journal of Microelectromechanical Systems, Volume: 20, Issue: 2, pp: 410.

35. Yamamoto, K., Nakamizo, K., Kameoka, H. and Namba, K., 2002, "High Performance Micro Heat Pipe", Furukawa review No. 27, pp. 3-8.

36. Sreenivasa, T. N., Sridhara, S.N. and Pundarika, G., 2005, "Working fluid inventory in miniature heat pipe", Proceedings of the International Conference on Mechanical Engineering Dhaka, Bangladesh, ICME05-TH-02.

37. Akhanda, M. A. R., Mahmood, S.L. and Ahmed, A., 2006, "An experimental investigation of an air-cooled miniature heat pipe (MHP) using different working fluids at different fill ratios", Proceedings of the 3rd BSME-ASME International Conference on Thermal Engineering Dhaka, Bangladesh, Paper No. BA 175.

38. Cao Y.and Gao, M., 2002, "Wickless network heat pipes for high heat flux spreading applications", International Journal of Heat and Mass Transfer, Vol. 45, pp. 2539-2547.

39. Eguchi, K., Mochizuki, M., Mashiko, K., Goto, K., Saito, Y., Takamiya, A. and Nguyen, T., 1997, "Cooling of CPU using micro heat pipe", Fujikuru Co., Technical Note, Vol. 9,pp. 64-68.

40. Xie H., Aghazadeh, M. and Toth. J., 1995, "The use of heat pipes in the cooling of portables with high power packages – A case study with the Pentium processor-based notebooks and sub-notebooks.", Proceedings of the 1995 Electronic Components and Technology Conference (ECTC), pp. 906-913.

41. Mochizuki, M., Mashiko, K., Nguyen, T.,Saito, Y. and Goto, K., "Cooling CPU using hinged heat pipe", 1996, 5th International Heat Pipe Symposium, Melbourne, Australia, pp. 218-229.

42. Kole, M. and Dey, T. K. "Thermal performance of screen mesh wick heat pipes using water based copper nanofluids", *www.researchgate.net/.../236892967_Thermal_performance_of_screen* Last visited on June 02, 2014.

43. Chiang**,** Y., Chieh, J. and Ho**,** C. **"**The magnetic-nanofluid heat pipe with superior thermal properties through magnetic enhancement", *www.nanoscalereslett.com/content/7/1/322,* Last visited on June 02, 2014.

44. Annamalai, A. S. and Ramalingam, V., 2011, "Experimental investigation and computational fluid dynamics analysis of an air cooled condenser heat pipe", Thermal Science, 15(3): 759-772.

45. Uhia, F. J., Campo, A. and Fernandez-Seara, J., 2013, "Uncertainty Aanalysis for Experimental Heat Transfer Data Obtained by the Wilson Plot Method

Application to condensation on horizontal plain tubes", Thermal Science, 17(2): pp. 471-487.

46. Coleman, H. W. Steele, W. G., 1998,"*Experimentation and Uncertainty Analysis for Engineers"*, 2nd ed., John Wiley & Sons, New York, USA.

47. Kline, S. J. and McClintock, F. A., 1953, "Describing the uncertainties in single sample experiments". Mechanical Engineering, pages 3–8.

Appendix A-1

Experimental Data for TMMHP

TMMHP: Circular, Fluid: Ethanol, Temperature: ^{o}C

Inclination: 0^{o}

Sl. No.	q (Watt)	T_1	T_{1s}	T_2	T_{2s}	T_3	T_{3s}	T_4	T_{4s}	T_5	T_{5s}
1	2.0	43.5	46.8	45.5	49.9	39.9	44.6	36.2	31.1	33.9	28.9
2	4.0	52.5	61.6	56.3	68.5	46.9	54.5	40.5	31.4	37.4	29.1
3	6.0	63.5	72.4	68.7	78.2	57.8	64.6	46.5	31.9	41.8	29.4
4	8.0	70.8	81.5	78.0	91.4	66.7	78.8	50.7	32.8	44.5	29.9
5	10.0	78.8	86.7	86.8	98.8	76.8	85.8	55.8	33.8	48.0	30.2
6	12.0	84.2	99.8	91.2	105.9	84.0	91.6	59.8	34.4	50.3	30.4
7	14.0	90.5	106.6	101.1	113.8	91.5	101.5	64.5	35.9	52.9	30.8
8	16.0	95.6	115.8	112.1	135.7	96.6	110.0	67.3	36.6	54.8	31.5

Inclination: 45^{o}

Sl. No.	q (Watt)	T_1	T_{1s}	T_2	T_{2s}	T_3	T_{3s}	T_4	T_{4s}	T_5	T_{5s}
1	2.0	41.2	44.2	43.3	48.4	39.9	43.1	36.1	31.4	34.1	29.1
2	4.0	50.3	58.3	53.2	67.4	47.5	56.4	40.6	31.7	37.6	29.5
3	6.0	61.2	68.5	68.0	79.3	59.6	66.3	47.4	32.4	42.6	30.1
4	8.0	69.8	80.1	76.5	89.7	68.0	75.7	52.0	32.6	45.8	30.4
5	10.0	77.6	85.5	82.4	97.9	73.8	81.8	55.5	33.8	48.4	30.9
6	12.0	85.1	98.9	88.5	105.8	79.5	91.6	58.6	34.2	50.7	31.2
7	14.0	99.5	112.5	101.8	118.8	88.6	97.9	64.2	35.8	55.1	31.6
8	16.0	105.9	120.7	111.0	137.7	96.0	106.6	68.7	37.7	58.4	32.4

Inclination: 90^{o}

Sl. No.	q (Watt)	T_1	T_{1s}	T_2	T_{2s}	T_3	T_{3s}	T_4	T_{4s}	T_5	T_{5s}
1	2.0	43.7	47.7	44.2	50.4	40.5	44.3	36.3	32.2	34.8	29.2
2	4.0	55.9	64.5	56.4	67.9	49.3	58.8	41.8	32.7	38.9	29.4
3	6.0	70.3	79.9	70.6	81.8	59.8	65.5	48.3	33.4	43.8	29.6
4	8.0	77.2	86.2	78.8	88.6	65.8	75.1	52.2	33.9	46.4	29.7
5	10.0	87.2	95.9	88.1	98.9	73.4	81.7	56.9	34.2	49.8	30.2
6	12.0	95.1	106.8	96.0	109.9	79.0	90.4	60.6	34.9	52.4	30.5
7	14.0	106.5	119.9	108.3	125.5	87.6	96.3	66.0	36.6	56.3	31.1
8	16.0	117.1	128.8	118.2	135.8	94.7	104.4	71.0	37.9	60.0	31.8

TMMHP: Circular
Fluid: Methanol
Temperature: ^{o}C

Inclination: 0^{o}

Sl. No.	q (Watt)	T_1	T_{1s}	T_2	T_{2s}	T_3	T_{3s}	T_4	T_{4s}	T_5	T_{5s}
1	2.0	35.1	41.1	42.4	51.7	36.9	44.8	35.0	33.3	33.7	28.9
2	4.0	37.6	46.8	51.0	62.8	41.2	51.5	37.3	33.8	36.1	29.1
3	6.0	41.3	52.4	58.7	71.5	44.2	58.7	40.2	33.9	39.0	29.3
4	8.0	43.9	56.9	62.4	77.4	47.3	62.9	42.6	34.2	40.7	29.5
5	10.0	46.8	62.9	66.3	79.2	49.1	63.6	43.4	34.8	42.2	29.9
6	12.0	48.3	66.7	69.1	81.8	52.8	65.7	44.5	35.0	43.7	30.2
7	14.0	50.5	72.4	70.2	83.9	55.3	68.2	46.2	35.2	44.1	30.6
8	16.0	52.0	76.3	72.7	87.9	58.7	70.9	48.1	36.2	45.3	31.1

Inclination: 45^{o}

Sl. No.	q (Watt)	T_1	T_{1s}	T_2	T_{2s}	T_3	T_{3s}	T_4	T_{4s}	T_5	T_{5s}
1	2.0	34.5	40.7	41.1	51.4	36.8	46.9	35.3	33.1	33.7	29.2
2	4.0	37.5	46.1	49.8	56.7	41.3	51.6	38.1	33.9	36.5	29.8
3	6.0	40.2	51.7	58.7	60.8	46.7	54.5	41.1	34.0	38.8	30.5
4	8.0	45.1	57.7	63.7	67.4	53.5	57.9	42.7	34.2	41.9	30.7
5	10.0	48.2	63.6	69.7	75.9	58.2	65.8	44.2	35.9	44.0	30.9
6	12.0	50.5	67.8	73.2	82.7	61.4	71.4	47.0	36.1	45.6	31.2
7	14.0	53.1	82.8	76.0	88.6	64.2	74.4	47.9	36.8	47.4	31.7
8	16.0	55.1	85.4	78.6	93.6	66.5	79.9	49.5	37.3	48.9	32.2

Inclination: 90^{o}

Sl. No.	q (Watt)	T_1	T_{1s}	T_2	T_{2s}	T_3	T_{3s}	T_4	T_{4s}	T_5	T_{5s}
1	2.0	35.3	41.1	36.8	44.3	35.4	40.2	33.8	33.3	33.1	28.9
2	4.0	36.4	46.8	39.9	51.4	37.9	45.8	36.6	33.8	35.5	29.2
3	6.0	41.8	52.5	48.8	60.2	45.0	54.7	40.1	34.1	39.1	30.1
4	8.0	45.2	58.4	56.6	62.8	50.3	57.6	43.5	34.5	41.4	30.8
5	10.0	48.5	64.8	61.9	67.8	54.2	62.4	45.5	34.7	43.6	31.1
6	12.0	52.4	68.6	68.5	72.9	59.5	67.5	48.4	35.0	45.8	31.5
7	14.0	54.9	72.9	73.7	84.4	61.5	70.4	49.5	35.4	47.5	31.9
8	16.0	58.2	79.5	80.7	89.4	64.0	74.6	51.0	36.4	50.0	32.1

TMMHP: Circular
Fluid: Iso-propanol
Temperature: ^{o}C

Inclination: 0^{o}

Sl. No.	q (Watt)	T_1	T_{1s}	T_2	T_{2s}	T_3	T_{3s}	T_4	T_{4s}	T_5	T_{5s}
1	2.0	34.7	39.1	36.8	46.3	35.1	44.9	33.1	28.9	32.0	28.9
2	4.0	36.4	45.9	41.1	54.7	37.9	48.5	35.7	30.2	34.0	29.9
3	6.0	39.9	52.6	48.2	68.8	43.1	54.7	37.5	31.1	36.9	30.5
4	8.0	44.5	68.1	59.3	72.7	50.8	71.3	40.2	31.8	39.0	30.8
5	10.0	46.7	70.4	60.1	76.1	52.3	73.9	41.1	32.0	39.9	31.0
6	12.0	48.5	72.9	63.1	77.2	54.1	75.3	42.4	32.2	40.3	31.4
7	14.0	49.9	74.4	65.9	77.9	55.4	76.9	43.8	32.9	40.8	31.9
8	16.0	54.2	79.9	69.3	87.3	57.9	78.2	45.7	33.3	42.8	32.3

Inclination: 45^{o}

Sl. No.	q (Watt)	T_1	T_{1s}	T_2	T_{2s}	T_3	T_{3s}	T_4	T_{4s}	T_5	T_{5s}
1	2.0	34.8	40.3	37.1	50.1	35.4	45.3	34.3	33.1	32.5	29.2
2	4.0	36.4	46.2	41.7	52.7	38.4	48.7	37.1	34.7	34.6	30.1
3	6.0	40.9	57.5	48.3	63.6	43.8	59.1	41.4	35.5	37.7	30.3
4	8.0	43.9	63.4	52.8	71.5	47.5	63.8	44.3	36.2	39.8	30.5
5	10.0	46.5	68.8	57.1	78.8	51	67.3	46.5	37.1	41.5	31.7
6	12.0	51.3	82.7	69.7	84.4	59.5	73.8	50.7	39.4	44.4	33.4
7	14.0	55.4	85.1	75.7	89.1	64.2	79.2	53.7	40.8	46.5	33.8
8	16.0	58.4	87.9	79.2	93.8	66.2	85.5	56.8	42.7	48.6	34.4

Inclination: 90^{o}

Sl. No.	q (Watt)	T_1	T_{1s}	T_2	T_{2s}	T_3	T_{3s}	T_4	T_{4s}	T_5	T_{5s}
1	2.0	34.0	40.1	37.6	48.5	35.3	44.7	34.0	33.2	32.2	29.0
2	4.0	34.7	41.6	42.1	52.1	37.7	48.4	37.1	34.5	32.5	30.3
3	6.0	37.0	47.5	49.1	63.1	42.3	57.5	41.7	35.1	33	31.2
4	8.0	38.0	50.2	51.9	70.3	44.2	62.7	43.3	35.8	33.3	31.8
5	10.0	41.5	56.4	57.2	78.1	48.6	66.1	46.6	36.9	34.3	32.0
6	12.0	42.8	60.1	61.7	80.2	51.2	69.4	48.6	38.2	35.6	32.6
7	14.0	45.5	65.8	66.2	82.7	54.3	72.9	51.3	39.3	36.2	33.1
8	16.0	48.0	70.5	73.4	86.4	58.6	78.6	55.2	41.5	36.8	33.8

TMMHP: Circular
Fluid: Water
Temperature: ^{o}C

Inclination: 0^{o}

Sl. No.	q (Watt)	T_1	T_{1s}	T_2	T_{2s}	T_3	T_{3s}	T_4	T_{4s}	T_5	T_{5s}
1	2.0	33.9	43.7	40.4	44.7	34.3	44.5	30.7	28.1	31.1	31.1
2	4.0	38.1	51.5	47.5	53.5	37.8	51.1	32.1	28.8	32.9	32.8
3	6.0	42.4	66.1	56.5	68.3	42.5	66.1	33.4	28.9	35.4	35.1
4	8.0	51.6	76.1	69.5	87.5	53.8	75.8	36.4	30.5	39.1	39.0
5	10.0	61.8	80.1	75.8	95.7	58.6	78.6	36.4	29.5	40.7	40.5
6	12.0	71.5	83.5	84.2	103.1	62.8	79.9	36.5	31.1	42.3	42.2
7	14.0	78.1	86.1	91.6	111.1	69.5	80.2	36.9	31.9	44.2	41.9
8	16.0	83.1	100.4	98.7	139.3	77.2	85.3	37.2	32.5	46.0	45.3

Inclination: 45^{o}

Sl. No.	q (Watt)	T_1	T_{1s}	T_2	T_{2s}	T_3	T_{3s}	T_4	T_{4s}	T_5	T_{5s}
1	2.0	32.1	42.1	37.4	43.7	31.2	40.3	29.2	28.5	29.7	29.3
2	4.0	35.8	52.0	46.7	54.8	36.4	52.3	30.0	29.5	32.2	32.1
3	6.0	42.6	68.1	61.0	70.8	43.3	68.8	31.1	30.0	35.6	35.5
4	8.0	45.7	77.0	68.1	80.2	46.6	72.6	31.6	30.3	37.3	37.1
5	10.0	49.7	83.5	80.3	94.5	52.4	75.9	33.8	31.4	39.5	39.4
6	12.0	56.0	85.7	87.2	110.3	55.2	77.2	34.3	31.9	41.3	39.9
7	14.0	65.2	90.2	93.5	121.9	59.0	79.8	35.2	32.4	43.8	42.7
8	16.0	71.1	96.7	98.3	130.5	65.2	87.7	35.7	33.4	46.3	46.1

Inclination: 90^{o}

Sl. No.	q (Watt)	T_1	T_{1s}	T_2	T_{2s}	T_3	T_{3s}	T_4	T_{4s}	T_5	T_{5s}
1	2.0	34.4	41.8	38.1	43.2	33.5	42.8	29.0	28.9	30.2	30.1
2	4.0	38.2	49.6	45.9	53.1	37.5	50.8	30.0	29.5	32.1	32.0
3	6.0	44.1	60.5	56.9	69.4	43.5	64.6	31.5	30.1	35.2	34.9
4	8.0	51.8	73.9	66.5	86.2	50.3	68.3	33.3	30.8	38.2	37.9
5	10.0	58.3	88.1	80.6	101.6	56.4	77.3	34.0	30.3	40.4	40.1
6	12.0	65.9	90.2	86.5	113.8	63.7	81.5	35.1	30.5	43.4	43.0
7	14.0	75.4	94.2	93.1	123.6	70.4	82.8	35.3	30.1	43.6	43.2
8	16.0	91.7	99.5	103.0	134.1	78.2	86.9	35.8	33.5	45.6	44.8

TMMHP: Triangular
Fluid: Ethanol
Temperature: ^{o}C

Inclination: 0^{o}

Sl. No.	q (Watt)	T_1	T_{1s}	T_2	T_{2s}	T_3	T_{3s}	T_4	T_{4s}	T_5	T_{5s}
1	2.0	34.0	45.1	36.7	55.2	28.7	31.1	24.5	24.5	24.4	22.2
2	4.0	51.4	67.8	58.3	76.5	38.0	41.1	29.8	28.3	30.0	22.4
3	6.0	58.8	71.4	68.3	81.8	46.1	53.2	33.1	29.8	33.5	22.6
4	8.0	69.2	80.2	78.6	89.8	57.1	64.8	34.5	29.9	34.3	22.7
5	10.0	71.2	83.4	85.8	95.8	63.7	71.8	34.7	30.1	34.4	22.7
6	12.0	75.4	89.8	91.1	97.3	70.4	78.6	34.8	30.2	34.5	22.8
7	14.0	82.5	94.9	97.2	102.7	74.9	82.9	41.2	33.8	34.8	22.9
8	16.0	88.8	105.4	103.4	112.2	78.5	86.6	45.5	34.1	35.1	23.2

Inclination: 45^{o}

Sl. No.	q (Watt)	T_1	T_{1s}	T_2	T_{2s}	T_3	T_{3s}	T_4	T_{4s}	T_5	T_{5s}
1	2.0	2.0	26.8	29.2	28.2	30.8	23.6	24.0	21.3	20.5	21.7
2	4.0	4.0	28.2	35.6	31.6	38.4	26.5	27.8	23.3	20.6	23.8
3	6.0	6.0	28.4	45.5	37.6	48.3	29.3	31.5	24.6	20.6	25.0
4	8.0	8.0	37.2	52.2	42.7	55.8	32.2	33.7	26.2	20.7	26.5
5	10.0	10.0	44.3	59.5	50.0	60.5	31.9	34.9	24.6	20.7	25.0
6	12.0	12.0	49.5	68.5	66.3	70.9	34.8	40.5	25.9	20.8	28.1
7	14.0	14.0	61.8	75.4	69.1	83.3	42.7	43.9	30.8	20.8	31.4
8	16.0	16.0	69.5	78.7	70.3	90.9	46.3	47.2	32.9	20.9	33.4

Inclination: 90^{o}

Sl. No.	q (Watt)	T_1	T_{1s}	T_2	T_{2s}	T_3	T_{3s}	T_4	T_{4s}	T_5	T_{5s}
1	2.0	22.1	21.4	24.1	24.8	19.9	22.2	20.5	20.1	20.2	20.1
2	4.0	24.0	25.2	29.7	31.3	25.8	26.4	23.5	20.2	22.6	20.1
3	6.0	36.5	60.1	46.4	54.2	35.6	37.4	28.4	23.0	28.1	20.1
4	8.0	35.7	65.6	50.3	59.6	38.1	40.5	30.6	24.0	29.8	20.0
5	10.0	35.9	70.6	53.3	64.0	40.1	41.6	31.5	25.1	30.2	20.1
6	12.0	38.2	76.8	57.8	69.0	41.8	43.0	33.6	25.7	31.7	20.1
7	14.0	55.1	77.9	60.8	74.6	42.4	43.8	33.7	26.9	32.5	20.0
8	16.0	56.6	80.8	67.6	85.0	45.7	48.2	37.1	28.2	34.5	20.2

TMMHP: Triangular
Fluid: Methanol
Temperature: ^{o}C

Inclination: 0^{o}

Sl. No.	q (Watt)	T_1	T_{1s}	T_2	T_{2s}	T_3	T_{3s}	T_4	T_{4s}	T_5	T_{5s}
1	2.0	39.7	56	43.1	63.2	36.4	40.1	32.6	32.4	32.1	28.6
2	4.0	45.9	70	54.6	77.8	42.1	45.2	36.0	35.2	35.3	28.8
3	6.0	54.3	84	66.7	88.9	51.4	55.5	43.0	38.0	38.9	29.9
4	8.0	58.6	91	70.5	98.8	53.4	57.8	46.6	40.2	39.8	31.0
5	10.0	60.9	97	73.6	103.5	56.7	61.5	50.4	44.8	40.5	31.2
6	12.0	63.5	103	76.0	109.4	60.8	65.4	56.8	50.7	41.3	31.5
7	14.0	65.9	109	77.6	114.6	61.3	66.2	59.6	55.7	42.0	31.8
8	16.0	68.8	117	77.2	126.2	63.2	69.8	53.0	56.5	42.3	32.0

Inclination: 45^{o}

Sl. No.	q (Watt)	T_1	T_{1s}	T_2	T_{2s}	T_3	T_{3s}	T_4	T_{4s}	T_5	T_{5s}
1	2.0	40.1	53.8	43.7	74.9	36.2	40.5	33.2	29.4	32.9	27.3
2	4.0	49.7	74.5	56.6	84.7	41.7	45.7	36.9	36.1	36.3	27.3
3	6.0	58.3	98.7	68.7	110.2	46.4	52.7	39.3	38.8	38.3	27.4
4	8.0	64.8	114.6	77.4	122.5	56.0	62.8	42.9	41.6	40.5	27.4
5	10.0	75.0	130.6	88.7	141.9	56.5	62.8	45.1	42.8	44.4	27.5
6	12.0	82.0	147.6	100.5	158.8	63.0	70.1	48.7	43.2	47.2	27.6
7	14.0	84.4	163.3	104.2	178.4	66.2	72.1	50.6	44.5	49.2	27.7
8	16.0	85.7	182.5	115.0	190.5	73.0	80.4	52.8	46.1	51.0	27.8

Inclination: 90^{o}

Sl. No.	q (Watt)	T_1	T_{1s}	T_2	T_{2s}	T_3	T_{3s}	T_4	T_{4s}	T_5	T_{5s}
1	2.0	33.1	45.0	34.8	49.8	32.4	35.9	32.5	30.4	30.4	30.3
2	4.0	37.7	57.5	39.8	61.5	34.9	38.2	33.6	31.8	32.3	31.3
3	6.0	44.5	83.5	49.2	85.4	40.3	45.6	36.1	34.0	34.4	31.8
4	8.0	46.1	99.3	55.5	108.4	43.2	49.5	36.8	35.5	35.8	34.5
5	10.0	53.0	111.7	60.5	121.6	46.0	53.6	38.8	37.8	37.0	35.7
6	12.0	56.3	127.3	70.5	139.8	51.4	58.8	39.7	39.0	40.5	36.8
7	14.0	63.8	130.5	72.4	147.8	51.8	59.1	41.4	39.2	40.1	39.3
8	16.0	66.9	134.2	75.6	157.9	54.7	64.9	41.9	39.9	41.2	40.4

TMMHP: Triangular
Fluid: Iso-Propanol
Temperature: ^{o}C

Inclination: 0^{o}

Sl. No.	q (Watt)	T_1	T_{1s}	T_2	T_{2s}	T_3	T_{3s}	T_4	T_{4s}	T_5	T_{5s}
1	2.0	22.6	22.6	25.1	27.5	20.7	21.4	19.9	18.1	20.1	21.3
2	4.0	26.6	30.1	35.9	38.3	24.2	26.1	22.9	19.0	22.9	21.2
3	6.0	27.9	36.1	46.1	48.3	28.5	29.9	25.0	19.4	25.1	21.1
4	8.0	42.5	46.9	56.1	65.1	32.1	31.0	27.1	19.8	27.2	21.1
5	10.0	49.1	55.2	65.9	74.9	35.9	35.1	28.2	20.2	28.1	21.1
6	12.0	54.2	61.2	72.2	83.7	39.1	37.8	31.7	20.5	30.2	21.1
7	14.0	57.1	67.5	73.3	80.6	40.2	40.6	29.2	20.5	28.7	21.1
8	16.0	65.3	84.9	75.3	85.9	43.1	44.6	32.0	21.2	32.1	21.1

Inclination: 45^{o}

Sl. No.	q (Watt)	T_1	T_{1s}	T_2	T_{2s}	T_3	T_{3s}	T_4	T_{4s}	T_5	T_{5s}
1	2.0	25.9	28.4	28.2	31.5	23.3	23.5	20.7	18.6	20.8	20.7
2	4.0	29.8	33.6	34.6	35.8	25.4	26.6	22.7	18.9	23.0	20.7
3	6.0	36.8	40.7	46.1	43.4	29.1	27.4	25.2	18.9	25.1	20.5
4	8.0	39.2	46.0	50.3	51.8	29.2	29.3	24.5	19.1	24.2	20.6
5	10.0	43.8	57.5	58.2	68.4	31.6	33.4	25.0	19.7	25.5	20.5
6	12.0	46.7	65.1	65.1	77.8	33.0	36.4	25.4	20.1	24.7	20.5
7	14.0	59.0	78.2	73.2	77.9	40.5	42.2	30.2	20.7	29.7	20.5
8	16.0	66.7	87.2	76.0	80.3	44.3	45.6	31.9	21.0	31.5	20.5

Inclination: 90^{o}

Sl. No.	q (Watt)	T_1	T_{1s}	T_2	T_{2s}	T_3	T_{3s}	T_4	T_{4s}	T_5	T_{5s}
1	2.0	25.3	28.3	26.3	33.3	20.6	22.3	20.3	18.7	20.1	20.2
2	4.0	29.0	33.6	31.5	41.1	23.4	23.9	21.5	18.8	21.3	20.2
3	6.0	37.5	48.9	41.9	65.3	28.1	27.8	23.3	20.4	23.3	20.2
4	8.0	40.1	54.3	46.3	71.2	30.3	28.4	23.1	21.2	22.2	20.1
5	10.0	46.6	64.7	51.6	84.9	34.8	33.8	26.9	22.5	25.6	20.2
6	12.0	53.3	81.8	59.8	90.3	35.6	37.6	30.2	25.0	28.3	20.2
7	14.0	64.3	85.3	74.3	86.5	44.7	43.3	32.8	25.2	30.2	20.1
8	16.0	67.5	85.4	74.9	91.3	48.1	44.9	34.4	26.9	34.1	20.2

TMMHP: Triangular
Fluid: Water
Temperature: ^{o}C
Inclination: 0^{o}

Sl. No.	q (Watt)	T_1	T_{1s}	T_2	T_{2s}	T_3	T_{3s}	T_4	T_{4s}	T_5	T_{5s}
1	2.0	45.3	48.6	46.6	56.3	43.3	45.3	35.6	33.2	35.6	32.0
2	4.0	49.2	56.5	52.1	66.1	46.5	49.8	37.2	33.7	37.2	32.2
3	6.0	53.3	61.8	59.7	71.9	50.5	56.1	38.8	34.1	38.8	32.3
4	8.0	56.3	66.8	65.1	77.4	54.1	61.8	39.7	34.8	39.5	32.6
5	10.0	57.5	68.9	68.5	81.5	55.1	64.4	40.3	35.2	40.1	32.9
6	12.0	60.3	71.2	73.4	86.4	57.6	69.2	41.6	35.4	41.3	33.0
7	14.0	67.9	81.8	78.2	91.4	60.6	72.4	43.4	35.8	42.6	33.1
8	16.0	75.4	88.5	84.6	98.9	64.9	79.3	45.6	36.1	45.5	33.2

Inclination: 45^{o}

Sl. No.	q (Watt)	T_1	T_{1s}	T_2	T_{2s}	T_3	T_{3s}	T_4	T_{4s}	T_5	T_{5s}
1	2.0	38.4	42.5	41.2	49.7	36.7	40.7	34.7	33.2	33.1	32.0
2	4.0	47.8	53.2	52.8	64.7	43.9	46.8	38.3	34.1	36.8	32.1
3	6.0	58.5	66.8	66.1	78.8	52.1	58.6	42.3	34.5	40.9	32.4
4	8.0	66.9	76.9	71.8	88.8	59.7	68.5	44.8	34.8	43.3	32.6
5	10.0	72.1	82.8	79.9	96.8	67.3	78.8	47.2	35.2	45.7	32.8
6	12.0	74.4	86.9	89.2	104.7	69.8	81.2	49	35.2	47.3	33.1
7	14.0	83.4	96.9	100.9	114.7	76.1	91.4	52.6	35.5	51	33.3
8	16.0	90.1	102.5	110.8	122.8	81	99.9	56.2	35.8	53.7	33.4

Inclination: 90^{o}

Sl. No.	q (Watt)	T_1	T_{1s}	T_2	T_{2s}	T_3	T_{3s}	T_4	T_{4s}	T_5	T_{5s}
1	2.0	40.2	43.2	43.5	49.5	38.4	41.4	35.7	33.2	34	32.1
2	4.0	50	55.8	56.2	64.8	46.1	50.5	39.6	33.4	37.8	32.3
3	6.0	61.8	68.8	72.3	82.8	55.4	61.6	44.8	35.4	42.4	32.6
4	8.0	69.1	78.4	82.5	95.2	61.7	68.5	47.8	35.9	45.3	32.9
5	10.0	77.1	89.4	93.1	108.8	69	76.6	51.1	36.2	48.3	33.1
6	12.0	86.6	98.6	106.1	123.1	76.7	83.8	54.9	36.5	52	33.6
7	14.0	95.4	109.4	115.7	134.5	82.5	92.8	59.3	36.9	55.2	33.9
8	16.0	104.7	119.8	119.8	140.8	89.8	95.5	66.3	37.2	59.8	34.4

TMMHP: Square
Fluid: Ethanol
Temperature: ^{o}C

Inclination: 0^{o}

Sl. No.	q (Watt)	T_1	T_{1s}	T_2	T_{2s}	T_3	T_{3s}	T_4	T_{4s}	T_5	T_{5s}
1	2.0	25.1	45.6	31.9	37.9	28.1	24.3	24.3	24.0	24.1	22.9
2	4.0	30.9	55.1	42.1	49.8	35.1	26.9	30.6	28.0	28.0	22.9
3	6.0	35.9	69.4	57.8	80.7	43.9	43.7	35.4	32.6	32.5	22.7
4	8.0	40.1	75.1	66.2	90.1	49	56.7	39.8	35.4	35.4	22.5
5	10.0	43.4	78.6	70.2	95.0	50.4	58.3	43.5	36.0	35.9	22.4
6	12.0	45.6	83.5	73.9	98.8	51.9	60.5	47.7	37.4	37.3	22.4
7	14.0	46.5	89.5	77.8	102.0	53.3	62.6	54.0	39.1	39.1	22.4
8	16.0	47.5	93.7	81.5	105.2	53.6	65.2	62.4	41.9	40.8	22.4

Inclination: 45^{o}

Sl. No.	q (Watt)	T_1	T_{1s}	T_2	T_{2s}	T_3	T_{3s}	T_4	T_{4s}	T_5	T_{5s}
1	2.0	25.0	42.4	35.0	41.0	29.6	27.8	26.0	25.6	24.3	22.0
2	4.0	33.0	47.0	57.2	61.7	36.1	32.7	31.0	30.1	29.8	21.9
3	6.0	36.2	59.8	81.6	119.3	47.4	32.9	33.3	31.7	31.4	21.6
4	8.0	39.9	67.0	92.4	136.4	52.3	35.1	35.7	33.9	33.8	22.1
5	10.0	41.6	79.9	107.3	159.3	59.9	38.3	36.8	34.5	36.8	22.3
6	12.0	43.8	86.9	123.0	171.4	67.2	41.9	41.8	39.5	39.1	22.4
7	14.0	45.6	99.3	141.1	188.1	76.4	43.8	44.8	42.1	41.9	22.3
8	16.0	50.9	107.6	153.8	198.4	81.0	66.2	48.0	46.1	45.5	21.8

Inclination: 90^{o}

Sl. No.	q (Watt)	T_1	T_{1s}	T_2	T_{2s}	T_3	T_{3s}	T_4	T_{4s}	T_5	T_{5s}
1	2.0	26.3	44.7	35.3	42.1	26.1	30.9	26.8	27.2	22.4	21.0
2	4.0	30.0	59.8	44.9	55.1	31.3	36.5	29.8	33.0	25.4	21.3
3	6.0	35.0	77.5	56.4	70.3	37.2	43.4	35.5	39.7	33.7	21.3
4	8.0	36.8	129.8	61.9	84.9	36.8	51.4	34.6	40.1	33.5	21.2
5	10.0	42.6	156.7	73.7	101.7	41.8	61.0	40.2	45.9	37.2	21.3
6	12.0	47.8	179.4	86.3	120.7	47.4	72.5	45.9	50.2	41.1	21.2
7	14.0	57.3	184.8	97.0	133.7	50.3	79.3	49.4	57.3	43.8	21.0
8	16.0	72.4	190.8	101.3	130.9	53.1	86.1	49.8	60.8	44.7	21.0

TMMHP: Square
Fluid: Methanol
Temperature: ^{o}C

Inclination: 0^{o}

Sl. No.	q (Watt)	T_1	T_{1s}	T_2	T_{2s}	T_3	T_{3s}	T_4	T_{4s}	T_5	T_{5s}
1	2.0	27	40.4	27.4	33.3	24.2	22.6	21.1	20.8	20.4	19.8
2	4.0	35.3	46.9	36.0	60.8	29.5	27.0	24.9	23.6	23.1	19.8
3	6.0	42.7	59.2	45.8	75.9	36.4	31.8	28.4	27.2	26.6	19.8
4	8.0	48.3	69.0	52.4	84.5	42.8	38.1	31.1	30.0	28.8	19.8
5	10.0	51	72.3	56.0	88.7	45.7	43.8	33.1	31.7	30.2	19.8
6	12.0	53.3	78.9	61.0	97.7	50.8	51.3	37.5	34.9	32.5	19.8
7	14.0	55.5	53.0	64.7	101.8	54.9	57.0	41.1	37.5	33.5	19.7
8	16.0	59.7	82.5	68.1	106.9	52.2	59.9	45.2	40.2	35.3	19.7

Inclination: 45^{o}

Sl. No.	q (Watt)	T_1	T_{1s}	T_2	T_{2s}	T_3	T_{3s}	T_4	T_{4s}	T_5	T_{5s}
1	2.0	24.1	28.4	28.0	40.7	23.4	22.7	20.7	20.5	20.0	19.5
2	4.0	30.0	36.4	36.3	59.6	26.9	26.5	23.5	23.1	22.5	19.3
3	6.0	34.4	52.4	44.3	81.5	32.2	30.1	25.7	25.3	24.5	19.2
4	8.0	37.1	59.5	49.0	94.4	35.5	32.4	30.6	27.3	25.9	19.5
5	10.0	47.9	59.3	59.3	111.3	40.0	37.9	36.8	31.5	29.6	19.5
6	12.0	54.1	66.2	67.5	130.5	45.8	52.1	42.3	34.3	33.2	19.4
7	14.0	62.5	91.5	80.2	165.3	59.3	54.0	38.3	36.7	35.4	19.4
8	16.0	72.7	105.8	84.6	172.2	63.0	54.6	39.2	37.6	35.6	19.4

Inclination: 90^{o}

Sl. No.	q (Watt)	T_1	T_{1s}	T_2	T_{2s}	T_3	T_{3s}	T_4	T_{4s}	T_5	T_{5s}
1	2.0	26.9	39.9	28.1	48.4	26.9	24.1	26.1	25.8	23.4	19.3
2	4.0	30.4	33.6	34.7	56.3	30.7	28.4	26.3	25.2	23.2	19.3
3	6.0	39.7	46.8	45.5	82.2	32.4	30.0	27.5	26.0	25.2	19.3
4	8.0	46.3	53.2	52.8	91.1	35.0	33.8	28.8	27.2	26.2	19.2
5	10.0	53.2	75.2	58.3	116.2	37.4	34.4	30.1	29.7	28.6	19.2
6	12.0	59.4	79.7	69.8	126.4	40.6	37.6	34.3	32.6	31.0	19.2
7	14.0	67.1	80.4	72.1	149.8	48.0	45.0	39.7	36.7	35.1	19.2
8	16.0	73.6	84.3	78.2	167.8	52.7	48.7	42.7	39.2	37.3	19.1

TMMHP: Square
Fluid: Iso-Propanol
Temperature: ^{o}C

Inclination: 0^{o}

Sl. No.	q (Watt)	T_1	T_{1s}	T_2	T_{2s}	T_3	T_{3s}	T_4	T_{4s}	T_5	T_{5s}
1	2.0	26.1	30.6	27.8	36.0	25.2	24.0	23.7	23.5	23.5	23.3
2	4.0	29.6	37.9	32.2	46.1	28.1	26.3	25.0	24.7	24.6	23.5
3	6.0	34.1	47.8	39.3	61.8	32.9	30.0	27.3	27.0	26.8	23.5
4	8.0	37.5	60.1	46.4	73.7	36.6	34.2	29.6	29.1	28.8	23.4
5	10.0	43.9	69.9	53.4	79.9	38.6	38.3	31.9	30.9	30.8	23.4
6	12.0	44.4	76.0	60.8	84.8	41.2	45.3	34.9	33.8	33.0	23.2
7	14.0	48.5	84.2	66.8	90.1	43.5	53.7	37.4	34.5	35.3	23.4
8	16.0	52.1	90.3	72.6	96.7	46.9	59.2	40.5	37.4	37.5	23.6

Inclination: 45^{o}

Sl. No.	q (Watt)	T_1	T_{1s}	T_2	T_{2s}	T_3	T_{3s}	T_4	T_{4s}	T_5	T_{5s}
1	2.0	25.2	35.7	26.0	26.9	23.9	23.5	22.5	22.4	22.2	25.2
2	4.0	26.4	42.7	29.1	31.6	24.9	24.3	22.8	21.4	22.4	26.4
3	6.0	29.1	52.8	32.8	37.5	26.9	26.1	24.1	22.2	23.7	29.1
4	8.0	32.1	62.8	36.7	43.2	29.2	28.1	25.4	22.7	24.9	32.1
5	10.0	35.9	68.4	40.7	48.0	31.5	30.5	26.8	23.8	26.1	35.9
6	12.0	39.1	78.2	45.2	55.0	34.7	33.1	28.1	23.6	27.4	39.1
7	14.0	42.2	86.0	48.6	59.1	36.6	35.1	29.3	24.2	28.5	42.2
8	16.0	44.8	94.5	52.8	65.2	38.9	37.0	30.6	24.4	29.7	44.8

Inclination: 90^{o}

Sl. No.	q (Watt)	T_1	T_{1s}	T_2	T_{2s}	T_3	T_{3s}	T_4	T_{4s}	T_5	T_{5s}
1	2.0	23.1	24.2	24.8	31.0	22.6	21.8	21.8	20.3	20.7	21.4
2	4.0	25.8	27.2	26.9	37.2	23.3	22.3	21.4	20.6	21.2	21.4
3	6.0	30.9	30.9	32.1	50.5	25.9	24.9	23.2	22.9	23.0	21.3
4	8.0	35.1	35.1	35.6	58.9	27.8	26.7	24.5	23.5	24.1	21.3
5	10.0	38.9	37.8	39.1	66.6	29.8	28.7	25.7	24.1	25.4	21.2
6	12.0	42.7	38.7	44.1	77.2	32.7	32.0	27.4	25.3	27.2	21.1
7	14.0	45.3	43.0	48.6	86.6	35.3	34.2	28.8	25.7	28.5	21.1
8	16.0	50.3	47.4	54.0	95.4	38.3	37.1	30.7	26.9	30.3	21.1

TMMHP: Square
Fluid: Water
Temperature: ^{o}C

Inclination: 0^{o}

Sl. No.	q (Watt)	T_1	T_{1s}	T_2	T_{2s}	T_3	T_{3s}	T_4	T_{4s}	T_5	T_{5s}
1	2.0	30.0	34.2	32.5	38.6	25.2	28.7	24.2	23.0	22.8	19.5
2	4.0	38.1	48.1	42.8	53.7	30.6	36.4	29.5	27.0	27.0	19.5
3	6.0	47.6	64.2	55.2	71.0	37.2	45.4	35.6	31.8	32.0	19.5
4	8.0	60.3	81.8	71.1	79.7	45.1	59.3	42.7	37.3	37.4	19.5
5	10.0	68.2	97.8	85.6	87.9	51.8	73.2	45.38	40.5	40.6	19.5
6	12.0	73.4	118.6	96.4	96.2	56.3	93.8	52.4	43.8	48.0	19.4
7	14.0	78.3	148.8	110.2	118.1	72.8	132.7	59.3	53.8	53.3	18.9
8	16.0	85.8	162.8	119.3	139.5	76.2	147.7	61.7	57.2	57.2	18.9

Inclination: 45^{o}

Sl. No.	q (Watt)	T_1	T_{1s}	T_2	T_{2s}	T_3	T_{3s}	T_4	T_{4s}	T_5	T_{5s}
1	2.0	26.8	35.2	29.3	38.8	26.0	21.4	22.4	21.1	21.1	19.2
2	4.0	35.6	51.2	40.9	57.9	34.3	25.9	27.7	26.2	25.5	19.2
3	6.0	46.4	71.4	54.5	109.1	44.2	31.4	34.6	32.0	31.0	19.3
4	8.0	57.8	92.1	69.9	122.4	55.6	38.7	40.8	38.1	36.3	19.3
5	10.0	69.0	117.4	83.5	148.0	64.9	44.7	54.8	44.6	42.9	19.2
6	12.0	118.1	124.8	115.4	162.9	72.5	65.3	57.9	46.0	47.7	19.1
7	14.0	129.7	131.5	125.5	175.8	80.1	76.8	60.6	48.1	54.4	19.0
8	16.0	139.2	165.5	134.2	185.2	85.5	86.8	66.4	56.3	61.6	19.1

Inclination: 90^{o}

Sl. No.	q (Watt)	T_1	T_{1s}	T_2	T_{2s}	T_3	T_{3s}	T_4	T_{4s}	T_5	T_{5s}
1	2.0	29.6	32.0	38.8	40.3	27.9	26.1	24.0	23.0	23.1	18.7
2	4.0	35.2	45.5	57.6	59.8	37.8	29.7	29.9	28.3	28.4	18.7
3	6.0	44.8	61.3	89.6	112.4	53.8	34.9	34.7	34.0	34.1	18.6
4	8.0	46.2	76.1	110.7	128.6	65.3	39.8	37.2	35.0	35.1	18.6
5	10.0	49.8	87.6	134.0	145.6	79.7	42.1	41.4	37.0	36.9	18.6
6	12.0	53.1	95.6	147.8	156.2	93.7	45.5	44.4	39.4	39.3	18.5
7	14.0	58.0	106.8	166.0	172.0	109.2	50.4	49.8	42.9	42.4	18.5
8	16.0	62.9	117.3	180.2	187.2	132.6	54.6	54.1	45.2	45.1	18.5

TMMHP: Convergent-Divergent
Fluid: Ethanol
Temperature: ^{o}C

Inclination: 0^{o}

Sl. No.	q (Watt)	T_1	T_{1s}	T_2	T_{2s}	T_3	T_{3s}	T_4	T_{4s}	T_5	T_{5s}
1	2.0	33.2	42.3	36.2	41.9	32.4	32.1	29.7	26.1	30.3	25.2
2	4.0	40.9	52.4	47.1	54.3	41.2	42.7	32.9	26.6	33.0	25.3
3	6.0	49.4	66.1	58.1	67.8	52.5	50.3	37.9	28.6	42.3	25.3
4	8.0	55.6	68.9	60.0	70.2	57	53.3	39.3	31.3	47.7	25.4
5	10.0	59.5	70.8	62.5	71.6	58.9	55.9	40.2	31.7	49.4	25.4
6	12.0	62.8	75.5	69.1	80.8	63.9	58.6	42.1	36.6	53.8	25.4
7	14.0	65.5	79.1	73.7	84.9	67.2	61.1	43.6	37.5	56.5	25.5
8	16.0	72.2	86.7	77.8	87.8	70.5	64.5	45.9	38.5	59.7	25.6

Inclination: 45^{o}

Sl. No.	q (Watt)	T_1	T_{1s}	T_2	T_{2s}	T_3	T_{3s}	T_4	T_{4s}	T_5	T_{5s}
1	2.0	33.1	40.3	35.6	41.6	31.8	31.0	29.0	24.6	29.2	24.7
2	4.0	39.5	53.1	43.4	53.5	37	36.4	31.9	24.8	32.2	24.8
3	6.0	51.2	70.9	61.0	73.5	55.4	55.0	32.8	25.4	38.3	24.9
4	8.0	57.0	78.0	67.2	109.1	60.6	60.5	38.5	25.7	40.5	24.9
5	10.0	71.5	84.4	75.8	120.0	72.4	70.9	42.1	26.6	46.8	24.9
6	12.0	73.5	91.7	79.1	128.9	74.1	73.1	43.4	27.7	49.7	25.0
7	14.0	75.6	96.3	86.5	141.6	78.1	75.9	45.0	28.5	50.0	25.1
8	16.0	77.8	98.6	87.8	172.5	80.1	77.8	46.6	29.4	52.9	25.1

Inclination: 90^{o}

Sl. No.	q (Watt)	T_1	T_{1s}	T_2	T_{2s}	T_3	T_{3s}	T_4	T_{4s}	T_5	T_{5s}
1	2.0	29.1	40.4	33.7	50.0	29.8	29.8	26.9	24.1	27.1	24.0
2	4.0	32.9	55.2	41.8	75.0	35.3	33.9	29.5	24.2	29.8	24.1
3	6.0	38.8	70.5	51.3	100.3	39.4	39.4	32.8	24.4	33.2	24.1
4	8.0	48.7	78.0	59.1	112.2	43.5	43.9	35.3	24.9	36.1	24.2
5	10.0	59.5	95.4	70.1	141.2	60.3	53.5	40.5	25.2	41.4	24.5
6	12.0	74.6	97.8	85.1	146.3	76.7	69.2	43.9	26.7	46.9	24.5
7	14.0	77.6	100.9	86.9	164.4	78.9	78.1	46.2	28.4	51.1	24.5
8	16.0	80.3	112.9	90.3	195.5	81.8	82.2	48.8	31.0	56.3	24.5

TMMHP: Convergent-Divergent
Fluid: Methanol
Temperature: ^{o}C

Inclination: 0^{o}

Sl. No.	q (Watt)	T_1	T_{1s}	T_2	T_{2s}	T_3	T_{3s}	T_4	T_{4s}	T_5	T_{5s}
1	2.0	35.6	49.5	40.7	51.9	37.1	34.7	31.0	30.7	31.7	25.5
2	4.0	41.8	64.1	65.9	69.3	50.3	45.3	38.8	35.0	39.8	25.6
3	6.0	46.6	80.1	76.6	104.6	54.6	48.6	42.6	36.2	43.9	25.7
4	8.0	53.8	93.2	83.4	145.7	64.3	58.5	44.8	40.0	45.8	25.7
5	10.0	61.8	96.6	88.8	171.9	69.8	62.5	48.7	42.4	51.9	25.7
6	12.0	66.0	104.6	89.7	199.4	73.5	66.2	53.3	45.2	55.1	25.8
7	14.0	72.5	117.7	89.8	212.8	76.1	69.3	57.1	47.3	61.1	25.9
8	16.0	--	--	--	--	--	--	--	--	--	--

Inclination: 45^{o}

Sl. No.	q (Watt)	T_1	T_{1s}	T_2	T_{2s}	T_3	T_{3s}	T_4	T_{4s}	T_5	T_{5s}
1	2.0	32.7	38.9	35.9	51.8	33.1	33.4	30.3	30.3	31.1	25.3
2	4.0	37.2	49.9	41.9	66.1	37.2	38.8	32.7	32.6	34.2	25.3
3	6.0	40.7	65.0	55.6	75.4	46.6	42.1	37.0	37.9	39.9	25.3
4	8.0	43.3	76.8	57.3	93.3	48.3	45.8	38.3	39.0	42.1	25.4
5	10.0	51.2	108.8	68.3	125.9	57.7	59.9	42.2	42.0	46.2	25.4
6	12.0	59.2	131.6	77.2	136.1	66	61.5	45.0	45.0	49.6	25.4
7	14.0	69.2	158.8	86.9	173.2	75.1	69.8	49.0	48.6	53.7	25.5
8	16.0	84.7	189.8	124.7	199.9	90.5	79.8	57.2	55.9	61.5	25.6

Inclination: 90^{o}

Sl. No.	q (Watt)	T_1	T_{1s}	T_2	T_{2s}	T_3	T_{3s}	T_4	T_{4s}	T_5	T_{5s}
1	2.0	29.1	51.6	32.9	55.2	30.3	28.9	28.2	28.4	28.5	24.8
2	4.0	33.8	61.7	38.9	62.7	33.9	34.6	31.8	32.7	32.8	24.8
3	6.0	40.9	68.7	51.3	88.2	37.5	41.5	36.6	37.6	39.0	24.9
4	8.0	47.8	72.8	65.9	98.5	40.9	44.2	37.5	36.9	43.9	24.9
5	10.0	50.7	80.5	77.1	113.4	42.9	53.6	41.0	41.0	46.9	24.9
6	12.0	55.6	92.8	80.8	151.8	47	55.6	43.5	43.6	48.9	24.9
7	14.0	60.5	102.5	89.3	166.8	50.1	58.8	45.7	45.8	49.7	24.9
8	16.0	62.4	112.5	97.7	193.9	53.6	62.3	47.7	48.3	52.0	24.9

TMMHP: Convergent-Divergent
Fluid: Iso-Propanol
Temperature: ^{o}C

Inclination: 0^{o}

Sl. No.	q (Watt)	T_1	T_{1s}	T_2	T_{2s}	T_3	T_{3s}	T_4	T_{4s}	T_5	T_{5s}
1	2.0	35.6	50.0	41.7	56.0	36.6	32.2	31.0	30.9	31.2	27.3
2	4.0	42.2	57.1	49.9	65.1	42.7	40.5	34.0	30.4	34.5	27.2
3	6.0	52.0	75.9	67.0	87.2	54.6	49.4	40.2	32.0	41.8	27.2
4	8.0	54.9	79.2	73.1	127.7	60.1	50.9	40.5	33.1	41.5	27.2
5	10.0	63.9	91.2	78.0	157.8	64.1	55.6	44.1	33.6	45.3	27.2
6	12.0	69.6	112.0	86.8	172.7	71.7	58.2	46.9	30.7	49.2	27.2
7	14.0	74.3	117.5	87.7	185.5	75.9	59.9	48.5	31.8	50.0	27.2
8	16.0	77.1	144.5	104.2	192.7	76.8	64.4	53.1	32.5	54.5	27.2

Inclination: 45^{o}

Sl. No.	q (Watt)	T_1	T_{1s}	T_2	T_{2s}	T_3	T_{3s}	T_4	T_{4s}	T_5	T_{5s}
1	2.0	31.9	43.6	33.1	45.1	31.5	30.6	29.5	26.4	29.9	26.4
2	4.0	37.9	60.4	40.2	70.3	36.7	36.2	30.5	27.2	31.7	26.4
3	6.0	43.5	86.1	47.0	94.9	40	38.5	33.8	27.5	34.5	25.7
4	8.0	53.6	94.9	58.1	130.7	48.5	43.8	44.2	27.8	45.2	26.3
5	10.0	61.2	135.3	62.5	147.9	57.8	56.1	46.8	29.9	47.5	26.3
6	12.0	62.0	147.7	68.2	167.8	59.4	61.4	49.1	30.3	51.3	29.3
7	14.0	68.5	170.2	80.6	188.6	68.7	64.7	50.1	32.1	53.5	29.8
8	16.0	74.8	197.7	90.1	200.4	77.3	68.5	53.6	32.3	55.2	30.2

Inclination: 90^{o}

Sl. No.	q (Watt)	T_1	T_{1s}	T_2	T_{2s}	T_3	T_{3s}	T_4	T_{4s}	T_5	T_{5s}
1	2.0	32.2	31.4	33.8	45.3	28.2	26.7	28.1	26.4	29.6	26.0
2	4.0	36.5	47.8	39.7	48.5	33.7	28.7	31.5	27.9	32.6	26.1
3	6.0	38.5	51.8	45.8	62.5	38.5	35.7	35.6	27.5	36.6	26.2
4	8.0	39.1	68.8	51.1	78.1	43.6	41.2	39	27.5	37.7	26.2
5	10.0	43.9	76.4	55.1	81.9	47.2	49.6	41.9	28.1	42.1	26.3
6	12.0	47.9	80.8	60.8	88.6	51.5	50.3	42.1	29.9	44	26.3
7	14.0	51.1	82.8	63.8	93.3	54	51.9	42.3	30.2	45.8	26.4
8	16.0	60.8	85.2	72.2	95.2	62.7	53.9	45.1	30.3	48.8	26.5

TMMHP: Convergent-Divergent
Fluid: Water
Temperature: ^{o}C

Inclination: 0^{o}

Sl. No.	q (Watt)	T_1	T_{1s}	T_2	T_{2s}	T_3	T_{3s}	T_4	T_{4s}	T_5	T_{5s}
1	2.0	45.8	53.7	52.9	54.2	48.4	47.4	34.1	33.1	34.3	26.2
2	4.0	50.1	58.1	58.5	58.9	52.7	54.1	35.8	35.1	36.3	26.3
3	6.0	55.0	62.4	62.0	63.4	56.9	56.5	38.2	37.1	38.6	26.3
4	8.0	59.7	67.5	66.9	72.1	61.1	61.8	39.7	37.5	40.6	26.4
5	10.0	65.1	73.5	72.4	78.9	65.7	64.7	41.4	39.8	42.1	26.4
6	12.0	70.9	80.1	78.0	86.1	70.4	71.6	44.2	41.2	44.8	26.5
7	14.0	77.3	90.5	81.6	100.3	75.1	73.6	45.6	43.1	45.9	26.5
8	16.0	--	--	--	--	--	--	--	--	--	--

Inclination: 45^{o}

Sl. No.	q (Watt)	T_1	T_{1s}	T_2	T_{2s}	T_3	T_{3s}	T_4	T_{4s}	T_5	T_{5s}
1	2.0	33.4	41.5	37.5	45.2	34.3	31.6	30.5	25.4	30.6	26.6
2	4.0	43.1	56.5	47.3	60.2	41.4	37.3	33.2	30.5	34.0	27.4
3	6.0	55.6	75.8	66.7	88.2	62.4	51.3	37.1	34.2	38.1	27.5
4	8.0	70.5	89.8	74.2	94.4	71.4	57.1	39.2	35.3	41.5	27.5
5	10.0	87.6	98.9	89.6	125.8	85.0	67.4	44.9	36.5	46.9	27.5
6	12.0	100.2	104.7	107.9	146.0	91.2	72.8	48.1	38.0	50.9	27.5
7	14.0	106.7	136.9	111.1	157.3	93.0	87.1	49.9	39.5	51.6	27.6
8	16.0	112.5	184.3	117.1	167.7	95.6	88.6	51.5	42.1	55.6	27.6

Inclination: 90^{o}

Sl. No.	q (Watt)	T_1	T_{1s}	T_2	T_{2s}	T_3	T_{3s}	T_4	T_{4s}	T_5	T_{5s}
1	2.0	34.7	44.7	36.6	57.3	32.5	31.1	27.8	27.1	28.6	26.2
2	4.0	39.8	58.9	43.0	83.7	37.7	34.8	29.4	27.2	30.6	26.2
3	6.0	55.2	86.1	60.2	129.3	48.3	44.1	33.7	31.2	36.0	26.3
4	8.0	65.8	101.0	71.8	153.7	56.7	51.3	36.3	32.5	37.1	26.3
5	10.0	78.1	113.7	83.6	184.9	71.6	61.3	40.1	38.4	44.3	26.4
6	12.0	80.2	122.5	89.3	188.9	83.0	74.0	42.8	40.0	46.1	26.5
7	14.0	86.2	128.6	99.4	192.5	87.5	82.8	45.5	43.2	52.5	26.5
8	16.0	89.1	138.2	100.1	198.8	90.7	84.2	47.2	45.2	56.1	26.6

Appendix A-2

Data and Plots from Validation Experiment [25]

SMMHP: Circular, Metal: Copper, Fluid: Ethanol, Temperature: ^{o}C
Inclination: 30^{o}

Sl. No.	q (Watt)	T_1	T_{1s}	T_2	T_{2s}	T_3	T_{3s}	T_4	T_{4s}	T_5	T_{5s}
1	0.61	43.4	45.8	42.5	43.9	42.3	42.1	41.4	40.3	34.2	33.1
2	1.56	46.6	48.7	44.6	42.8	43.2	42.4	35.7	33.8	30.6	28.2
3	3.67	52.1	57.3	47.1	47.8	46	45.8	39.9	37.6	32.2	30.9
4	8.71	66.4	78.1	56.8	57.4	56.1	55.7	55.4	52.5	47.5	46.1

Inclination: 50^{o}

Sl. No.	q (Watt)	T_1	T_{1s}	T_2	T_{2s}	T_3	T_{3s}	T_4	T_{4s}	T_5	T_{5s}
1	0.61	36.6	38.8	35.9	35.3	35.5	34.9	35.2	33.7	30.6	28.5
2	1.56	44.5	48	39.2	40.8	38.1	37.5	36.2	35.2	31.3	28.9
3	3.67	49.8	51.9	46.4	48.5	44.6	45.2	40.8	38.5	32.5	30.6
4	8.71	66.1	68.1	60	64.7	58.2	57.8	52.6	48.2	47.8	46.6

Inclination: 70^{o}

Sl. No.	q (Watt)	T_1	T_{1s}	T_2	T_{2s}	T_3	T_{3s}	T_4	T_{4s}	T_5	T_{5s}
1	0.61	37.8	39.4	36.1	37	35.8	35.2	35.2	33.6	32.6	30.8
2	1.56	46.1	54.1	40.2	39.9	38.9	37.1	37.5	34.2	33.4	31.8
3	3.67	58.8	65.1	49.8	46.8	46.3	43.2	42.7	39.6	35.9	33.5
4	8.71	63.9	76.5	55.9	57.4	55	53.2	53.2	52.5	48.2	46.1

Inclination: 90^{o}

Sl. No.	q (Watt)	T_1	T_{1s}	T_2	T_{2s}	T_3	T_{3s}	T_4	T_{4s}	T_5	T_{5s}
1	0.61	34.7	36.6	32.9	33.4	32.7	32.4	32.4	30.2	30.3	28.1
2	1.56	37.1	40.5	36.1	37.5	35.8	35.2	33.6	31.4	31.7	29.1
3	3.67	50.3	54.8	45.1	46.4	44.6	42.8	36.4	32.8	33.9	31.5
4	8.71	63.2	70.5	57	60.1	56.1	54.8	52.7	48	44.4	42.1

Appendix B

Performance Parameters and Data Reduction

Positions of thermocouples on the TMMHP

There are ten K-type thermocouples attached with the TMMHP at different locations as those are shown in the Fig. App-B.1.

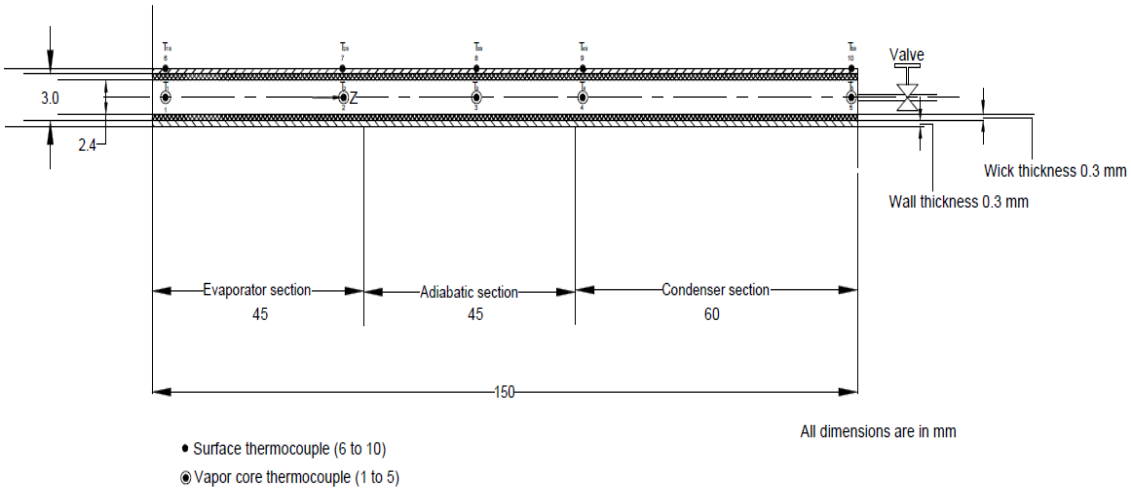

Figure App-B.1: Positions of thermocouples along the TMMHP

T_1, T_2 = temperature of sat.vapor

T_3 = temp. of sat. vapor in adiab. sect.

T_4, T_5 = temperature of the condensate

T_{1s}, T_{2s} = surface temp. of the evaporator

T_{3s} = surface temp. of the adiabatic section

T_{4s}, T_{5s} = surface temp. of the condenser

Thermal performances of TMMHPs are measured by heat transfer coefficient, *h*, obtained by using Newton's law of cooling. Then the values of *h* are cross checked by measuring, h_{eff} , and the thermal resistance, R_{eff} , of the system. The value of *h* indicates the overall heat transfer capability of the fluid calculated from the internal working fluid's terminal temperature difference between evaporator and condenser. Thus the *h* may also be considered the overall heat transfer coefficient for the respective fluid.

Then h_{eff} of the fluid is calculated by taking the average temperature of the evaporator and condenser respectively. Similarly, the heat transfer coefficients at the evaporator and condenser, h_e and h_c, can be calculated, which are shown below.

I. $h = \frac{q}{A_e(T_1 - T_5)}$ $kW/m^2.^oC$

II. $h_{eff} = \frac{q}{A_e(T_e - T_c)}$ $kW/m^2.^oC$

III. $h_e = \frac{q}{A_e(T_e - T_{sat})}$ $kW/m^2.^oC$

IV. $h_c = \frac{q}{A_c(T_{sat} - T_c)}$ $kW/m^2.^oC$

V. $U = \frac{q}{A_e(T_{es} - T_{cs})}$ $kW/m^2.^oC$

Thermal resistance is inversely related to the heat transfer coefficient. R_{eff} is calculated by using the following equation.

$$R_{eff} = \frac{T_e - T_c}{q} \quad {}^oC/W$$

Heat transfer through the shell of the heat pipe is calculated by using the conduction equation, $q = -k\frac{\Delta T}{\Delta l}$ W/m^2

And the heat transfer by coolant water at the condenser is calculated by using the energy equation $q_{c,s} = \dot{m}c_{p,w}(T_{w,c} - T_{w,\infty})/A_c$ W/m^2

Effective temperatures at evaporator and condenser are calculated from the average values at each respectively, and the steps are as follows.

I. $T_e = \frac{T_1 + T_2}{2}$

II. $T_c = \frac{T_4 + T_5}{2}$

Similarly, the effective length is calculated as follows.

$$l_{eff} = l_a + \frac{l_e + l_c}{2}$$

All the effective performance and thermal parameters are calculated by using the average values. The dimensional correlation coefficient, $\frac{d_H}{d_T}$, and the orientation coefficient, $sin\theta cos\theta$, are chosen by trial and error method using the trends of the experimental data.

Appendix C

Calibration of Ammeter, Voltmeter and Thermocouples (K-type)

In measuring heat input to the evaporator one ammeter and one voltmeter, and in measuring temperatures, a digital thermometer fitted with K-type thermocouple is used. Following are the calibration data on ammeter, voltmeter and thermocouple respectively.

Ammeter, Type: Digital
Full scale deflection: 20 A

Voltmeter, Type: Digital
Full scale deflection: 600V

Table. App-C.1 Standard and measured current

Std. Current. (A)	Mesd. Current (A)
1.9	2.00
2	2.10
2.25	2.30
2.85	2.90
3.2	3.29
3.9	4.10
4.3	4.40
4.7	4.85
5.1	5.25
5.3	5.38

Table App-C.2 Standard and measured voltage

Std. Voltage (V)	**Mesd. Voltage (V)**
80	74
100	91
120	112
130	122
150	141
160	152
170	161
180	168
200	185
250	231

Table. App-C.1 contains the standard and measured current data.

Table. App-C.2contains the standard and measured voltage data.

Thermocouple, Type: K (90% Ni, 10% Cr)

Thermocouple is a device to measure temperature of a system by attaching it to a digital thermometer. An electromagnetic force (emf) is generated in the circuit of dissimilar materials of thermocouples when the junctions are submerged in the sources of different temperature. This emf can be related to temperature of the junction. Ten sets of K-type thermocouples are used in this experiment. The schematic view of the

thermocouple calibration circuit is shown in Fig. App-C.3. Then keeping the cold or reference junction at constant ice-cold temperature, the temperature of hot junction is gradually raised to the boiling-hot temperature using water heater. The emf is measured for each step of heat addition to the hot junction. Table App-C.3 shows the values of emf as follows.

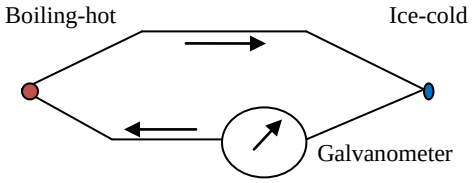

Figure App-C.3 Thermocouple calibration circuit

Table App-C.3 Comparison of Th. Temp. with TC Table Temp.

Emf (mV)	Th. Temp. ^{o}C	TC Table Temp. ^{o}C
1.201	30	29.95
1.689	42	41.90
2.101	52	51.90
3.179	78	77.92
4.091	100	99.90

Note. Digital thermometer is found to be with almost 0% error.

Appendix D

Uncertainty Analysis for TMMHP

Statistical analysis of an experiment requires multi-sample test, and the data are collected by multiple observations using many similar but different equipment. Hence, the experiment becomes more expensive and time consuming. However, this experiment is typically developed on a two different conductivity metal (Cu-Ag) tube which contains the working fluid to transfer heat by *boiling and condensation* mode wherein convective heat transfer coefficient, *h,* plays the most important role. Therefore, this kind of single-sample experiment can be evaluated from the uncertainties developed in operating parameters and field variables that are measured by different equipment. In solving the errors developed within the equipment (bias or systematic errors), calibrations are done for ammeter and voltmeter as well as for thermocouples with digital thermometer. The eye-estimation errors (random errors) in measuring the length and thickness of the tube are also considered in the uncertainty analysis. To minimize the errors developed from geometrical varieties, and the errors in using a common hydraulic diameter are included in the analysis. Finally the collected data are processed through different data reduction methods to reach the final result. The effort ends in finding convective heat transfer coefficient to check the cumulative uncertainties by percent. However, uncertainties can be expressed in three ways: relative uncertainties, standard uncertainties and expanded uncertainties. Following is the details of the procedure used in this case, Uhia, F. J. *et al*. [45] and Coleman and Steele [46]. According to Kline and McClintock [47] the total uncertainty propagation for $r = f(v_{j=1\ldots n})$ is summarized in *eqn. 1* which is commonly used in calculating the related uncertainties in any experiment.

$$u(r) = \sqrt{\sum_{j=1}^{n} [\frac{\partial r}{\partial v_j} u(v_j)]^2} \ldots\ldots\ldots (1)$$

Here, *u* stands for the standard uncertainty, which is equivalent to the standard deviation, and v_j stands for the variables that contribute to the uncertainty in the result *r*

that revolves around any data reduction equation. To calculate the uncertainty for individual quantities, the equation needs to be expanded. Now squaring both sides and then dividing each term by r^2 and multiplying right hand side with $\left(\frac{X_i}{X_i}\right)^2$ yields a non-dimensional equation which is shown in *eqn. 2* [46].

$$\left(\frac{U_r}{r}\right)^2 = \left(\frac{X_1}{r}\frac{\partial_r}{\partial X_1}\right)^2 \left(\frac{U_{X_1}}{X_1}\right)^2 + \left(\frac{X_2}{r}\frac{\partial_r}{\partial X_2}\right)^2 \left(\frac{U_{X_2}}{X_2}\right)^2 + \cdots (2)$$

where,

$\frac{U_r}{r}$ = relative uncertainty in the result

$\frac{\partial_r}{\partial X_1}$ = sensitivity coefficient (SC)

$\left(\frac{X_1}{r}\frac{\partial_r}{\partial X_1}\right)$ = uncertainty magnification factors (UMFs)

$\frac{U_{X_1}}{X_1}$ = relative uncertainty of each variable

By substituting the UMFs into *eqn. 2* and simplifying, the equation becomes

$$\left(\frac{U_r}{r}\right)^2 = \left(\frac{U_{X_1}}{X_1}\right)^2 + \left(\frac{U_{X_2}}{X_2}\right)^2 + \cdots (3)$$

The *eqn. 3* relates the relative uncertainty of the results with the uncertainties of measured variables which affect the results.

The convective heat transfer coefficient *h* is defined by the Newton's law of cooling,

$$q = hA(T_w - T_\infty) \ldots\ldots\ldots\ldots (4)$$

where the subscript *w* and ∞ indicates wall and faraway distance from the surface of interest. As it is seen, $h = f(q, T, A)$, then with respect to the *eqn. 4*, *eqn. 3* will take a look like the following equations as *eqn. 5*, *eqn. 6*, *eqn. 7* and *eqn. 8*.

$\left(\frac{U_q}{q}\right)^2 = \left(\frac{U_V}{V}\right)^2 + \left(\frac{U_A}{A}\right)^2 \ldots\ldots (5)$ where *V* for volts and *A* for amperes.

$\left(\frac{U_T}{T}\right)^2 = \left(\frac{U_{Tc}}{Tc}\right)^2 + \left(\frac{U_{Dt}}{Dt}\right)^2 \ldots\ldots (6)$ where *Tc* for thermocouple and *Dt* for digital thermometer to indicate ^oC.

$$\left(\frac{U_A}{A}\right)^2 = \left(\frac{U_d}{d_h}\right)^2 + \left(\frac{U_l}{l}\right)^2 \dots\dots(7)$$ where d_h for hydraulic diameter and l for length of the tube in meter *(m)* and π is assumed to have no error.

$$\left(\frac{U_h}{h}\right)^2 = \left(\frac{U_q}{q}\right)^2 + \left(\frac{U_T}{T}\right)^2 + \left(\frac{U_A}{A}\right)^2 \dots\dots\dots(8)$$

Since the TMMHP has three different sections – evaporator, adiabatic and condenser—through which *h* is involved, thus *eqn. 8* will be split into three equations as *eqn. 9, eqn. 10* and *eqn. 11*.

$$\left(\frac{U_{h_e}}{h_e}\right)^2 = \left(\frac{U_{q_e}}{q_e}\right)^2 + \left(\frac{U_{T_e}}{T_e}\right)^2 + \left(\frac{U_{A_e}}{A_e}\right)^2 \dots\dots\dots(9)$$

$$\left(\frac{U_{h_a}}{h_a}\right)^2 = \left(\frac{U_{q_a}}{q_a}\right)^2 + \left(\frac{U_{T_a}}{T_a}\right)^2 + \left(\frac{U_{A_a}}{A_a}\right)^2 \dots\dots\dots(10)$$

$$\left(\frac{U_{h_c}}{h_c}\right)^2 = \left(\frac{U_{q_c}}{q_c}\right)^2 + \left(\frac{U_{T_c}}{T_c}\right)^2 + \left(\frac{U_{A_c}}{A_c}\right)^2 \dots\dots\dots(11)$$

Thus finally, the relative uncertainties for *h* can be cumulatively expressed as in *eqn. 12*

$$\left(\frac{U_h}{h}\right)^2 = \left\{\left(\frac{U_{h_e}}{h_e}\right)^2 + \left(\frac{U_{h_a}}{h_a}\right)^2 + \left(\frac{U_{h_c}}{h_c}\right)^2\right\} \times 100\% \dots\dots\dots(12)$$ or, it can be re-written for standard uncertainty in the form of *eqn. 1* as shown in *eqn. 13*.

$$u(h) = \left\{\sqrt{\sum_{j=e}^{c} \frac{\partial h}{\partial q_j} h(q_j) + \sum_{j=e}^{c} \frac{\partial h}{\partial T_j} h(T_j) + \sum_{j=e}^{c} \frac{\partial h}{\partial A_j} h(A_j)}\right\} \times 100\% \dots\dots\dots(13)$$

where *j* = *e, a* and *c* which represents "evaporator, adiabatic and condenser" respectively.

While developing the uncertainty relation for the experiment, the following assumptions were made for simplification.

- Errors are negligible for the dissipation of heat through adiabatic section.
- Errors in pressure drop in the adiabatic section are negligible.
- Errors in density change in the adiabatic section are not significant.
- "Dry out" and "Flooding" related errors are not recognized because of the unsteady state.

- Errors caused by time elapse during recording data at the steady state are also insignificant.

The maximum errors are detected in the evaporator section which contains many sources of error, i.e. power input where volts and current are involved, heater coil, insulating material, fire proof tape etc. The condenser section releases heat at a temperature with a little variation and with coolant flow at a constant rate at ambient temperature, thus keeps the error at minimum.

The standard uncertainty, 4.54%, obtained by ***eqn. 13*** implies that the true value is expected to fall within the band $\pm u(h)$ around the measured value with an embedded 68% (2:1odds) confidence level. However, the most widely used procedure is to express the uncertainty of results with 95% (20:1odds) confidence level. The uncertainty with a 95% confidence level or expanded uncertainty (U) is related with the standard uncertainty (u) by means of a coverage factor (CF), as indicated in *eqn.14*. Herein, CF = 1.96 is the recommended value for the CF to improve the confidence interval up to 95% assuming a normal distribution in the experimental results, h_e, h_a and h_c.

$$U(h) = 1.96u(h) \dots\dots\dots (14)$$

Now by employing ***eqn. 13*** and ***eqn.14***, the cumulative percentile error is calculated with a confidence level of 95% ($\pm 1.96\sigma$) which is found to be 8.90%. Although theoretically, the expanded uncertainty should not exceed 5%, the excess of 3.90% is a bit higher than expected. This may happen because of few simplifications made during the analysis as stated earlier.

Appendix E

Thermophysical Properties of Ethanol (C_2H_5OH)

Ethanol, C_2H5OH, Molecular Mass: 46.0, (T_{sat} = 78.3 °C; T_m = -114.5 °C)											
˚C	p_v saturation pressure (10^5 Pa)	latent heat (kJ/kg)	ρ_ℓ liquid density (10^3 kg/m³)	ρ_v vapor density (kg/m³)	μ_ℓ liquid viscosity (10^{-3} N-s/m²)	μ_v vapor viscosity (10^{-5} N-s/m²)	k_ℓ liquid thermal conductivity (W/m-K)	k_v vapor thermal conductivity a (W/m-K)	σ liquid surface tension (10^{-3}N/m)	$c_{p,\ell}$ liquid specific heat b (kJ/kg-K)	$c_{p,v}$ vapor specific heat c (kJ/kg-K)
0	0.012	1048.4	0.901	0.036	1.7990	0.774	0.183	0.0117	24.4	2.27	1.34
20	0.058	1030.0	0.800	0.085	1.1980	0.835	0.179	0.0139	22.8	2.40	1.40
40	0.180	1011.9	0.789	0.316	0.8190	0.900	0.175	0.0160	21.0	2.57	1.48
60	0.472	988.9	0.770	0.748	0.5880	0.959	0.171	0.0179	19.2	2.78	1.54
80	1.086	960.0	0.757	1.430	0.4320	1.030	0.169	0.0199	17.3	3.03	1.61
100	2.260	927.0	0.730	3.410	0.3180	1.092	0.167	0.0219	15.5	3.30	1.68
120	4.290	885.5	0.710	6.010	0.2430	1.157	0.165	0.0238	13.4	3.61	1.75
140	7.530	834.0	0.680	10.670	0.1900	1.219	0.163	0.0256	11.2	3.96	
160	12.756	772.9	0.650	17.450	0.1500	1.293	0.161	0.0272	9.0		
180	19.600	698.8	0.610	27.650	0.1200	1.369	0.159	0.0288	6.7		
200	29.400	598.3	0.564	44.480	0.0950	1.464	0.157	0.0395	4.3		
220	42.800	468.5	0.510	74.350	0.0725	1.618	0.155	0.0321	2.2		
240	60.200	280.5	0.415	135.500	0.0488	1.948	0.153		0.1		

Property[a]	Temp.	α_0	α_1	α_2	α_3	α_4	α_5	Error(%)
p_v (10^5Pa)	0 – 240 °C	-4.4114	8.7650-2b	-6.3182-4	3.9958-6	-1.4340-8	2.0359-11	1.24
c (kJ/kg)	0 – 240 °C	1048.6	-1.0921	1.0651-2	-2.0693-4	1.1231-6	-2.4928-9	0.12
ρ_ℓ (10^3kg/m³)	0 – 240 °C	-1.0791-1	-7.7201-3	1.5906-4	-1.6139-6	7.1873-9	-1.2075-11	0.50
ρ_v (kg/m³)	0 – 240 °C	-3.3681	5.2492-2	5.1630-5	-1.9542-6	8.6893-9	-1.1451-11	4.95
μ_ℓ (10^{-3}Ns/m²)	0 – 240 °C	5.8942-1	-2.2540-2	1.0283-4	-8.8574-7	4.7884-9	-9.7493-12	0.39
μ_v (10^{-5} Ns/m²)	0 – 240 °C	-2.5759-1	4.5249-3	-3.1212-5	3.9144-7	-2.3733-9	5.1450-12	0.29
k_ℓ (W/m-K)	0 – 240 °C	-1.6976	-1.2505-3	7.5291-7	5.2361-8	-3.4986-10	6.4599-13	0.10
k_v (W/m-K)	0 – 220 °C	-4.4346	3.3797-3	2.1001-4	-3.4778-6	2.0462-8	-4.0325-11	3.75
σ[c] (10^{-3} N/m)	0 – 240 °C	24.419	-8.1477-2	-1.1450-4	8.6540-7	-7.6432-9	1.9148-11	2.15
$c_{p,\ell}$ (kJ/kg-K)	0 – 140 °C	0.81763	2.6793-3	1.3888-5	-4.3856-11	-4.4424-10	1.5104-12	0.01
$c_{p,v}$ (kJ/kg-K)	0 – 120 °C	2.9255-1	1.2271-3	8.0938-5	-1.8513-6	1.6850-8	-5.3880-11	0.11

a Polynomial Function: $\ln(\text{Property}) = \alpha_0 + \alpha_1 T + \alpha_2 T^2 + \alpha_3 T^3 + \alpha_4 T^4 + \alpha_5 T^5$
b The notation 8.7650-2 signifies 8.7650×10-2
c Polynomial Function: $\text{Property} = \alpha_0 + \alpha_1 T + \alpha_2 T^2 + \alpha_3 T^3 + \alpha_4 T^4 + \alpha_5 T^5$
Source: Wikipedia

Thermophysical Properties of Methanol (CH_4O)

Methanol, CH_4O, Molecular Mass: 32.0, (T_{sat} = 64.7 °C; T_m = -98 °C)											
T Temp. °C	p_v saturation pressure (10^5 Pa)	h_{lv} latent heat (kJ/kg)	ρ_ℓ liquid density (10^3 kg/m³)	ρ_v vapor density (10^3 kg/m³)	μ_ℓ liquid viscosity (10^{-3} N-s/m²)	μ_v vapor viscosity (10^{-7} N-s/m²)	k_ℓ liquid thermal conductivity a (W/m-K)	k_v vapor thermal conductivity a (W/m-K)	σ liquid surface tension (10^{-3} N/m)	$c_{p,\ell}$ liquid specific heat (kJ/kg-K)	$c_{p,v}$ vapor specific heat b (kJ/kg-K)
0	0.0411	1210.0	0.8100		0.8170	88	0.205		24.5	2.42	1.37
20	0.103	1191.1	0.7915		0.5780	95	0.204		22.6	2.46	1.44
40	0.358	1163.9	0.7740		0.4460	101	0.203	0.00157	20.9	2.52	1.50
60	0.861	1130.4	0.7555	0.0001006	0.3470	108	0.202	0.00178	19.3		1.57
80	1.819	1084.4	0.7355	0.0020840	0.2710	115	0.200	0.00199	17.5		1.70
100	3.731	1030.0	0.7140	0.0039840	0.2140	123	0.198	0.00220	15.7		1.86
120	6.551	971.3	0.6900	0.0071420	0.1700	130	0.196	0.00241	13.6		1.92
140	10.810	904.3	0.6640	0.0121600	0.1360	136	0.194	0.00262	11.5		1.92
160	17.609	828.0	0.6340	0.0199400	0.1090	143		0.00283	9.3		
180	16.869	741.1	0.5980	0.0318600	0.0883	150		0.00303	6.9		
200	38.434	636.4	0.5530	0.0507500	0.0716	157		0.00324	4.5		
220	56.728	473.1	0.4900	0.0863500	0.0583	166		0.00344	2.1		
240	79.700		0.2750	0.2750000	0.0460	174					

Property$_a$	Temp.	α_0	α_1	α_2	α_3	α_4	α_5	Error (%)
p_v (10^5Pa)	0– 240 ˚C	-3.2260	5.2299-2b	1.0307-4	-2.9204-6	1.4369-8	-2.2852-11	3.52
h_{lv} (kJ/kg) 0– 240 ˚C	7.1001	-1.6650-3	4.2482-5	-8.2591-7	5.2087-9	-1.1710-11	0.39	
ρ_ℓ (10^3kg/m³)	60– 220 ˚C	-2.0054-1	-5.5461-3	1.8492-4	-2.6081-6	1.4646-8	-2.8794-11	1.96
ρ_v (10^3 kg/m³)	0– 240 ˚C	-67.300	2.1944	-3.0858-2	2.1359-4	-7.2014-7	9.4732-10	6.77
μ_ℓ (10^{-3}Ns/m²)	0– 240 ˚C	-2.0529-1	-1.8685-2	1.2225-4	-1.0701-6	4.5665-9	-7.2697-12	0.35
μ_v (10^{-7} Ns/m²)	0– 240 ˚C	4.4794	3.3930-3	4.0163-6	-7.3376-8	2.4641-10	-2.1042-13	0.28
k_ℓ (W/m-K)	0– 140 ˚C	-1.5847	-4.0650-4	1.1186-5	-2.2761-7	1.6087-9	-3.9220-12	0.03
k_v (W/m-K)	40– 220 ˚C	-6.7646	8.9038-3	-3.5238-5	1.4232-7	-4.0030-10	5.0729-13	0.03
σ (10^{-3}N/m)	0– 220 ˚C	3.2019	-6.2365-3	1.1123-4	-1.7652-6	1.0660-8	-2.4530-11	0.65
$c_{p,\ell}$ (kJ/kg-K)	0– 40 ˚C	8.8377-1	6.2710-4	9.6297-6	0.0	0.0	0.0	0.01
$c_{p,v}$ (kJ/kg-K)	0– 140 ˚C	3.1404-1	5.0100-3	-1.7365-4	3.4376-6	-2.5001-8	5.9705-11	0.40

Polynomial function: $\ln(\text{Property}) = \alpha_0 + \alpha_1 T + \alpha_2 T^2 + \alpha_3 T^3 + \alpha_4 T^4 + \alpha_5 T^5$
Source: Wikipedia

Thermophysical Properties of Iso-propanol (C_3H_8O)

Working liquid	Density(ρ), kg/m^3	Viscosity(μ) mPa.s	Specific heat(c_p) kJ/kg.^oC	Boiling point (^oC)
Iso-Propanol	786.0	4.5646 mPa·s at 0°C	2.68 kJ/kg.^oC at 20°C-25°C (liquid)	82.2 (at STP)
		2.3703 mPa·s at 20°C	1.54 kJ/kg.K at 25°C (gas)	
		1.3311 mPa·s at 40°		

Vapor pressure of liquid

P in mm Hg	1	10	40	100	400	760	1520	3800	7600	15200	30400	45600
T in °C	-26.1	2.4	23.8	39.5	67.8	82.5	101.3	130.2	155.7	186.0	220.2	-

Table data obtained from *CRC Handbook of Chemistry and Physics* 44th ed.

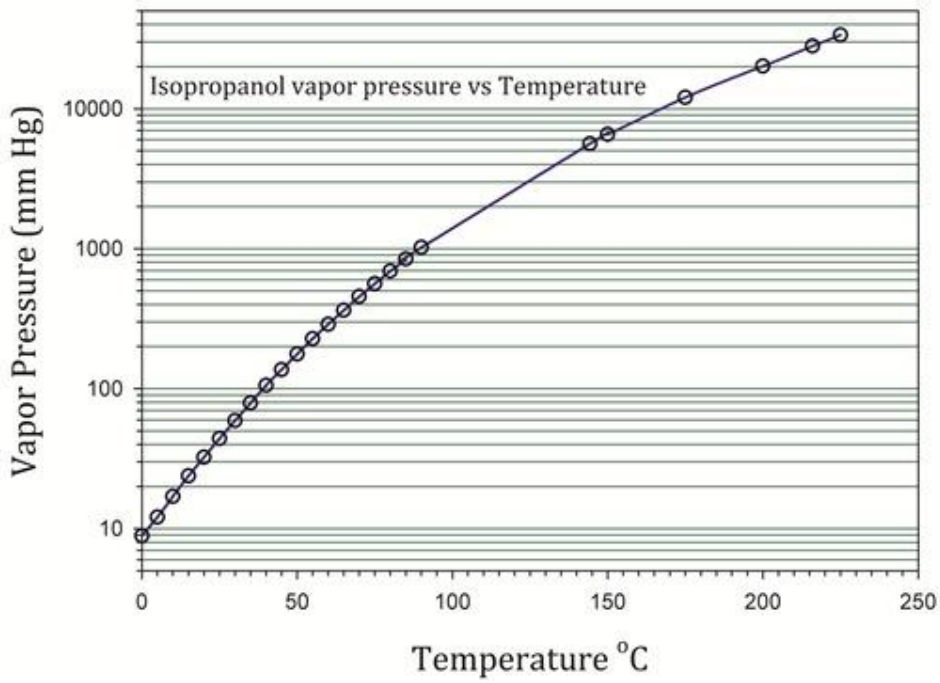

Figure App-E.1 $\log_{10}$ of Iso-propanol Vapor Pressure vs. Temperature

Source: Wikipedia

Thermophysical Properties of Water (H_2O)

Some commonly used thermal properties of water:

- Maximum density at *4 ^oC - 1,000 kg/m^3, 1.940 slugs/ft^3*
- Specific Weight at *4 ^oC - 9.807 kN/m^3*
- Freezing temperature - *0 ^oC (Official Ice at 0 ^oC)*
- Boiling temperature - *100 ^oC*
- Latent heat of melting - *334 kJ/kg*
- Latent heat of evaporation - *2,270 kJ/kg*
- Critical temperature - *380 ^oC - 386 ^oC*
- Critical pressure - *221.2 bar, 22.1 MPa (MN/m^2)*
- Specific heat water - *4.187 kJ/kgK*
- Specific heat ice - *2.108 kJ/kgK*
- Specific heat water vapor - *1.996 kJ/kgK*
- Thermal expansion from *4 ^oC to 100 ^oC - 4.2x10^{-2}*
- Bulk modulus elasticity - *2.15 x 10^9 (Pa, N/m^2)*

Temperature - *t* -	**Absolute pressure - *p* -**	**Density - *ρ* -**	**Specific volume - *v* -**	**Specific Heat - c_p -**	**Specific entropy - *e* -**
(^oC)	*(kN/m^2)*	*(kg/m^3)*	*10^{-3} (m^3/kg)*	*(kJ/kgK)*	*(kJ/kgK)*
0		916.8			
0.01	0.6	999.8	1.00	4.210	0
4	0.9	1000.0			
5	0.9	1000.0	1.00	4.204	0.075
10	1.2	999.8	1.00	4.193	0.150
15	1.7	999.2	1.00	4.186	0.223
20	2.3	998.3	1.00	4.183	0.296
25	3.2	997.1	1.00	4.181	0.367
30	4.3	995.7	1.00	4.179	0.438
35	5.6	994.1	1.01	4.178	0.505
40	7.7	992.3	1.01	4.179	0.581
45	9.6	990.2	1.01	4.181	0.637
50	12.5	988	1.01	4.182	0.707
55	15.7	986	1.01	4.183	0.767
60	20.0	983	1.02	4.185	0.832
65	25.0	980	1.02	4.188	0.893
70	31.3	978	1.02	4.191	0.966
75	38.6	975	1.03	4.194	1.016
80	47.5	972	1.03	4.198	1.076
85	57.8	968	1.03	4.203	1.134
90	70.0	965	1.04	4.208	1.192

Temperature ***- t -***	**Absolute pressure** ***- p -***	**Density** ***- ρ -***	**Specific volume** ***- v -***	**Specific Heat** ***- c_p -***	**Specific entropy** ***- e -***
(^oC)	*(kN/m^2)*	*(kg/m^3)*	*(10^{-3} (m^3/kg)*	*(kJ/kgK)*	*(kJ/kgK)*
95	84.5	962	1.04	4.213	1.250
100	101.33	958	1.04	4.219	1.307
105	121	954	1.05	4.226	1.382
110	143	951	1.05	4.233	1.418
115	169	947	1.06	4.240	1.473
120	199	943	1.06	4.248	1.527
125	228	939	1.06	4.26	1.565
130	270	935	1.07	4.27	1.635
135	313	931	1.07	4.28	1.687
140	361	926	1.08	4.29	1.739
145	416	922	1.08	4.30	1.790
150	477	918	1.09	4.32	1.842
155	543	912	1.10	4.34	1.892
160	618	907	1.10	4.35	1.942
165	701	902	1.11	4.36	1.992
170	792	897	1.11	4.38	2.041
175	890	893	1.12	4.39	2.090
180	1000	887	1.13	4.42	2.138
185	1120	882	1.13	4.45	2.187
190	1260	876	1.14	4.46	2.236
195	1400	870	1.15		2.282
200	1550	864	1.16	4.51	2.329
220		840		4.63	
225	2550	834	1.20	4.65	2.569
240		814		4.78	
250	3990	799	125	4.87	2.797
260		784		4.98	
275	5950	756	1.32	5.20	3.022
300	8600	714	1.40	5.65	3.256
325	12130	654	1.53	6.86	3.501
350	16540	575	1.74	10.1	3.781
360	18680	528	1.90	14.6	3.921

Source: Wikipedia